Calculation of Negative Lyapunov Exponents Using a Time Series for Potentially Stable Robotic Systems

By

Xinzheng Wang

A Thesis submitted to the Faculty of Graduate Studies of

The University of Manitoba

in partial fulfilment of the requirements for the degree of

MASTER OF SCIENCE

Mechanical and Manufacturing Engineering

Winnipeg, Manitoba, Canada

THE UNIVERSITY OF MANITOBA

FACULTY OF GRADUATE STUDIES

*****

COPYRIGHT PERMISSION

Calculation of Negative Lyapunov Exponents

Using a Time Series for Potentially

Stable Robotic Systems

BY

Xinzheng Wang

A Thesis/Practicum submitted to the Faculty of Graduate Studies of The University of

Manitoba in partial fulfillment of the requirement of the degree

MASTER OF SCIENCE

Abstract

It is believed that Lyapunov Exponents can characterize the stability of nonlinear dynamic systems. Lyapunov Exponents can be calculated from the mathematic model or time series data of the system, which are independent of the initial conditions within the same stability region. Lyapunov Exponents have been mainly used for diagnosing chaotic systems, where at least one Lyapunov Exponent is positive. Little work has been done on calculating Lyapunov Exponents from a time series of a potentially stable system, where the largest Lyapunov Exponent is negative or zero. Most mechanical systems are complex, of which, the mathematical models are sketchy or even not available. For such systems, it is extremely difficult, even impossible, to derive a Lyapunov function for stability analysis. Therefore, an alternative method for stability analysis of nonlinear engineering systems is needed.

The objective of this thesis is to explore the possibility and limitations of applying Wolf's method to calculate the largest Lyapunov exponent from a time series of potential stable systems. Two fundamentally different robotic systems are used as examples. One is a robotic arm with two rigid links moving in the horizontal plane. A position-controlled pneumatic actuator system is used as the second example. In addition to the different nature in their nonlinearity between the above two robotic systems, the pneumatic system has a set of infinite non-isolated equilibrium points, while the two-link robotic arm has one equilibrium point.

Lyapunov Exponents for each of the above systems are calculated using the mathematic models and the largest exponent is calculated from the time series. The results show that for the two-link position-controlled robotic system which has an isolated equilibrium point, the largest negative Lyapunov exponent calculated from the time series matches the one from the mathematic model very well. This indicates that Wolf's method has good potential for calculating largest negative Lyapunov exponent. However, for systems with a stable periodic motion, the stability should be studied using Lyapunov exponents calculated from mathematical model. For the pneumatic system, which has a set of infinite non-isolated equilibrium points, zero exponents are obtained from the mathematic model, which conflict with the conventional interpretation of the Lyapunov Exponents. However, the largest Lyapunov exponent calculated using a time series for the pneumatic system does not match the one from the mathematic model, and the cause is also explored. It is concluded based on the examples for systems with a set of infinite non-isolated equilibrium points, The largest Lyapunov Exponents can not be calculated using Wolf's method. Systems with infinite non-isolated equilibrium points occur naturally and frequently in mechanical engineering systems.

This work is the first step in applying the concept of Lyapunov Exponents for stable mechanical engineering systems. It enables us to understand the possibility and procedure for applying Wolf's method using time series for potentially stable robotic systems. More importantly, this work shows the limitations of the applications of Wolf's method to engineering systems.

Table of Contents

Acknowledgements

I would like to thank my Supervisor, Dr. Christine Q. Wu. I could not have imagined having a better advisor and mentor for my M.Sc., and without her common-sense, knowledge, perceptiveness and cracking-of-the-whip I would never have finished. I am grateful for the highly responsive support from my co-advisor Dr. N. Sepehri, for providing me with the background knowledge in nonlinear control and robots.

Thank-you to my advisory committee members, Dr. Q. Wang and Dr. Wai-Keung Fung for their careful review and suggestions regarding this thesis. I would also like to thank all of the rest of the academic and support staff of the Department of Mechanical and Manufacturing Engineering at the University of Manitoba.

My gratitude also goes to all of the members in the Nonlinear System Research Laboratory for their help and support.

I thank all of my friends, in particular Kubla, Weiwei, Jilu, Jane and Irene; and my extended family, wherever they are. Special thanks, goes to my landlady Heather and landlord Rick. I could not live as happily as I do, without their care. Special thanks go to Wu Yi for her encouragement. Lastly, but most importantly, I thank my Mom and Dad for their love.

List of Figures

List of Tables

List of Symbols

λ_i	The i^{th} Lyapunov Exponent
ψ	The state transition matrix
m	The embedding dimension
P_{t1}	The initial point in reconstruction
P_{t2}	The nearest neighbor to P_{t1}
$L(t)$	The involution length
V_{noise}	The average noise power
$V_{noise\ n}$	The noise power at a time instant
V_{signal}	The average noise power
$V_{signal\ n}$	The system signal power at a time instant
dB	The ratio of a signal power to the noise power
l_1	The rigid link 1 length in two-link pendulum system
l_2	The rigid link 2 length in two-link pendulum system
m_1	The mass of link 1 in two-link pendulum system
m_2	The mass of link 2 in two-link pendulum system
r_1	The location of the mass center of the link 1 in two-link pendulum system

r_2 The location of the mass center of the link 2 in two-link pendulum system

θ_1 The joint angle 1 in two-link pendulum system

θ_2 The joint angle 2 in two-link pendulum system

τ_1 The control torque applied at joint 1 in two-link pendulum system

τ_2 The control torque applied at joint 2 in two-link pendulum system

C A vector of the torque related to the centrifugal and Coriolis forces

$f(\dot{\theta})$ The vector of the torque related to the viscous friction

$g(\theta)$ The vector of the torque related to the gravity

k_{p_i} The proportional gains

k_{v_i} The derivative gains

x_p The position of the piston

M The combined mass of the piston-rod assembly and the external load mass

P_1 The absolute pressure in the actuator chamber 2

P_2 The absolute pressure in the actuator chamber 2

A The annulus area of the piston

b The viscous friction coefficient

F_f The dry friction force

F_l The externally applied load

ρ The mass density of the working fluid

R The ideal gas constant

$\dot{m}$ The mass flow rate

V The chamber volume

c_v The specific heat at constant volume

c_p The specific heat at constant pressure

$\dot{Q}$ The rate of heat transfer across the cylinder wall

P_s The supply pressure and

P_d The return pressure, the area of each valve orifice

A_v A function of the displacement of the valve spool

x_v The control valve position

u The input voltage

σ_0 The stiffness of the bristles in LuGre model

σ_1 The damping in LuGre model

$g(v)$ The Stribeck effect in LuGre model

$f(v)$ The viscous friction in LuGre model

F_s Static friction

F_c Coulomb friction

$\dot{e}_{deadband}$ The estimate of the velocity error caused by deadband

β The experimental constant found though trial and error

P_{atm} Atmospheric pressure

b Viscous damping coefficient

L Actuator stroke

V_{o1}, V_{o2} Cylinder dead volume

T Temperature of air source

γ Ratio of specific hearts

α Pressure-volume work correction factor

C_d Valve coefficient of discharge

w Valve orifice area gradient

$x_{v,\max} / x_{v,\min}$ Min/Max valve spool displacement

K_{valve} Valve spool position gain

μ Valve first-order time constant

P_{cr} Valve critical pressure ratio

K_I The Integral gain

U_{lower} The lowest control voltage

U_{upper} The highest control voltage

$\dot{e}_{\min}$ The controller with this modification will overcome the error accumulate of the deadband

List of Abbreviations

AMI, Average Mutual Information

COM, Center of Mass

DOF, Degrees of Freedom

GFNN, Global False Nearest Neighbors

GSR, Gram-Schmidt Reothonormalization

GWN, Gaussian White Noise

L.E., Lyapunov Exponent

PD, Proportional and Derivative

PI, Proportional-Integral

PID, Proportional-Integral-Derivative

QFT, Quantitative Feedback Theory

RPS, Reconstructed Phase Space

SNR, Signal to Noise Ratio

Chapter 1

Introduction

1.1 Motivations

Control Engineering uses control theory to cause diverse, mathematically modeled systems behave in a desired manner. In order to create the controller, the dynamic behavior of a modeled system needs to be fully analyzed and understood.

Control Engineering has a wide range of applications, from the flight and propulsion systems of commercial airliners to the automatic control present in many modern robot systems. The stability of the control systems is the most important consideration when applying the controllers.

With background technologies of behavior, navigation and path planning solved using basic wheeled robots; Roboticists are now moving on to develop stable walking robots. Over the past two decades, numerous bipedal walking robots have been created including Asimo (Honda Motor CO. 2002) and QRIO (Sony Co. 2003). Initial work focused on multi-legged

robots such as Aibo (Sony Co. 1999); which were statically stable and easier to work with.

A difficulty in the development of bipedal and naturally gaited robots is that the human body utilizes a large number of muscles to keep balanced and stable when moving. Replicating what is required for stabilization mechanically is very difficult and expensive.

Since an unstable robotic system is typically useless and potentially dangerous; the stability analysis is always the important part in control engineering. The controller is applied to ensure that the system follows the desired trajectory or moves to the desired position. In the majority of cases, automatic control systems involve complex devices, consisting of objects (plants or processes) to be controlled, and controllers. The task of a controller is to continuously support either the stationary operating conditions, or those conditions of the plant that change according to a given law. All deviations from the desired conditions that may arise in the control system must be reduced to zero. In other words, the control system must be asymptotically stable (David R Merkn, 1996). The stability analysis of robotic motion can be traced back to the time when robots were first invented. In recent years, many studies on the stability analysis relating to robotic control have been done. Several theories and methods have been successfully developed to support the stability analysis of robotic motion.

Lyapunov's stability theory is widely used for stability analysis of nonlinear dynamic systems. It includes two methods. One is the Linearization Method and the other is the Direct Method. The Linearization Method draws conclusions about a nonlinear system's local

stability around an equilibrium point from the stability properties of its linear approximation. The Direct Method is not restricted to local motion. It determines the stability properties of nonlinear system by constructing a scalar energy-like function for the system and examining the derivative of the function with respect to time. The key to applying the Lyapunov stability analysis is to find a Lyapunov function. However, there are no general and constructive methods for deriving Lyapunov functions for nonlinear systems.

As there are no constructive rules for deriving a Lyapunov function, the applications of this otherwise powerful tool are extremely limited and the stability of many nonlinear systems cannot be studied. Lyapunov exponents quantify the average rate of convergence or divergence of nearby trajectories. A positive exponent implies a divergence of orbits, a negative one shows convergence of orbits, and a zero exponent indicates the temporally continuous nature of a flow (i.e. the trajectory show periodic motion).

There are two ways to calculate Lyapunov Exponents. One method calculates Lyapunov Exponents from the mathematic model of the system, and the other method calculates Lyapunov Exponents directly from one series of the simulation or experiment data. The method which calculates Lyapunov Exponents from the time series data is very convenient and powerful. Until now, most of the work on the method which calculates Lyapunov Exponents from the time series data has been focused on the chaotic system, where at least one Lyapunov Exponent is positive. Further exploration of Lyapunov Exponents using the time series method of stability analysis, where the largest Lyapunov exponent is negative or

zero, is needed.

1.2 Literature survey

1.2.1 Stability analysis of nonlinear robotic systems

"The General Problem of Motion Stability" was developed by Alexandr Mikhailovich Lyapunov in the late 19th century. Since then, Lyapunov's direct method has been applied to many mathematic, electrical and mechanical systems. These studies focus on the variation of the Lyapunov function measurements of the motion amplitude. The Lyapunov function is not restricted to linear systems but requires the construction of a suitable measure, done on a case by case basis. Lyapunov's stability theory does not give the method for deriving a Lyapunov function. Consequently, the construction of a Lyapunov function for a nonlinear system remains a great challenge which restricts applications for this otherwise powerful theory (Wu, 1996). Non-smooth systems, defined by ordinary differential equations containing discontinuous terms, frequently appear in mechanical engineering. For non-smooth systems, which violate the Lipschitz-continuous requirement, the solution and stability analysis of such systems using classical techniques is questionable. Due to the existence of the above challenges, many studies on Lyapunov stability analysis have been carried out and are summarized below.

The stability of multi Degrees of Freedom (DOF) robot systems have been studied under the Lyapunov direct method. A considerable amount of work has been done on developing methods for deriving Lyapunov functions including: the method of analogy with linear

systems by Barbasin (1960), the method of integration by parts by Ponzo (1965) and Huaux (1967), the method of system energy by Marimo and Nicosia (1983), the integral methods, the scalar-Lyapunov-function method and the intrinsic method by Chin (1986, 1987, 1988 and 1989), extended integral method by Wu et. al. (1995). These methods provide a robust basis for the stability analysis, especially the Wu et. al. (1995) extended Chin's integral method which constructs Lyapunov functions for the general nonlinear systems represented by state space models. All of the above research is based on the conventional Lyapunov's stability theory. They can only be applied to the smooth system. Smooth systems, are systems where every term in the ordinary differential equations is continuous. In spite of the importance of non-smooth systems which has been mentioned by several researchers (Slotine and Sastry 1983, Southwar et al. 1991, Utkin 1977 and 1991 and Corles 1993), there are no effective methods developed. A solution theory, which allows for the study of differential equations with discontinuous terms, is needed for non-smooth systems. The pioneer in the research of the non-smooth system is Filippov (1960, 1979 and 1988). He developed a solution theory (Filoppov's solution theory) for non-smooth systems that is used to define solutions for the proposed piece-wise continuous control systems and the existence and uniqueness of such solutions. Wu et al., (1996) proved the uniqueness of Filippov's solution for a base-excited inverted pendulum system where the Lyapunov feedback control law is discontinuous. Wu et al. (1998, 2001), further extended the Lyapunov's second method to non-smooth dynamic systems and methods for constructing smooth/non-smooth Lyapunov functions have been developed. It has been demonstrated that with such methods, it is much

easier to construct Lyapunov functions for some non-smooth engineering systems.

Although Lyapunov's stability theory is a powerful tool for stability analysis, the lack of rules for deriving Lyapunov functions has severely limited the applications of Lyapunov's stability theory. Therefore, a new method to analyze the stablity of nonlinear systems is needed.

1.2.2 Chaos phenomena in mechanical engineering

There are many studies on the presence of bifurcations and chaos in mechanical and electrical systems. Moon (1987) describes many phenomena where chaos has been detected. In the particular case of robot manipulators however, little work exists on bifurcations and chaos. For example, Nakamura et al. (1997) analyzed an underactuated, frictionless manipulator lying on a horizontal plane. They considered chaos as a motion characterized by sensitive dependence on initial conditions and topological transitivity, and show numerically that the system can display these two properties. They proposed some controllers to accomplish several control objectives, showing dynamical properties from numerical experiments. Mahout et al. (1993) presented simulations of a 2-DOF robot manipulator executing repetitive tasks controlled with a PD algorithm, which gave rise to complex dynamics. Lankalapalli and Ghosal (1996, 1997) analyzed a controlled 2-DOF robot manipulator (a PD and a model-based controller). They verified the existence of chaotic motions using numerical simulations and by calculating the largest Lyapunov exponent.

Several analytical results of bifurcations and chaos have also been obtained for special configurations of the dynamic systems. Burov (1986) and Dullin (1994) have proved the non-integrability of the double pendulum using the method of splitting, separatrices and Melnikov's method, respectively. Lindtner et al. (1989) gave all the generic codimension-one cases of stability loss in a driven double pendulum where the prescribed motion of the endpoint is a circle. Verduzco and Alvarez (1999) made a theoretical study of bifurcations in a 2-DOF underactuated robot manipulator driven by constant torques.

Among the procedures proposed to regulate mechanical robots, the PD compensator is widely used (Takegaki et al. 1981). Under some circumstances, a complex dynamical behavior may arise in this system. In particular, the PD-controlled pendulum may exhibit a chaotic behavior when the reference for the angular position is periodic and the total dissipation and proportional gain satisfy some conditions (Alvarez et al. 1998). Lypapunov's direct method is not suitable to the stability analysis of chaos. For this new phenomenon, a method to diagnosing and analyzing chaos is required.

1.2.3 Concept of Lyapunov Exponents

Chaotic behavior has been observed in the laboratory in a variety of systems including oscillating chemical reactions and fluid dynamics. Chaotic behavior has been observed in nature including the dynamics of satellites in the solar system, weather and climate. Lyapunov Exponents have been considered to be the most useful dynamc diagnostic tool for chaotic systems.

Lyapunov Exponents quantify the rate at which orbits on an attractor converge or diverge as the system evolves in time (Rosenstein et al., 1993, Abarbanel, 1996), and provide a direct measure of the stability of those orbits. One exponent is defined for each dimension, representing the average rate of growth or decay along each of the principal axes in the d_E-dimensional state space (Abarbanel, 1996). The largest Lyapunov exponent specifies the maximum average rate of divergence, or convergence of the orbits. A positive exponent implies divergence of the orbits and indicates global instability and sensitivity to initial conditions that define the presence of chaos. A negative one indicates convergence of the orbits. A zero exponent indicates the temporally continuous nature of a flow (i.e. the trajectory show periodic motion). Consequently, a system with positive exponents has positive entropy, in that trajectories which are initially close move apart over time. The more positive the exponent, the faster they move apart. Similarly, for negative Lyapunov Exponents, the trajectories converge. Determining the Lyapunov Exponents analytically is extremely difficult, especially for robot systems. Most of the work on determining Lyapunov Exponents for robot systems is based on numeric calculations.

1.2.4 Calculation of Lyapunov Exponents

1.2.4.1 Calculation of Lyapunov Exponents from the mathematic model

For systems of which the equations of motion are explicity known, there is a well developed and straightforward technique to compute the entire Lyapunov Exponents' spectrum (Benettin et. al., 1980). The concept of Lyapunov Exponents was given in a form

adapted to the needs of the theory of dyamic systems and of the ergodic system by Oseledec (1968). Benettin et al. (1980) developed a method for determining the analytical results of all Lyapunov Exponents. It is the basic background for the calculation of Lyapunov Exponents numerically.

One chaotic system was introduced by Lorenz (1984) which has 3 ordinary differential equations, where the Lyapunov Exponents of the system were calculated. The most used method which calculates Lyapunov Exponents from the mathematic model was developed by Wolf et al. (1985). Muller (1995) extended Wolf's method to the non-smooth system and pointed out that the required linearized equations have to be supplemented by certain transition conditions at the instance of discontinuities. The accuracy of the calculated Lyapunov Exponents is always important. However in Wolf's method, the first order ODE numerical method was used. Despite the success of the methods for determining Lyapunov Exponents based on mathematical models, it has many limitations.

Better algorithms are needed. Adequate mathematical models have not yet been found even for the simplest chaotic flows in hydrodynamic systems (Harry 1986). The above method can not be applied directly to the experimental data, and even due to the known system's high order non-linear systems, heavy mathematic calculation is required and the method for determining Lyapunov Exponents based on mathematical models is not feasible for some systems.

1.2.4.2 Calculation of Lyapunov Exponents from a time series

Calculating the Lyapunov Exponents from a time series is another way to analyze the stability of a system. Usually, time series data is a set of data for a variable and consists of discrete measurements. This method allows for the calculation of Lyapunov Exponents from one time series data which can often be collected from experiments. These advantages of this method attract many researchers to employ it. A considerable amount of work has been done for chaotic systems. Applying this method to stable systems, suggests a bright future for stability analysis.

Before calculating Lyapunov Exponents, the attractor has to be reconstructed. The Takens theorem (1981) implies that for a wide class of deterministic systems, there exists a diffeomorphism (one to one differential mapping) between a finite "window" of the time series data. Several related approaches which use a state/space reconstruction method (Packard et. al., 1980) to predict the input/output data, include local linear method (Price and Prichard, 1993; Vassiliadis et al. 1994) AutoRegressive Moving-Average method (Detman and Vassiliadis, 1997) and neural network models (Her et al. 1993).

Given a scalar time series produced from a measurement of an autonomous system with many degrees of freedom, it was shown by Packard et al (1980) that if the dynamics of the system lies on a low dimensional attractor, the attractor can be reconstructed by creating a delayed coordinate vector. It was shown by Takens (1981) that this attractor reconstruction is one to one. Most observed data, reflect just a few of the many physical variables of a system and measurements of all variables are rarely possible. This difficulty is overcome if the

variables are nonlinearly coupled, in which case the time delay embedding technique can be used to reconstruct the phase space from the time series data. The Embedding Theorem (Takens, 1981, Sauer et al., 1991) states that the topological structure of a dynamical system can be "unfolded" from a single time series using the original data and its time-delayed copies:

$$Y(n) = [X(t), X(t+\tau), ..., X(t+(d_E-1)\tau)] \tag{1.1}$$

where $Y(n)$ is the reconstructed d_E -dimensional state vector, $X(t)$ is the original 1-dimensional data, τ is a time lag, and d_E is the embedding dimension. The time lag, τ, can be calculated from the first minimum of the Average Mutual Information (AMI) function, which evaluates the amount of information shared between two sets of data over a range of time lags (Fraser and Swinney, 1986, Abarbanel, 1996). An appropriate value for d_E can be computed from a Global False Nearest Neighbors (GFNN) analysis (Abarbanel, 1996) by determining the dimension where the total percentage of false neighbors (produced by projection of an attractor onto a state space of too small a dimension) drops close to zero.

A major breakthrough came with the discovery that a measured time series carries the information necessary to estimate the above quantities. In particular, the method of embedding using time delay coordinates, first introduced by Packard et al. (1980), provided a general tool for the identification and analysis of complex systems in terms of low dimensional systems. The Embedding Theorem guarantees that the dynamical properties of the system are the same

in both the original and reconstructed state spaces, providing a powerful tool for extracting multidimensional dynamic information from unidimensional time series.

In the calculation of Lyapunov Exponents from time seres data, the samples of the data are very important for the calculation. Here, the basic signal sample concepts and theorem (Shenoi 2006, Cover and Thomas 1991) are reviewed. Time series data include two kinds of time signal, the continuous-time signal (analog signal) and discrete-time signal (digital signal). A continuous-time signal is a function of an independent variable that is continuous. A one dimensional continuous-time signal $f(t)$ is expressed as a funtion of time that varies continuously from $-\infty$ and ∞. A discrete-time signal is a function that is defined only at discrete instances of time and is undefined at all other values of time. Although a discrete-time function may be defined at arbitrary values to time in the interval $-\infty$ and ∞, in this work we consider only a function defined at equal intervals of time and defined at $t = n\tau$, where τ is a fixed interval in seconds known as the sampling period and n is an integer variable defined over $-\infty$ and ∞. If it is chosen to sample $f(t)$ at equal intervals of τ seconds, the function $f(n\tau) = f(t)|_{t=n\tau}$ as a sequence of number (samples). Since τ is fixed, $f(n\tau)$ is a function of only the integer variable n and hence can be considered as a function of n or expressed by $f(n)$. For a continuous function, $f(t)$ is band-limited to $f_{\max}$. Namely, the spectrum of the function is 0 for all frequencies greater than $f_{\max}$. Then, the function is completely determined by samples of the function spaced $\frac{1}{2f_{\max}}$ seconds apart. The Nyquist-Shannon theorem shows that a band-limited function has only $2f_{\max}$ degrees of freedom per second. The values of the

function at the sample points can be chosen independently, and this specifies the entire function (Cover et. al., 1991). Graphically, if the sampling rate is sufficiently high, i.e. greater than the Nyaquist rate, there will be no overlapped frequency components in the frequency domain. Most mechanical signals have frequency limited to below 100Hz. Therefore, a 200Hz sampling rate should satisfy most mechanical engineering applications.

After the attractor is reconstructed, a method for calculating Lyapunov Exponents needs to be developed. Several methods for estimating Lyapunov Exponents from experimental data have been developed. The most frequently used methods are due to Wolf et al. (1985), which follow the separation between nearby points on the attractor to estimate the largest Lyapunov exponent. Eckaman et al. (1990) follows groups of nearby points to compute a least square estimate of the Jacobian at each point, which is then used to integrate the variational equations, from which the Lyapunov Exponents are calculated. Although these techniques give an estimate of the Lyapunov Exponents, large amounts of experimental data are necessary (Mayer-Kress 1986). This is due in part, to the need to obtain an accurate reproduction of the attractor geometry from the observed data. Stoop and Parisi (1991) advocated the use of the singular value decompostition to restrict the dynamics to the tangent plane of the attractor, prior to approximating the local linear dynamics. Rosenstein et al. (1993) developed an algorithm to compute the largest Lyapunov exponent by directly estimating the separation between pairs of neighboring points in the state space as they diverge over time. By plotting the log of the divergence versus time, the largest Lyapunov exponent is estimated by computing a

least squares fit to the linear region of the resulting curve (Rosenstein et al., 1993). A less data required method was developed by Rauf and Ahmed (1992). The studies related to this method were done to get more precise Lyapunov Exponents with short data (Zeng et al. 1991; Brown, Henry 1991). This method was applied to the daily-averaged data of surface temperature observed at two locations in the United States, to quantitatively evaluate atmospheric predictability. Carretero-Gonzlez et al. (2000) described methods of estimating the entire Lyapunov sepectrum of a spatially extended system from multivariate time series observations. Kinsner (2003) developed the method to measure and analyze chaos using Lyapunov metrics. Until now, most of the works on Lyapunov Exponents are about the low dimensional chaotic systems (the Lorenz attractor is the most famous one). Although this method suggests a bright future for stability analysis, difficulties do exist in getting accurate Lyapunov Exponents i.e., for calculating negative Lyapunov Exponents.

Noise imported from the environment is also a problem which affects the accuracy of the calculation of Lyapunov Exponents. Sauer and Yorke (1999) investigated the computational artifacts due to observtional noise in the experimental time series data, and gave the formulae for the expected values of the reconstructed Jacobian in some simple cases. More information about measurement noise is presented in the next section.

1.2.5 The effects of noise on calculation of Lyapunov Exponents from time series

The experimental data is usually accompanied with noise. Although filters can remove some of the noise it can not be eliminated completely. As noise will affect the accuracy of the

Lyapunov Exponents, the effects of noise must be reduced. There are two methods to do that. One is using filters to reduce the noise from the experimental data; the other is setting the evolution length scales, which only work when scales larger than the noise contain accurate information. Since larger neighborhoods yield poorer linear approximations due to the nonlinearity, errors in the dynamics increase with the noise level. White Gaussian Noise (WGN) is the most common noise in the mechanical systems. Removing the noise from experimental data and studying the sensitivity of the method to noise which calculates Lyapunov Exponents from time series are both challenging problems.

The theory of filtering of stationary time series for a variety of purposes; was developed by Norbert Wiener in the 1940s for continuous time processes in a notable feat of mathematics (Wiener, 1949). In an important paper, Levinson (1947) showed that in discrete time, the entire theory could be reduced to least squares, which makes it mathematically simple. Conventional approaches to noise reduction like the Weiner and the Kalman filters are not suitable for signals measured from chaotic systems because the underlying dynamics of the chaotic system is not localized in either the time or the frequency domain. Methods of noise reduction are extensively used in communication, physical systems and experimental measurements. There are many methods for reducing noise in a chaotic time series. Hammel (1990) has presented a method which can reduce the noise of a chaotic orbit on an attractor by more than ten orders of magnitude. This method is simple and fast. Its performance was analysed for several two-dimensional systems at moderate noise levels. A simple nonlinear

noise reduction method can be used in the Wolf's method. This involves choosing the replacement neighborhood points which selects trajectories that stay closed, for a few time steps to the segment to be cleaned.

Overall, the concept of Lyapunov Exponents is a powerful tool to analyze the stability of nonlinear systems. The method which calculates the Lyapunov Exponents from the mathematic model has been well developed. A considerable amount of work has been focused on developing the method which calculates the Lyapunov Exponents directly from the time series. Until now, a large body of research has been completed on the analysis of chaotic systems, which have at least one positive Lyapunov exponent. The concept of Lyapunov Exponents has rarely been used to study potentially stable systems where the largest Lyapunov exponent is negative or zero. This is true especially for the method calculating Lyapunov Exponents directly from the time series. The pioneering explorations for applying the concept of Lyapunov Exponents directly from the time series for stable systems are needed.

1.3 The systems studied in this thesis

Two typical robotic systems will be used in this study to test the applicability of methods for calculating negative Lyapunov Exponents based on a time series. Research related to the two robotic systems studied in this work, are discussed briefly in this section.

1.3.1 Multiple pendulum systems

The inverse pendulum plays an important role in robotic research. For research on

bipedal robots, a chain of inverted pendulums is often used as a physical model. An inverted pendulm is an inherently unstable system and the studies of control and stability of such a system is one of the challenging problems in the field of automatic control (Mori, 1972). For natural human walking, more than 20-degrees of freedom may be involved (Golliday and Hemami, 1977). It is extremely challenging to study such a complicated system and to get some desired results. So in robotic research, the first step is to select a simpler mathematical model to describe the motion and test the controller. Previous studies about the stability of the bipedal robot systems still rest on the Lyapunov's stability theory. Although the previous works provided a solid framework in the study of posture stability and control of biped movement, it is difficult to apply them to more complicated models.

With more than 20-degrees of freedom involved in human walking, it is complicated to model the systems and the dynamic equations which have highly coupled nonlinearities. To address this, several simplified models have been developed. The majority of these approaches used the inverted pendulum to study human/biped systems (Chow and Jacobson 1971, 1972, Hemami et al. 1973, Hemami and Golliday 1977, Hemami et al. 178, Katbab 1982, Muri 1984, Kajita and Tanie 1991, Wu et al. 1998). Wu et al. (1998) studied a base-excited (in 3D space) inverted pendulum with two degrees of rotational freedom to predict major features of upper body dynamics and stability. However, the single pendulum is too simple to adequately study the complete dynamic motion of humans. The model to describe bipedal locomotion was then increased to 2-DOF and the idea of using a two-link

inverted pendulum model was introduced (Golliday and Hemami 1976, Hemami and Camana 1976, Hmami 1978, Hurmuzlu and Moskowitz 1986, Wu and Swain 2002). The three-link biped model which has an upright trunk and two lower limbs were developed by Hemami (1977) and Hurmuzlu (1984). The five-link model was studied by many researchers (Hemami et al 1977, Urmuzlu 1993, Wu and Chan 2002, Ma and Wu 2002, and Wu et al. 2002, 2004). The five-link inverted pendulum system became a seven-link system when two links were added as the two feet. Onyshko and Winter (1980) and Shih (1996) studied human locomation using a seven-link bipedal model. The more complicated nine-link biped was sudied by Tagawa and Yamashita (1981), Furusho and Sano (1990) and Zheng and Shen (1990). Although the multi DOF inverted pendulum system can describe the human being motion better, it is sometimes too complicated to feasibly analyze the stability.

A very strange phenomenon, chaos, appeared when changing the controller gains. Although literature exists on chaotic motion in Duffing's oscillator, in inverted pendulum maps and several other systems (Holmes, 1983); there are very few works on chaos in robots reported. Striet et al (1989) have investigated the non-linear response of a flexible manipulator performimg a repetitive task. They showed that the flexible variables can undergo period doubling bifurcations leading to chaos. Buhler and Koditschek (1990) have discussed robotic juggling and have shown that incrementing controller gains of a planar juggling robot can lead to period doubling and chaotic motions. Vakakis and Burdick (1990) and M'Closkey and Burdick (1993) have looked at periodic and chaotic motions in a hopping

robot with a non-linear spring in the leg. Mahout et al. (1992) have numerically studied the equations of a planar 2R robot with a proportional and derivative (PD) controller. They have shown that the 2R robot, under PD control, can exhibit harmonic, subharmonic, higher harmonic, fractional harmonic and possible chaotic motions as the gains changed.

1.3.2 Pneumatic actuation systems

Pneumatic actuators have been widely used in manufacturing and industry because of their low cost and neatness. Many complete mathematical models for the thermodynamics and flow equations in the charging-discharging processes were developed (Shearer, 1956). As a result, more complex position controllers; based on the linearization around the mid stroke position, were developed (Burrows, 1966; Liu et. al., 1988). There are lots of control methods, from point-to-point position control to high accuracy tracking and force control. A comparison between linear and nonlinear controllers applied to a rotary pneumatic actuator is presented by Richard and Scavarda (1996). It is difficult to make the actuator reach the desired performance level using either the standard proportional-integral (PI) or proportional-integral-derivative (PID) control. Karpenko and Sepeheri (2003) developed a practical, yet accurate, position controller for an experimental pneumatic actuator. Based on the quantitative feedback theory (QFT) they used a fixed-gain PI control law which minimizes the effects of the plant parametric uncertainty on the closed-loop position responses (Karpenko, 2003). Due to the complexity of the peumanic system the stability analysis has not been carried out.

Both of the systems studied in this thesis, are very typical systems in robotic control engineering. Due to the complexity of the systems and lack of rules for generating Lyapunov functions, stability analysis of the above control systems has been extremely limited. In this work, the concept of Lyapunov Exponents is applied to these two systems for stability analysis.

1.4 Objective and scope of this Thesis

A considerable amount of work on determining Lyapunov Exponents based on a time series has been done, for chaotic systems and for low dimensional systems. Most of the work on the noise analysis is in physics and electrical engineering. In the mechanical engineering area, only a limited amount of work has been done calculating the Lyapunov Exponents for a potentially stable system or in calculating Lyapunov Exponents from time series with noise.

The objective of this thesis is to explore the possible applications of the concept of Lyapunov Exponents for stability analysis in a potentially stable system, i.e., the possibility of calculating negative Lyapunov Exponents from a time series using Wolf's method (1985).

Two robotic systems are selected for stability analysis. One is a two-link pendulum system and the other is a pneumatic actuator system. Firstly, the time series is generated from the mathematical model of both robotic systems, i.e., the time series is noise-free. Both methods calculating the Lyapunov Exponents from the mathematic model and a time series, specifically Wolf's method (Wolf, 1984) are applied to the two systems. The Lyapunov Exponents calculated from both methods will be compared. Secondly, White Gaussian Noise

will be imposed to the time series generated from the mathematical models. The Lyapunov Exponents will then be calculated from the data with noise. The sensitivity of the method to the noise is very important for its applicability.

1.5 Thesis Organization

The remainder of this thesis is organized as following. Chapter 2 introduces the theoretical fundamentals of this research. The concept of Lyapunov Exponents will be introduced first. Then, the methods for calculating the exponents are presented. Chapter 3 contains the application of the Lyapunov Exponents' theory to the two-link pendulum system. The chaotic motion, stability to a set point and trajectory tracking will be generated. The exponents will be calculated for both the mathematical model and the time series. Such exponents will be compared. The noise is inputted to the time series data to study the sensitivity of the method to the noise. In Chapter 4, Wolf's method will be applied to the high dimensional system-a pneumatic actuator. The limitation of the method will be identified and reasons will be given to explain it. Conclusions and recommended future work is outlined in Chapter 5.

Chapter 2

Theoretical Preliminaries

In this chapter, the theoretical background needed for this research is presented. The concept of Lyapunov Exponents will be introduced first. Then, two methods for calculating the exponents will be discussed. One method calculates Lyapunov Exponents from the mathematical model. The other method calculates the exponents from time series data. Since the reconstruction of the attractor is the important part for the second method, the embedding method for reconstruction is also presented in this chapter. When the time series is collected from experiments, it is inevitable to include noise to the original signals. The basic knowledge of noise and its effects on the accuracy of the calculating Lyapunov Exponents are introduced in the last section in this chapter.

2.1 The concept of Lyapunov Exponents

The concept of Lyapunov Exponents plays an important role in the modern theory of nonlinear dynamics. They characterize the exponential rates of changes in the response of

dynamical systems. The concept of Lyapunov Exponents was first developed in mathematics. The Oseledec ergodic theorem (1968) provides the theoretical background for the computation of Lyapunov Exponents of a nonlinear dynamical system. The theorem states conditions for the existence of the defining limits and describes the properties of the Lyapunov Exponents. Since 1968, a considerable amount of research has been carried out in the studies of chaotic systems using the concept of Lyapunov Exponents. However, little work has been done on studying potentially stable systems using the concept of Lyapunov Exponents. The only works on applying the concept of Lyapunov Exponents to stability analysis of robotic systems are from Grune (1998), Ravishankar and Ghosal (1999), Wu et al. (2001) and Pooya (2004), where Lyapunov Exponents were calculated using mathematical models.

Definition of Lyapunov Exponents: Consider a dynamic system of dimension N, defined by equations

$$\dot{x}(t) = f(x(t)), \quad x(0) = x_0, x \in R^n \tag{2.1}$$

where $x(t)$ is a state vector and function f is generally a nonlinear, continuous differentiable function. The movements of the state vector $x(t)$ in the state space, results in a system's trajectories. After the transient stage, the trajectories generated by different initial conditions x_0 settle near an attractor. The time evolution of a small perturbation to a trajectory is governed by a linearized equation in the tangent space:

$$\delta\dot{x}(t) = Df(x(t))\delta x(t) \qquad \delta x(0) = \delta x_0 \tag{2.2}$$

where δx is a small perturbation to a trajectory, δx_0 denotes the initial perturbation, Df is the Jacobi matrix of the function f. Oseledec (1968) introduced a measure of average contraction of the perturbation to a given trajectory as:

$$\lambda_i = \lim_{t\to\infty} \frac{1}{t} \log_2 \left(\frac{\|\delta x_i(t)\|}{\|\delta x_i(t_0)\|} \right) \qquad (i = 1, 2, ..., n) \tag{2.3}$$

known as the Lyapunov Exponents. In equation (2.3), $\|\delta x_i(t)\|$ and $\|\delta x_i(t_0)\|$ denote the length of the i^{th} principal axis of the infinitesimal n-dimensional hyper-ellipsoid at final and initial times, t and t_0. A common approach in visualizing state space motion is to imagine how a small length, area, volume or higher-dimensional element might evolve in time. For example, the long term evolution of an infinitesimal $n-$ sphere of initial condition is monitored as the Lyapunov Exponents; the sphere will become an $n-$ ellipsoid due to the locally deforming nature of the trajectory in a $n-$ dimensional state space. The i^{th} Lyapunov exponent is then defined in terms of the length of the i^{th} principal axis. The existence of the $\lim_{t\to\infty}$ can be proved using the Oseledecs' multiplicative ergodic theorem (Oseledec, 1968).

The Lyapunov Exponents of a system are a set of invariant geometric measures, which describe in an intuitive way, the dynamic content of the system. In particular, they serve as a measure of ease in predicting the system performance. The system is referred to here, as a set of trajectories in the state space. Lyapunov Exponents quantify the average rate of convergence or divergence of nearby trajectories in a global sense. A positive exponent implies divergence of orbits, a negative one shows convergence of orbits, and a zero

exponent indicates the temporally continuous nature of a flow (i.e. the trajectory shows periodic motion). Consequently, a system with positive exponents has positive entropy, in that trajectories that are initially close together move apart over time. The more positive the exponent, the faster they move apart.

For the Lyapunov Exponents, the signs of the spectrum are usually used to analyze the stability of the system. Any continuous dynamic system without a fixed point will have at least one zero exponent. A stable steady state associated with an attracting periodic orbit has one zero and all other negative Lyapunov Exponents. Similarly, a stable quasiperiodic (superposition of periodic) attractor with K frequencies has K zero Lyapunov Exponents and the others are negative (Eckmann and Ruelle, 1985). If all of the Lyapunov Exponents of a system are negative, this indicates that the system has an attractive fix point. The sum of the Lyapunov Exponents is the time-averaged divergence of the state space velocity. Hence any dissipative dynamic system will have at least one negative exponent, the sum of all of the Exponents is negative, and the post-transient motion of trajectories will occur on a zero volume limit set (an attractor). From the equation (2.3) the Lyapunov exponent λ_i generally indicates in the i^{th} dimension:

$\lambda_i < 0$: The orbit attracts to a stable fixed point. Negative Lyapunov Exponents are characteristic of dissipative or non-conservative systems (the damped harmonic oscillator for instance). Such systems exhibit exponential stability. The more negative the exponent, the faster the systems move to the steady state. Super-stable fixed points have a Lyapunov

exponent of $\lambda_i \to -\infty$. This is akin to a critically damped oscillator in that the system heads towards its equilibrium point as quickly as possible. Nearby points on the trajectory will converge closer and closer as shown in Fig. 2.1.a.

$\lambda_i = 0$: A Lyapunov exponent of zero indicates that the system is in some sort of steady state mode. A physical system with this exponent is conservative. Such systems exhibit stability in the Lyapunov sense. Nearby points on the trajectory will stay at the same separation all of the time, as shown in Fig. 2.1.b.

$\lambda_i > 0$ The orbit is unstable and chaotic. Nearby points on the trajectory no matter how close will diverge to arbitrary separation, as shown in Fig. 2.1.c.

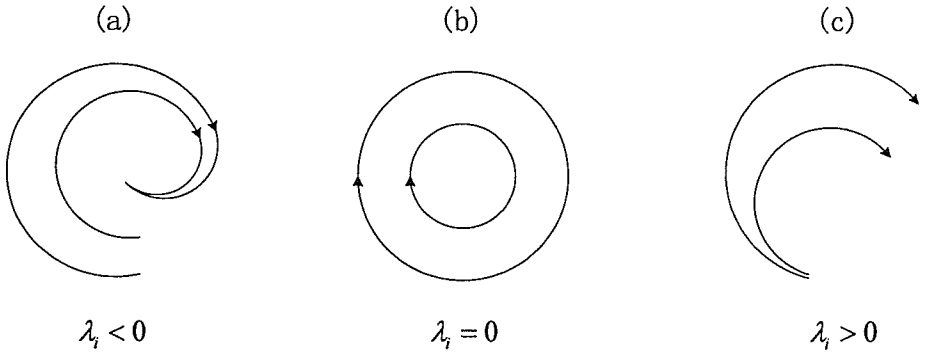

Fig. 2.1 Different orbits projected on the i^{th} dimension with different Lyapunov Exponents

For the special one-dimensional to a three or more dimensional system, the Lyapunov exponents can appear as follows:

For a one-dimensional state space, there are three types of equilibrium points:

a) $\lambda < 0$, Nodes(sinks): equilibrium points that attract nearby trajectories

b) $\lambda = 0$, Repellors(sources): equilibrium points that repel nearby trajectories

c) $\lambda > 0$, Saddle points: equilibrium points that attract trajectories on one side but repel

them on the other.

For a two-dimensional state space:

a) λ_1 and λ_2 both nonvanishing (non-zero exponent): the system will have a hyperbolic equilibrium point. Depending on the signs of λ_1 and λ_2, the equilibrium point can be attracting or stable ($\lambda_1 < 0$ and $\lambda_2 < 0$), repelling or unstable ($\lambda_1 > 0$ and $\lambda_2 > 0$), or saddle type ($\lambda_1 > 0$ and $\lambda_2 < 0$).

b) $\lambda_1 = 0$, $\lambda_2 < 0$: the system will have an attracting periodical orbit.

c) $\lambda_1 > 0$, $\lambda_2 = 0$: the system will have no equilibrium points or a repelling period orbit.

For three or higher dimensional systems, the positive Lyapunov Exponents introduce a new concept of chaos. Chaos is an aperiodic long-time behavior arising in a deterministic dynamic system that exhibits a sensitive dependence on initial conditions. Any systems containing at least one positive Lyapunov exponent is defined to be chaotic, with the magnitude of the exponent reflecting the time scale on which system dynamics become unpredictable (Wolf et. al., 1985). Chaos is sensitive to the initial conditions and the trajectories are not converging to any steady state. The signs of Lyapunov Exponents provide a qualitative picture of a system's dynamics. For a general continuous four dimensional system, the positive Lyapunov can only show up in three possible types. The Lyapunov spectra are $(+,+,0,-)$, $(+,0,0,-)$ and $(+,0,-,-)$. For a given system a change in parameters will generally change the Lyapunov spectrum and may also change both the type of spectrum and type of attractor. For example for a two-link pendulum system, stable motion and chaotic

motion can be shown just from changing the parameters of the controller.

The magnitude of the Lyapunov Exponents measures the rate of the convergence or divergence of the attractor. The higher the magnitude, the faster the system converges or diverges.

2.2 Calculation of Lyapunov Exponents

Since it is extremely difficult to determine Lyapunov Exponents analytically, especially for robotic systems, most of the work on determining Lyapunov Exponents is based on numerical calculations. Generally, there are two methods to calculate Lyapunov Exponents. One method calculates Lyapunov Exponents from the mathematical model, the other method calculates from the time series.

2.2.1 Calculation of Lyapunov Exponents from the mathematical model

The methods for calculating Lyapunov Exponents were originally developed for smooth systems, where every term in the ordinary differential equations is continuous and differentiable. Non-smooth systems, defined in this work are the differential equations containing non-differentiable terms, which occur naturally and frequently in engineering applications. The calculation procedure outlined in Section 2.3.1.2 is generalized for the calculation of Lyapunov Exponents in systems with discontinuity (Muller, 1995; Kunze, 2000). The methods for calculating Lyapunov Exponents for both smooth and non-smooth systems are summarized here.

2.2.1.1 Calculation of Lyapunov Exponents from the mathematical model for smooth systems

The method for calculating Lyapunov Exponents from the mathematical model is based on the theorem developed by Oseledec (1968), who introduced the analytical way to calculate Lyapunov Exponents known as the multiplicative ergodic theorem. The process could be implemented by defining the principal axes with initial conditions whose separations are as small as computer limitations allow and evolving these with the nonlinear equations of motion. An efficient algorithm for the calculation of Lyapunov Exponents, which is based on Oseledec's theorem, was developed by Shimada et al. (1979), Bennetin et al. (1980), and Wolf et al. (1985). Since Wolf's method is the most widely used, in this thesis, Wolf's method will be used to calculate the Lyapunov Exponents.

In order to calculate Lyapunov Exponents, a fiducial trajectory (i.e., the centre of a sphere) is defined by the action of the nonlinear equations of motion with some initial conditions. Trajectories of points on the surface of the sphere are defined by the action of the linearized equations of motion on points infinitesimally separated from the fiducial trajectory. The fiducial trajectory is created by integrating the nonlinear equations of motion for some post-transient initial condition. Simultaneously, for a $N-$dimensional system, the linearized equations of motion are integrated for N different initial vectors defining an arbitrarily oriented frame of N orthonormal vectors anchored to the fiducial trajectory (Wolf et al., 1985). This leads to the following set of combined nonlinear system and the linearized equations:

$$\begin{Bmatrix} \dot{x} \\ \dot{\psi} \end{Bmatrix} = \begin{Bmatrix} f(x) \\ F(t)\psi \end{Bmatrix} \tag{2.4}$$

where ψ is called the state transition matrix of the linearized system $\delta x = \psi \delta x_0$ and the variational equation $\dot{\psi} = F(t)\psi$ is a matrix-valued time-varying linear differential equation derived by linearization of the nonlinear vector field along the trajectory $x(t)$. The Jacobian $F(t)$ is defined as

$$F(t) = \left. \frac{\partial f}{\partial x^T} \right|_{x=x(t)} \tag{2.5}$$

And the initial conditions for numerical integrations are $\begin{Bmatrix} x(t_0) \\ \psi(t_0) \end{Bmatrix} = \begin{Bmatrix} x_0 \\ I \end{Bmatrix}$ where I, is the identity matrix. Lyapunov Exponents are calculated by following the evolution of the area of the hyper-ellipsoid spanned by $\delta x_1, \delta x_2 ..., \delta x_n$ via separately following the evolutions of $\delta x_1, \delta x_2 ..., \delta x_n$ using any integration method. The problem is that $\delta x_1, \delta x_2 ..., \delta x_n$ may tend to line up as $t \to \infty$. This alignment makes the calculations unreliable (Parker and Chua, 1989). To resolve this problem, $\delta x_1, \delta x_2 ..., \delta x_n$ are reorthonormalized at each integration step. This is done by including the Gram-Schmidt reorthonormalization (GSR) scheme in the calculation procedure. This procedure starts with an orthogonal collection of unit vectors $v_1, ..., v_n$, where the GSR generates an orthonormal set $u_1, ..., u_n$ as:

$$\begin{aligned} u_1 &= \frac{v_1}{\|v_1\|} \\ u_2 &= \frac{v_2 - < v_2, u_1 > u_1}{\|v_2 - < v_2, u_1 > u_1\|} \\ &... \\ u_n &= \frac{v_n - < v_n, u_{n-1} > u_{n-1} - ... - < v_n, u_1 > u_1}{\|v_n - < v_n, u_{n-1} > u_{n-1} - ... - < v_n, u_1 > u_1\|} \end{aligned} \tag{2.6}$$

where v_i^k is equal to δx_i^k, vector u_i^k is a normalized version of v_i^k, and <,> signifies the inner product. The frequency of reorthonormalization is not critical, as long as neither the magnitude nor the orientation divergences have exceeded computer limitations.

Fig. 2.2 shows the geometrical interpretation of the reorthonormalization for two vectors, δx_1^k and δx_2^k ($k=1,2,...,K$, K is the number of total integration steps), i.e., their orthogonalization into v_1^k and v_2^k, normalization into u_1^k and u_2^k. The vector v_1^k is equal to δx_1^k, and vector u_1^k is a normalized version of v_1^k. The factor $<\delta x_2^k, u_1^k>$ is the length of the orthogonal projection of δx_2^k onto u_1^k. Normalization of v_2^k yields the orthonormal vector u_2^k and the area of the hyper-ellipsoid spanned by $\{\delta x_1^k, \delta x_2^k\}$ is

$$\{\delta x_1^k, \delta x_2^k\} = \left\| v_1^k \right\| \bullet \left\| v_2^k \right\| \tag{2.7}$$

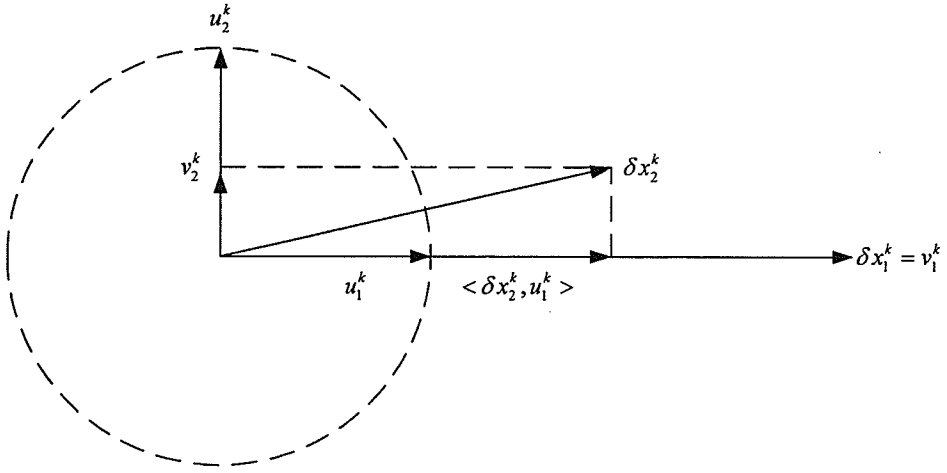

Fig. 2.2 Ortho-normalization of two vectors δx_1^k and δx_2^k

Then the Lyapunov Exponents can be calculated as:

$$\lambda_i \approx \frac{1}{Kh} \sum_{k=1}^{K} \log_2 \left\| v_i^k \right\|$$

where K is the number of total calculation steps, h is the time step.

Example of calculating Lyapunov Exponents from a mathematical model

The Lorenz attractor is a chaotic map noted for its butterfly shape, shown in Fig. 2.3.

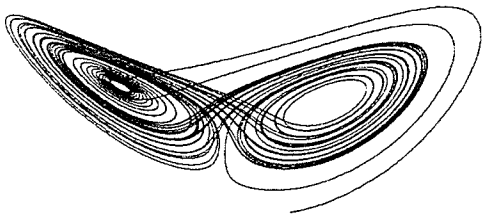

Fig. 2.3 Lorenz attractor (Lorenz, 1963)

The map shows how the states of a dynamical system (the three variables of a three-dimensional system) evolves over time in a complex, non-repeating beautiful pattern. The attractor, and the equations from which it was derived, were introduced by Edward Lorenz in 1963 (Lorenz, 1963). He based his work on the simplified equations of convection rolls arising in the equations of the atmosphere. The dynamic equations are shown below:

$$\begin{cases} \dot{x}_1 = a(x_1 + x_2) \\ \dot{x}_2 = x_1(c - x_3) - x_2 \\ \dot{x}_3 = x_1 x_2 - b x_3 \end{cases} \tag{2.8}$$

Where a, b, c are the constants. x_1, x_2 and x_3 are the coordinates of vector x.

Then, from equation (2.6), the linear variation equation is

$$\begin{bmatrix} \dot{\psi}_{11} & \dot{\psi}_{12} & \dot{\psi}_{13} \\ \dot{\psi}_{21} & \dot{\psi}_{22} & \dot{\psi}_{23} \\ \dot{\psi}_{31} & \dot{\psi}_{32} & \dot{\psi}_{33} \end{bmatrix} = \begin{bmatrix} a & a & 0 \\ c - x_3 & -1 & -x_1 \\ x_2 & x_1 & -b \end{bmatrix} \begin{bmatrix} \psi_{11} & \psi_{12} & \psi_{13} \\ \psi_{21} & \psi_{22} & \psi_{23} \\ \psi_{31} & \psi_{32} & \psi_{33} \end{bmatrix} \tag{2.9}$$

Let δx_1, δx_2 *and* δx_3 be three linearly independent vectors anchored to the fiducial trajectory of the above three dimensional system at $x = (x_1, x_2, x_3)$. The initial perturbation vectors are $\delta\tilde{x}_1^0, \delta\tilde{x}_2^0, \delta\tilde{x}_3^0$ and arbitrary states $x^0 = (x_1^0, x_2^0, x_3^0)$ belong to the basin of attraction of the attractor under study.

Define $\delta u_1^0 := \frac{\delta \tilde{x}_1^0}{\left\| \delta \tilde{x}_1^0 \right\|}$. Similarly define $\delta u_2^0 := \frac{\delta \tilde{x}_2^0}{\left\| \delta \tilde{x}_2^0 \right\|}$ and $\delta u_3^0 := \frac{\delta \tilde{x}_3^0}{\left\| \delta \tilde{x}_3^0 \right\|}$. Also, define $\delta \tilde{x}_i^k := \gamma(x_i^{k-1})$ for $k = 1,...,K$, $i = 1,2,3$ where γ is the solution of original nonlinear equation $\dot{x} = f(x)$ at the $k-1$ loop. Calculation of the Lyapunov exponent $\lambda_i (i = 1...3)$ evolves step by step integration of the variational equation from $u_i^0 (i = 1...3)$ with the time-step of h seconds.

At the first step:

$$\begin{cases} \delta \tilde{x}_1^1 := \delta \tilde{x}(h; u_1^0, x^0) := \psi(x^0) u_1^0 \\ \delta \tilde{x}_2^1 = \delta \tilde{x}(h; u_2^0, x^0) := \psi(x^0) u_2^0 \\ \delta \tilde{x}_3^1 = \delta \tilde{x}(h; u_3^0, x^0) := \psi(x^0) u_3^0 \end{cases} \tag{2.10}$$

To find all three Lyapunov Exponents, the set of three linearly independent perturbation vectors δx_i is repeatedly integrated and orthonormalized.

At the k^{th} step, the perturbation equations are

$$\begin{cases} \delta \tilde{x}_1^k := \delta \tilde{x}(h; u_1^{k-1}, x^{k-1}) := \psi(x^{k-1}) u_1^{k-1} \\ \delta \tilde{x}_2^k = \delta \tilde{x}(h; u_2^{k-1}, x^{k-1}) := \psi(x^{k-1}) u_3^{k-1} \\ \delta \tilde{x}_3^k = \delta \tilde{x}(h; u_3^{k-1}, x^{k-1}) := \psi(x^{k-1}) u_2^{k-1} \end{cases} \tag{2.11}$$

And the orthonormalization equations are

$$\begin{cases} v_1^k = \delta x_1^k \\ u_1^k := v_1^k / \left\| v_1^k \right\| \\ v_2^k = \delta \tilde{x}_2^k - < \delta \tilde{x}_2^k, u_1^k > u_1^k \\ u_2^k := v_2^k / \left\| v_2^k \right\| \\ v_3^k = \delta x_3^k - < \delta \tilde{x}_3^k, u_1^k > u_1^k - < \delta \tilde{x}_3^k, u_2^k > u_2^k \\ u_3^k := v_3^k / \left\| v_3^k \right\| \end{cases} \tag{2.12}$$

At the k^{th} step, the orthonormalization produces three vectors v_1, v_2, v_3 and for the K chosen large enough, the Lyapunov Exponents are:

$$\begin{cases} \lambda_1 \approx \dfrac{1}{Kh}\sum_{k=1}^{K}\log_2\left\|v_1^k\right\| \\ \lambda_2 \approx \dfrac{1}{Kh}\sum_{k=1}^{K}\log_2\left\|v_2^k\right\| \\ \lambda_3 \approx \dfrac{1}{Kh}\sum_{k=1}^{K}\log_2\left\|v_3^k\right\| \end{cases} \tag{2.13}$$

For example, if the parameters are $a=16$, $b=45.92$ and $c=4.0$ the Lyapunov Exponents of the Lorenz attractor are: $\lambda_1=2.16$, $\lambda_2=0.00$ and $\lambda_3=-32.4$.

2.2.1.2 Calculation of Lyapunov Exponents from the mathematical model for non-smooth systems

For the non-smooth system, the challenge comes from the fact that the derivative of the right-hand side of the state space model does not exist. Muller (1995) and Kunze (2000) extended the method of calculating the Lyapunov Exponents that behave smoothly in each interval between discontinuity instants t_i (i is the number of discontinuity instants). The system trajectory, starting from $t=t_{initial}$, is assumed to have reached to the discontinuity surface at $t=t_1$. The system equations can be expressed as:

Region 1: $\dot{x}=f_1(x), x(t_{initial})=x_0$ $(t_{initial}<t<t_1)$

Region 2: $\dot{x}=f_2(x), x(t_1)=x(t_1^+)$ $(t_1<t)$ (2.14)

Where t_1^+ denotes the time immediately after the discontinuity instant and t_1^- denotes the time immediately before the discontinuity instant. This yields the following linearized equations:

Region 1: $\delta\dot{x}=F_1(t)\delta x, \delta x(t_{initial})=\delta x_0$ $(t_{initial}<t<t_1)$

Region 2: $\delta\dot{x}=F_2(t), \delta x(t_1)=\delta x_1$ $(t_1<t)$ (2.15)

where $F_1(t)$ and $F_2(t)$ are Jacobians defined as:

$$F_1(t)=\frac{\partial f_1(x)}{\partial x^T}\Big|_{x=x(t)},\quad F_2(t)=\frac{\partial f_2(x)}{\partial x^T}\Big|_{x=x(t)} \tag{2.16}$$

At each instant of discontinuity, the linearized equations are evaluated using the indicator function, $h(x)$, and the transition function, $g(x)$. Both are defined based on the physical behaviour of the system. The indicator function is at least one time continuously differentiable and determines the instant of the discontinuity. The transition function describes the transition conditions at each instant of discontinuity. The linearized equations of motion at the instant of discontinuity ($t=t_1$) are derived as (Muller, 1995; Kunze, 2000)

$$\delta x^+ = G_1(x^-)\delta x^- - \left[G_1(x^-)f_1(x^-)-f_2(x^+)\right]\frac{H_1(x^-)\delta x^-}{H_1(x^-)f_1(x^-)} \tag{2.17}$$

where $x^+=x(t_1^+)$, $x^-=x(t_1^-)$, $\delta x^+=\delta x(t_1^+)$, and $\delta x^-=\delta x(t_1^-)$. $H_1(x^-)=\frac{\partial h_1(x)}{\partial x^T}\Big|_{x=x(t_1^-)}$ is the Jacobian of the indicator function, $h_1(x)$, and $G_1(x^-)=\frac{\partial g_1(x)}{\partial x^T}\Big|_{x=x(t_1^-)}$ is the Jacobian of the transition function, $g_1(x)$. If the system trajectory returns to the original region at the discontinuity instant ($t=t_2$), the transition condition of the linearized equations is:

$$\delta x^+ = G_2(x^-)\delta x^- - \left[G_2(x^-)f_2(x^-)-f_1(x^+)\right]\frac{H_2(x^-)\delta x^-}{H_2(x^-)f_2(x^-)} \tag{2.18}$$

where $x^+=x(t_2^+)$, $x^-=x(t_2^-)$, $\delta x^+=\delta x(t_2^+)$, and $\delta x^-=\delta x(t_2^-)$. The Jacobian matrices H_2 and G_2 are similarly derived using the indicator and transition functions $h_2(x)$ and $g_2(x)$, respectively. Equations (2.14)-(2.18) represent the generalized method for determining the variational equation, which can be used to calculate the Lyapunov Exponents of the system with discontinuity (Muller, 1995). The remaining procedure is the same as the one shown in Section 2.2.1.1.

Overall, the calculation of the Lyapunov Exponents from the system's mathematical model can be shown in the following Fig. 2.4:

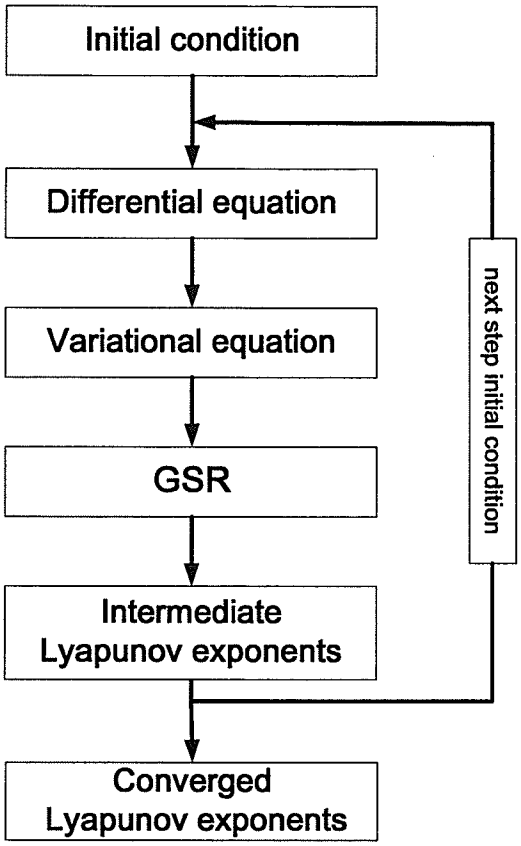

Fig. 2.4 Flow chart of Lyapunov Exponents' calculation from mathematical model

2.2.2 Calculation of Lyapunov Exponents from the time series data

The limitation of using mathematical models is that such models are not always available. Even if the models are available, due to their complexities and uncertainties, the calculations of Lyapunov Exponents can be infeasible. The most attractive advantage of using a time series is that the data for only one state is required, which can often be measured experimentally. Methods for calculating Lyapunov Exponents based on a time series have been developed. The first and one of most important step in calculating the Lyapunov

exponent from the time series, is the reconstruction of the system's attractor from a time series.

2.2.2.1 Reconstruction of the attractor

The foundation of the method calculating the largest Lyapunov exponent using a time series is the reconstruction of the attractor. The Embedding method is mapping a one-dimensional system (a time series) to an $m-$dimensional space. For the reconstruction according to the embedding theorem developed by Takens (1981), an $n-$dimensional dynamic system can be reconstructed in a phase space "equivalent" to the original phase space by embedding:

$$m \geq 2n+1 \tag{2.19}$$

Given a time series $x(t)$, an $m-$dimensional phase portrait is reconstructed with delay coordinates, i.e. a point on the attractor is given by $\{x(t), x(t+\tau), ..., x(t+(m-1)\tau)\}$ where τ is the chosen time delay. This method is termed Time Delay method for reconstruction of the phase space. The reconstructed phase space is equivalent to the original phase space. The equivalence means that the system's invariants characterizing the attractor are the same. However, it does not mean that the reconstructed phase space is exactly the same as original phase space. Using delayed copies of the original time series as components of reconstructed phase space to form an attractor, then:

$$X = \left\{ \left(x_0 \quad x_\tau \quad \cdots \quad x_{(m-1)\tau} \right), \left(x_1 \quad x_{(1+\tau)} \quad \cdots \quad x_{1+(m-1)\tau} \right), \ldots \right\} \tag{2.20}$$

where m is the embedding dimension, and τ is the time delay.

In the reconstruction, the dimension m and the time delay τ are two important

parameters that affect calculating the Lyapunov exponent. If m is too low the characteristics of the dynamic system can not be detected. For example, Fig. 2.5 shows that when a 3-dimensional Lorenz attractor is shown in 2-dimentional space, several points are overlapped, suggesting the wrong information for the original 3-dimensional attractor. However, if m is too large, among other problems, the noise in the data will tend to decrease the density of points defining the attractor, making it harder to find replacement points. It is advisable to check the stationarity of results with different embedding dimension m to ensure robust exponent estimates, *i.e.*, to calculate the largest Lyapunov exponent with different embedding dimensional reconstructed attractors.

2-dimensional space 3-dimensional space

Fig. 2.5 The reconstructed Lorenz attractors in different dimensional space

Time delay is also governed by the need to avoid catastrophes on reconstructing the attractor. If the time delay chosen is too small, the attractor stretches out along the $x = y = z = ...$ The successive points in the state space may be too close together to be sufficiently independent. Excessively low time delay, τ, leads to highly correlated vector elements which are concentrated around the diagonal in embedding space. Structure perpendicular to the diagonal is not captured adequately. If the time delay chosen is too large

the $m \times \tau$ will be much larger than the orbital period. The points may be so independent as to be essentially random. Thus, evolutionary information in the system is lost. A check of the stationarity of exponent estimates with different time delays is again recommended, i.e., calculate the largest Lyapunov exponent with different time delay.

In Fig. 2.6, the original and reconstructed Lorenz attractor based on the embedding theorem is shown. The reconstructed attractor with different time delay can be significantly different from the Lorenz attractor as an example. Therefore, careful selection of time delay in the reconstruction of the phase space is extremely important.

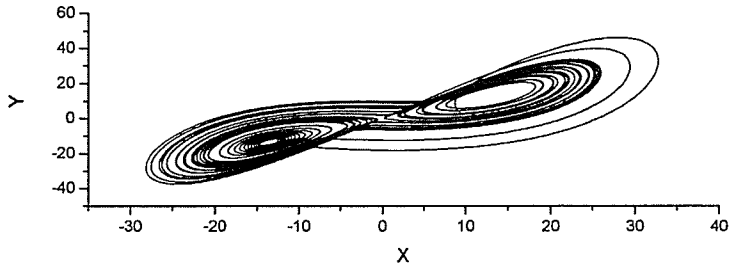

a. The original Lorenz attractor from the mathematical model

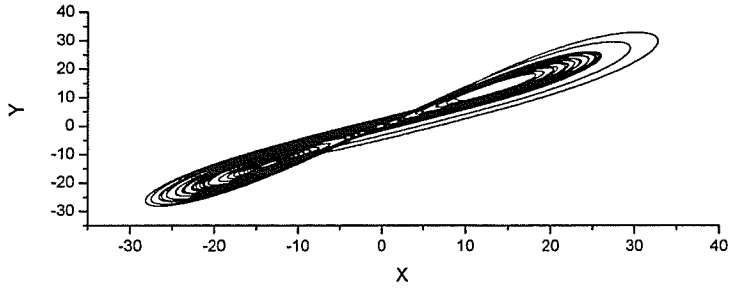

b. The reconstructed Lorenz attractor using delay embedding with τ =5, m =7

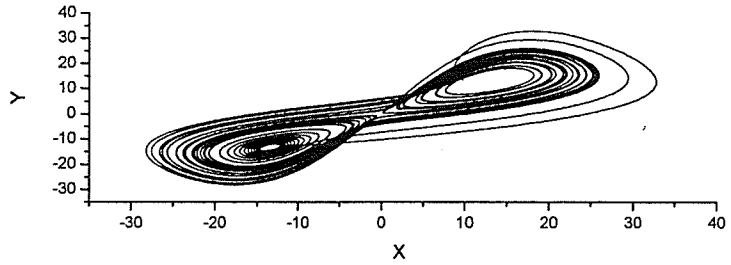

c. The reconstructed Lorenz attractor using delay embedding with τ =15, m =7

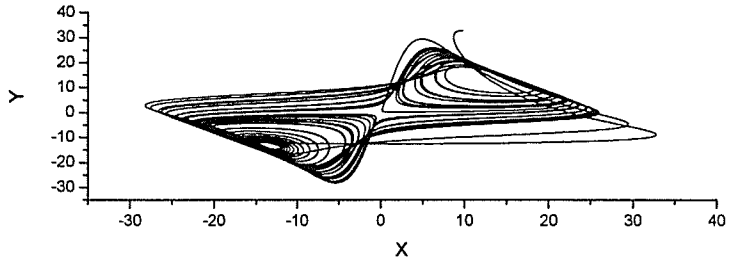

d. The reconstructed Lorenz attractor using delay embedding with τ =25, m =7

Fig. 2.6 Lorenz attractor in the original and reconstructed phase space

The advantages of using the time delay method for reconstruction of the phase space is the relative ease in computing and the fact that the attractor structure is left undistorted since no extra processing is imposed on it. The time-delay method has disadvantages including a less than obvious choice of delay parameter value; and poor reconstructed phase space (RPS) in the presence of noise.

2.2.2.2 Calculation of the Lyapunov exponent from time series data

Fig. 2.7 shows the details of the evolution method for the calculation of Lyapunov Exponents. In Fig. 2.7 a part of the reconstructed attractor is shown. At initial time t_0, the

lengths between the any points after 10^{th} point to the initial point P_{t0} are calculated as suggested by Wolf (Wolf et. al., 1985). The shortest length, $L(t_0)$, locates the nearest neighbor P_{t1}. At a later time t_1, the initial point P_{t0} evolves to $P_{t0}^{'}$. Then the nearest neighbor point, $P_{t1}^{'}$, is located again with the same method. The initial length, $L(t_0)$, evolves to length $L^{'}(t_0)$. The same procedures are repeated until all of the points on the reconstructed attractor are located. The length element is propagated through the attractor for a time short enough so that only a small scale attractor structure is likely to be examined.

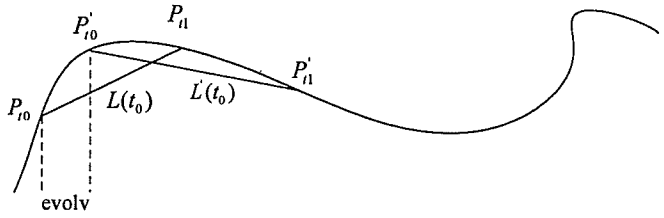

Fig. 2.7 Evolution and replacement procedure

Based on the reconstruction of one n dimensional trajectory, which is outlined in section 2.3.2.1 and Fig. 2.7, the largest Lyapunov exponent λ_1 is defined as:

$$\lambda_1 = \frac{1}{t_M - t_0} \sum_{k=1}^{M} \log_2 \frac{L_k^{'}(t)}{L_k(t)} \tag{2.21}$$

where M is the total number of replacement steps, t_M is the total time.

In the calculation of the largest Lyapunov exponent if the evolution time is too large, $L^{'}$ shrinks when the two trajectories pass through a folding region of the attractor. This would lead to an underestimation of the Lyapunov exponent. If the evolution time is too small, there are no changes of $L^{'}$ that can be detected. A new data point should satisfy the two criteria

reasonably well: L' from the evolved fiducial point is small and the angular separation between the evolved and replacement elements is small (Wolf et. al., 1985).

Based on the definition of the Lyapunov exponent, the calculation from the time series should be carried out for $t \to \infty$. However, it has been found that the estimation of Lyapunov Exponents can be done in finite-time (Alligood et al., 1997). A successful calculation requires that one time series has enough data to approach the appropriate length scales, ignores the effects of the noise on the length scale, and has an attractor with a macroscopic stretching/folding mechanism. Overall, the procedure of the calculation of the Lyapunov Exponents from a time series can be shown as follows:

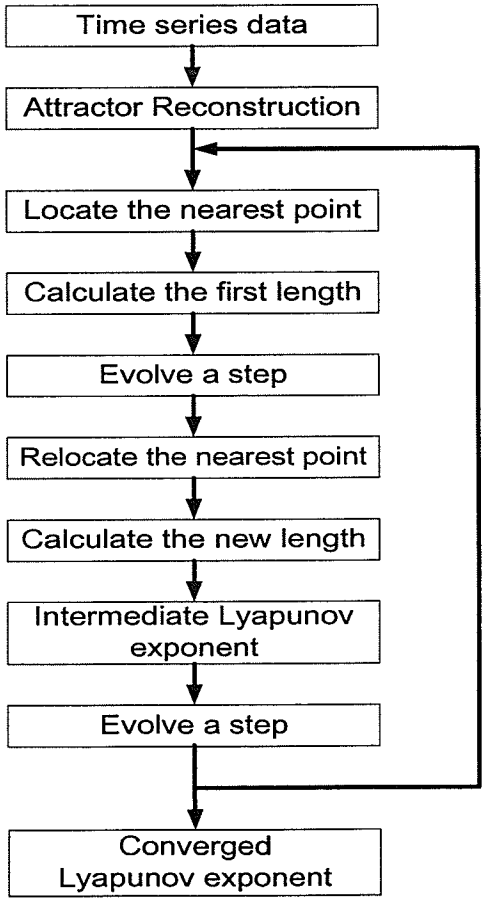

Fig. 2.8 The flow chart of Lyapunov exponent calculation from the time series

2.3 Basics of noise

As the time series is collected from experiments, noise is inevitably involved. When the attractor is reconstructed, the noise is also transformed. They will show the misleading characteristics of the characters for the system. With the advanced technology of filters, much noise can be filtered but they can not be eliminated.

2.3.1 Gaussian White noise (GWN)

Gaussian White noise (GWN) is the one of most common measurement noise in mechanical engineering. Gaussian White noise is a white noise process with a normal distribution and its power density is constant over a finite frequency range.

Fundamentals

As noise is random, it can only be predicted by statistical means, usually by a Gaussian probability density function with a bell-shaped curve as shown below:

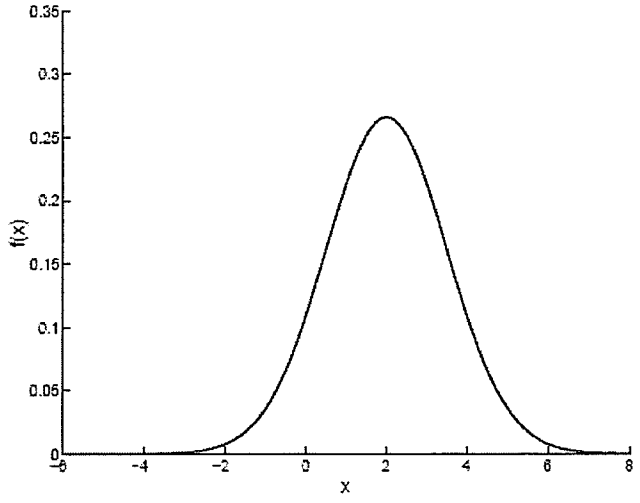

Fig. 2.9 Gaussian probability density function $f(x)$

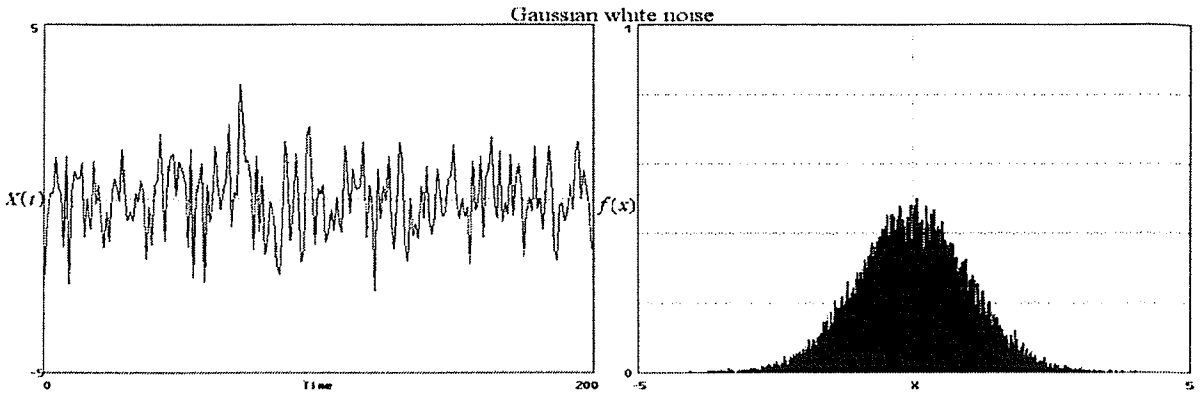

Fig. 2.10 A sample of Gaussian White noise

Fig. 2.10 shows an example of GWN. In Fig. 2.10.a the white noise process is shown for 200 seconds. Fig. 2.10.b $f(x)$ shows the probability density of the sample's value $X(t)$. As noise is random, its mean value is zero. Hence, we use mean square values which are measurements of the dissipated noise power. For the Guassian White noise, the average noise power is $V_{noise} = \frac{1}{n}\sqrt{\sum_{1}^{n} V_{noise\ n}^{2}}, n = 1,2,...N$, where V_{noise} is the average noise power and $V_{noise\ n}$ is the noise power at a time instant. The average of the system signal power is $V_{signal} = \frac{1}{n}\sqrt{\sum_{1}^{n} V_{signal\ n}^{2}}, n = 1,2,...N$, where V_{signal} is the system signal power at a time instant.

Since, in this work, GWN is added to the simulation data randomly, the amplitude of the noise is the main problem which affects the Lyapunov exponent's calculation. The signal to noise ratio (SNR) is defined as the ratio of a signal power to the noise power which is shown as the formula $dB = 10\log_{10}\left(\frac{V_{signal}}{V_{noise}}\right)$. From the definition of SNR, it is easy to find that the

noise can not be zero. In this thesis, the noise-to-signal ratio, $NSR = \frac{V_{signal}}{V_{noise}}\%$, is used to analyze how the noise affects the system in order to see the noise change from 0 to some value.

2.3.2 Noise filters

The theory of filtering stationary time series for a variety of purposes was developed by Norbert Wiener in the 1940's for continuous time processes, which was a notable feat of mathematics. In an important paper, Levinson (1947) showed that in discrete time, the entire theory can be reduced to least squares which were mathematically very simple. Kalman (1960) set out to extend Wiener filters to non-stationary processes. The immediate need was of a military nature, to forecast the trajectories of ballistic missiles, which in their launch and re-entry phases would have a very different character than a stationary process could describe. The formalism is less complicated than the one from Wiener theory (Wunsch, 1966).

In this research, the noise will be changed from 0 to 10% of the signal value ($\frac{V_{noise}}{V_{signal}}\%$) to observe its effects on the calculated Lyapunov exponent. In the simulations, the C++ code is used to generate the Gaussian White noise, which is added to the simulation data when the program imports data from a file.

2.3.3 Noise reduction in Wolf's method

In Wolf's method there is an approach to reduce the effects of noise. This is done by avoiding principal axis vectors whose magnitude is lower than the selected threshold value, i.e., the minimum cutoff length of evolution length. If this value is chosen to be somewhat

larger than the noise level, the fractional error in determining initial vector magnitudes may be reduced to an acceptable level. Avoiding noise effects is not a trivial matter, as noise may not be of constant amplitude throughout an attractor and the noise length scale may be difficult to determine. Again, this approach can only work if scales larger than the noise contain accurate information about orbital divergence rates in the zero length scale limit.

2.4 Summary

In this chapter, the concept of Lyapunov Exponents, the calculation of Lyapunov Exponents based on mathematic models and a time series, and basic information about Gaussian White noise have been reviewed. Specifically, Wolf's method for calculating Lyapunov Exponents using a time series has been discussed in details. Issues of selecting the key parameters (time delay, evolve time and embedding dimensions) have also been raised. Wolf's method will be used in this work.

Chapter 3

Exploration of Lyapunov Exponents on a two-link pendulum system

Mechanical oscillators constitute a family of important systems widely used as models to explain a diversity of phenomena, or to design engineering systems accomplishing a variety of tasks. Among many mechanical oscillator systems, those which are built with pendulums are of special interests since the dynamic systems have a wide variety of limit sets, from equilibrium points to strange sets. Pendulum systems are of specific interests in robotics as many robotic systems can be modeled as a chain of pendulums.

A two-link pendulum system is a pendulum with a second pendulum attached to its end, exhibiting rich dynamic behaviors. For the two-link pendulum in the vertical plane, the upper pendulum acts as a simple pendulum with a moving base and is under the effects of the gravity, joint force and controlled join torque. The lower pendulum behaves like a pendulum under the effects of gravity. The force and torque come from the upper pendulum and the

force and the control torque are applied at the basic joint. Depending on the control torques and the system parameters, such double pendulum system can exhibit either stable or chaotic motion. The stability analysis of the system is an important and challenging problem.

The concept of Lyapunov Exponents can characterize the system stability. Since it is extremely challenging to determine Lyapunov Exponents analytically, complex engineering systems are often calculated numerically. There are two approaches. One, is to calculate Lyapunov Exponents using the mathematical models of the dynamic systems and the other, is to calculate Lyapunov Exponents using a time series. In the previous work the concept of Lyapunov Exponents has mainly been used to diagnose a chaotic system. Wolf's method (1985) for calculating Lyapunov Exponents based on a time series has been considered valid for chaotic systems, i.e. for calculating positive Lyapunov Exponents. It is has been documented that such a method has been considered unreliable for calculating Lyapunov Exponents for potentially stable systems, i.e., for calculating negative or zero Lyapunov Exponents.

In this chapter, the possibility of calculating negative and zero Lyapunov Exponents for a two-link pendulum system based on a time series using Wolf's method is explored. The time series is generated from the mathematical model of a two-link pendulum system. The two-link pendulum system is used here mainly because the motion of a two-link pendulum is governed by a set of coupled ordinary differential equations, making it relatively easy to apply the concept of Lyapunov Exponents. On the other hand, the two-link pendulum system

exhibits rich dynamic behaviors having a wide variety of limit sets, from equilibrium points to strange sets.

In this work, Lyapunov Exponents are first calculated from the mathematical models. The time series is generated from the same model and the largest Lyapunov exponent is calculated from the time series data. The results are compared to demonstrate the applicability of Wolf's method, calculating the largest Lyapunov exponent from time series to potentially stable systems. In Wolf's method, several parameters such as time delay and evolution time have significant effects on the numerical Lyapunov Exponents. This has not been investigated before. The effects of such parameters on the calculated Lyapunov Exponents will also be studied.

In this work, the two-pendulum system is simplified to move on the horizontal plane. The proportional and derivative (PD) controller will be applied on the system to produce various motions. Under some special control gains, the two-link pendulum system is chaotic and positive Lyapunov Exponents are obtained. For the chaotic motion, Lyapunov Exponents will be calculated from the mathematical model and the largest Lyapunov exponent will be calculated from the time series. The results will be compared to confirm the validity of the algorithms and the program will be developed during this work. The gains in the controller will then be adjusted to keep the system stable.

Two types of stable motion will be generated. One involves the two-link pendulum moving to the desired position and remaining there. The stability of the pendulums will be

studied by using the concept of Lyapunov exponent as the negative Lyapunov Exponents are expected. Usually the more negative the Lyapunov Exponents are, the faster the pendulums reach the desired position. The second stable motion, involves the system being controlled to follow a desired sinusoid function trajectory, with a zero Lyapunov Exponent expected.

As discussed in Chapter 2, one advantage of calculating Lyapunov Exponents using a time series is that the time series can be collected from experiments without knowing the mathematical model of the system. The experimentally collected data contain noise, which is believed to have significant effects on the calculated Lyapunov Exponents (Wolf et. al., 1985, Zeng, et al., 1992). Such effects should be studied. In this work, Gaussian White Noise will be added to the time series generated from the simulation. The Lyapunov Exponent will then be calculated to check the robustness of the method with respect to the noise. In the simulations, the power of the Gaussian White noise will change from 0 to 10% of the power of the signal.

3.1 Dynamic model of a two-link pendulum

As shown in Fig. 3.1, the pendulum system consists of two rigid links with length l_1 and l_2. The base of the system is fixed at O. m_1 and m_2 are the masses of the two links. r_1 and r_2 are the locations of the mass centers of the two links. θ_1 and θ_2 are the joint angles which are positive in the clockwise direction. T_1 and T_2 are the control torques applied at both joints which are positive in the counter clockwise direction. The equations of motion can be derived from the Lagrangian formulation as follows:

$$M(\theta)\ddot{\theta}+C(\theta,\dot{\theta})+f(\dot{\theta})+g(\theta)=T \tag{3.1}$$

where θ is a 2×1 vector of joint angles, and M is the inertia matrix. C is a vector of the torque related to the centrifugal and Coriolis forces. $f(\dot{\theta})$ is the vector of the torque related to the viscous friction, and $g(\theta)$ is the vector of the torque related to the gravity. T is the control torque. The detailed deviation is presented in Appendix A.

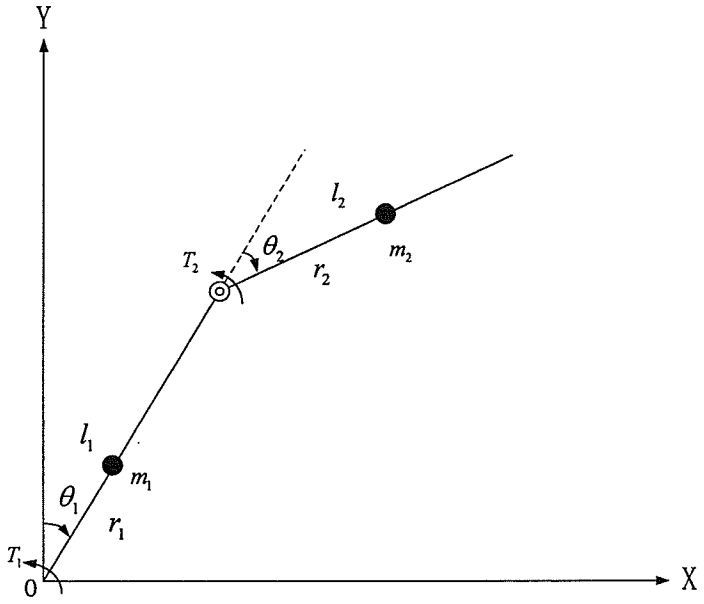

Fig. 3.1 Two-link pendulum

To apply the concept of Lyapunov Exponents to the two-link system, it is desirable to start from a simpler model. First, it is assumed that there is no viscous friction. Second, the system is assumed to move in the horizontal plane in order to remove the gravity effect. Then mathematical model of the system becomes:

$$M(\theta)\ddot{\theta}+C(\theta,\dot{\theta})=T \tag{3.2.a}$$

$$\text{Where } M=\begin{bmatrix} d_{11} & d_{12} \\ d_{21} & d_{22} \end{bmatrix}=\begin{bmatrix} J_1+J_2+2p\cos\theta_2 & J_2+p\cos\theta_2 \\ J_2+p\cos\theta_2 & J_2 \end{bmatrix} \tag{3.2.b}$$

$$C=\begin{bmatrix} d_{111} \\ d_{112} \end{bmatrix}=\begin{bmatrix} -p(\theta_1\dot{\theta}_2+\dot{\theta}_2^2)\sin\theta_2 \\ p\dot{\theta}_1^2\sin\theta_2 \end{bmatrix} \tag{3.2.c}$$

$$J_1=I_1+m_1r_1^2+m_2l_1^2,\ J_2=I_2+m_2r_2^2,\ p=m_2l_1r_2 \tag{3.2.d}$$

The proportional and derivative (PD) controller will be used to control the two-link pendulum system having stable and chaotic motion, respectively. For the PD controller, the torque at each joint is:

$$T_i=k_{p_i}(\theta_{d_i}-\theta_i)+k_{v_i}(\dot{\theta}_{d_i}-\dot{\theta}_i) \qquad i=1,2 \tag{3.3}$$

where θ_{d_i} is the desired position or a periodic trajectory to be tracked at each joint, k_{p_i} and k_{v_i} are the positive proportional and derivative gains. By changing the control gains k_{p_i} and k_{v_i}, the system can exhibit either chaotic motion or stable motion. For the stable motion, two simulations are carried out. One is to keep the pendulum system at a set point, and the other is to track a desired motion. For the chaotic motion, the system is intended to track the desired trajectory. It is documented that chaotic motion happens when the control gain k_{v_i} is small in the simulations. Since the time series is used for calculating Lyapunov Exponents, the simulations of the above discussed motion are first carried out. The parameters of the two-link pendulum are as follows:

Table 3.1 Parameters of the two-link pendulum

link	Length(m)	Mass(kg)	CG(m)	Inertia (kgm^2)
1	0.5	20	0.2	6
2	0.4	8	0.3	1.5

3.2 Simulations of two-link pendulum system

Our research will start with changing the controller gains, thereby controlling the two-link pendulum to exhibit chaotic motion. For a dynamic system classified as chaotic, one of the important characteristics of such a system is the sensitivity to initial conditions. Sensitivity to initial conditions means that an arbitrarily small perturbation of the current trajectory may lead to significantly different future behavior. As a result of this sensitivity, the behavior of systems that exhibit chaos appears to be random, exhibiting exponential error dispersion, even though the system is deterministic in the sense that it is well defined and contains no random parameters. Every chaotic system has a strange attractor. An attractor is a set to which the system evolves after a long enough time. Attractors are parts of the state space of the dynamic system and are considered geometrical subsets of the state space: points, lines, surfaces, volumes. Chaotic motion gives rise to what are known as strange attractors, attractors that can have great details and complexity. Because the system is deterministic, chaotic behavior is not random even though its aperiodicity and unpredictability may make it appear to be so. On the other hand, because of the instability, aperiodicity and sensitivity to initial conditions; the behavior of chaotic systems is not predictable even though it is deterministic.

3.2.1 Simulations of chaotic motion

The simulated chaotic motion for the 2-link pendulum is shown in Fig. 3.2. The desired angular displacements of link 1 and 2 are shown in Fig. 3.2.a which are

$\theta_d^1 = 1.57\sin(2t)$ and $\theta_d^2 = \frac{1.57}{2}\sin(2t)$ The actual angular displacements of link 1 and 2 are shown in Fig. 3.2.b. The controller gains are selected as $K_{p_i} = 50(N/rad)$ and $K_{vi} = 1(N{\bullet}S/rad)$, where $i = 1,2$ and the initial condition is $\{0.0(rad), 0(rad/s), 0.0(rad), 0(rad/s)\}$. It is easily to see that the system does not follow the desired trajectories. Fig. 3.3 shows the strange attractor of the angular displacement of link 2 in a phase place.

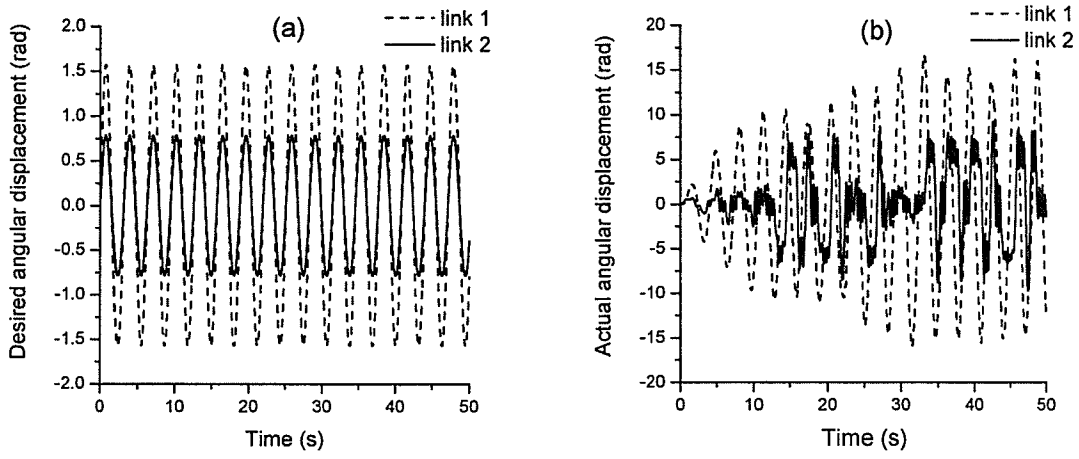

Fig. 3.2 (a) Desired angular displacement (b) Actual angular displacement

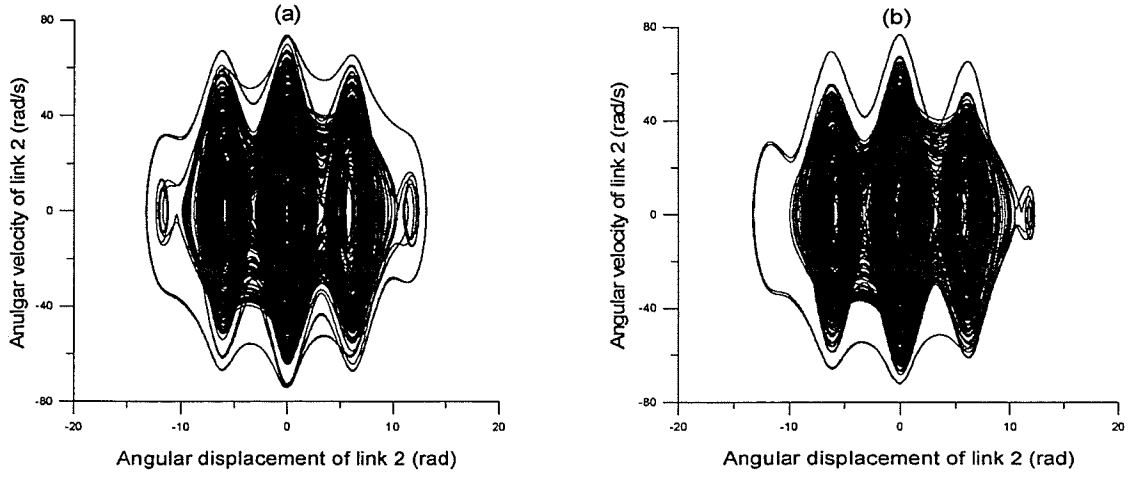

Fig 3.3 Attractor of chaotic motion of link 2
(a) initial angular displacement is 0 (rad) (b) initial angular displacement is 0.0001(rad)

In Fig. 3.3.b, the initial angular displacement was changed $10^{-4}(rad)$ from the one for Fig. 3.3.a with the same initial angular velocity ($0(rad/s)$). The result of the attractor is changed significantly, which demonstrates that the system is sensitive to the initial condition. In the context of the concept of Lyapunov Exponents, the system which has at least one positive Lyapunov Exponent is defined to be chaotic. The largest Lyapunov Exponent of the double pendulum system is indeed positive, which is studied in the following sections.

3.2.2 Simulations of stable tracking motion

By changing the gains in the PD controllers, the two-link pendulum system can exhibit the stable motion. In the case of stable tracking motion that the system follows, the desired trajectory, $\theta_d^1 = 1.57\sin(2t)$ and $\theta_d^2 = \frac{1.57}{2}\sin(2t)$, the gains were set as $K_{p1} = 30(N/rad)$, $K_{p2} = 50(N/rad)$ and $K_{v1} = K_{v2} = 80(N \bullet S/rad)$ in the simulations. The initial condition is $\{0.0(rad), 0(rad/s), 0.0(rad), 0(rad/s)\}$.

In Fig. 3.4 the angular displacements of link 1 and 2 are recorded. The vertical axis is the angle value and the horizontal axis is the time. The dash lines are the desired trajectories and the solid lines are the actual trajectories. Fig. 3.4 shows that the pendulum system can successfully follow the desired trajectory by using suitable controller gains. The state space model is the four dimensional system and its attractor can not be shown in the figure. But for link 2, Fig. 3.5 shows the attractor.

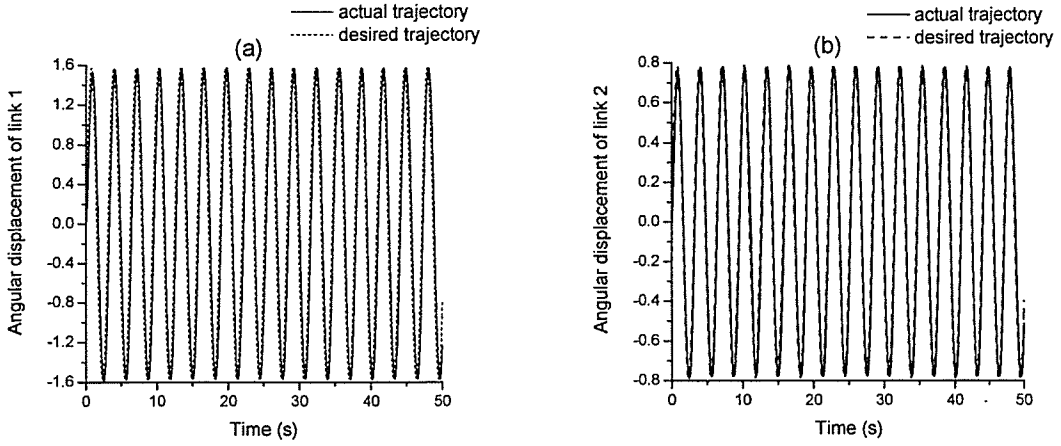

Fig. 3.4 Desired and actual angular displacements (a) link 1 and (b) link 2

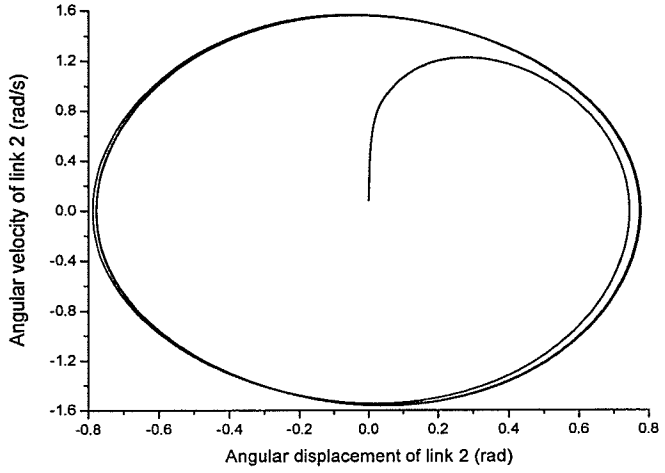

Fig. 3.5 Attractor of stable tracking motion

Note that the intersections are due to the reduced dimensions from four to two. By changing the initial condition, the system was found to always approach the attractor.

3.2.3 Simulations of stable motion with a set point

The second case for the simulation of stable motions is that the pendulum system is controlled to approach the set point. The gains in the PD controller are still set as $K_{p1} = K_{p2} = 20(N/rad)$ and $K_{v1} = K_{v2} = 5(N \bullet S/rad)$. The system will start from the

initial condition $\{1.0(rad), 0(rad/s), 1.0(rad), 0(rad/s)\}$, then controlled by the PD controller to approach the point $\{0.0(rad), 0.0(rad/s), 0.0(rad), 0.0(rad/s)\}$. The angular displacements of link 1 and link 2 are simulated and are shown in Fig. 3.6. The vertical axis is the angular displacement and the horizontal axis is the time.

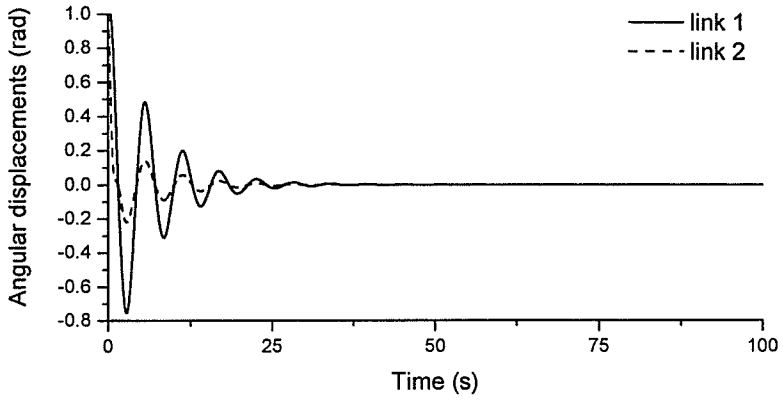

Fig. 3.6 Close-loop stable response with a set point

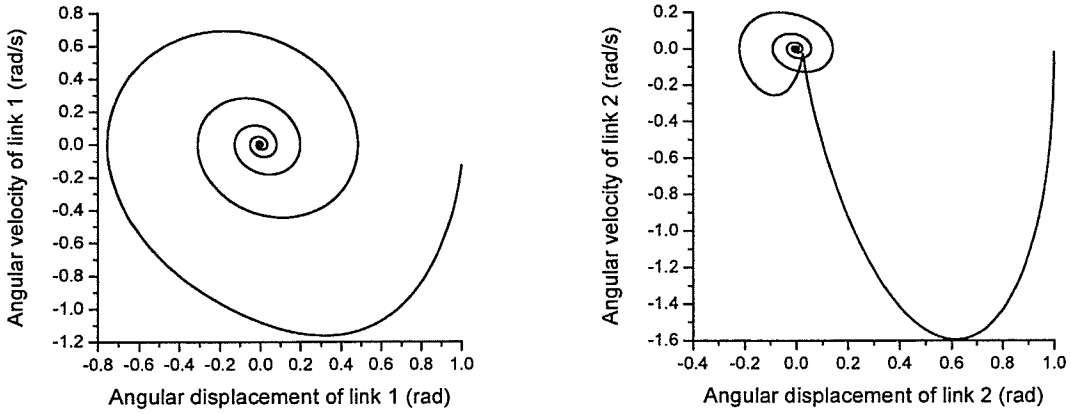

Fig. 3.7 State space response for the stable motion with a set point

The equilibrium point $\{0,0,0,0\}$ is shown in the phase space in Fig. 3.7. The vertical axis is the angular velocity and the horizontal axis is the angular displacement. In Fig. 3.7 the trajectory appears to intersect. This is because the system is 4-dimensional, shown as a 2-dimensional figure.

The angular displacement of each link is simulated in this section. The attractors of chaotic, stable motion are also shown. The results show that the two-link pendulum can exhibit different motion under different control parameters.

In the next section, the Lyapunov Exponents are calculated from the mathematical model and the largest Lyapunov Exponent is calculated from the time series based on Wolf's method. The object is to explore the possibility of using Wolf's method to calculate negative and zero Lyapunov Exponents.

3.3 Calculations of Lyapunov Exponents

3.3.1 Lyapunov Exponents from mathematical model

In this section the Lypuanov Exponents will be calculated from the mathematical model of the two-link pendulum system. The results are generated as the reference for Lyapunov Exponents which will be compared with those calculated from the time series. The simulation program is developed based on Wolf's method.

In the state space, let $x_1 = \theta_1, x_2 = \dot{\theta}_1, x_3 = \theta_2$ and $x_4 = \dot{\theta}_2$, equation (3.2) becomes:

$$\begin{aligned} \dot{x}_1 &= x_2 \\ \dot{x}_2 &= \frac{(\tau_1 - d_{111})d_{22} - (\tau_2 - d_{112})d_{12}}{d_{11}d_{22} - d_{12}d_{21}} \\ \dot{x}_3 &= x_4 \\ \dot{x}_4 &= \frac{(\tau_2 - d_{112})d_{11} - (\tau_1 - d_{111})d_{21}}{d_{11}d_{22} - d_{12}d_{21}} \end{aligned} \tag{3.4}$$

where

$J_1 = I_1 + m_1 r_1^2 + m_2 l_1^2$, $J_2 = I_2 + m_2 r_2^2$, $p = m_2 l_1 r_2$

$d_{11} = J_1 + J_2 + 2p\cos x_3$, $d_{12} = d_{21} = J_2 + p\cos x_3$, $d_{22} = J_2$,

$d_{111} = -p(2x_2x_4 + x_4^2)\sin x_3$, $d_{112} = px_2^2 \sin x_3$

Based on Wolf's method and the procedure outlined in Section 2.3.1, the variation equation is shown below

$$\dot{\psi}_t = F(t)\psi_t \tag{3.5.a}$$

The Jacobian matrix is shown as follows:

$$F(t) = \begin{bmatrix} 0 & 1 & 0 & 0 \\ a_{21} & a_{22} & a_{23} & a_{24} \\ 0 & 0 & 0 & 1 \\ a_{41} & a_{42} & a_{43} & a_{44} \end{bmatrix} \tag{3.5.b}$$

where

$$a_{21} = \frac{-k_{p1}d_{22}}{d_{11}d_{22} - d_{12}d_{21}} \tag{3.5.c}$$

$$a_{22} = \frac{(-k_{v1} + 2px_4 \sin x_3)d_{22} + 2pd_{12}x_2 \sin x_3}{d_{11}d_{22} - d_{12}d_{21}} \tag{3.5.d}$$

$$a_{23} = \frac{p(2x_2x_4 + x_4^2)\cos x_3 d_{22} + (k_{p2} + px_2 \cos x_3)d_{12} + p\sin x_3(T_1 - px_2^2 \sin x_3)}{d_{11}d_{22} - d_{12}d_{21}} - \frac{[(T_1 - d_{111})d_{22} - (T_2 - d_{112})d_{12}]p^2 \sin(2x_3)}{(d_{11}d_{22} - d_{12}d_{21})^2} \tag{3.5.e}$$

$$a_{24} = \frac{2p(x_2 + x_4)\sin x_3 d_{22} + k_{v2}d_{12}}{d_{11}d_{22} - d_{12}d_{21}} \tag{3.5.f}$$

$$a_{41} = \frac{k_{p1}d_{21}}{d_{11}d_{22} - d_{12}d_{21}} \tag{3.5.g}$$

$$a_{42} = \frac{2pd_{11}x_2 \sin x_3 + (k_{d1} + 2px_4 \sin x_3)d_{21}}{d_{11}d_{22} - d_{12}d_{21}} \tag{3.5.h}$$

$$a_{44} = \frac{-k_{v2}d_{11} - 2p(x_2 + x_4)\sin x_3 d_{21}}{d_{11}d_{22} - d_{12}d_{21}} \tag{3.5.i}$$

$$a_{43} = \frac{(-k_{p2} - px_2^2\cos x_3)d_{11} - 2(T_2 - d_{112})p\sin x_3 - pd_{21}(2x_2x_4 + x_4^2)\cos x_3 + p(T_1 - d_{111})\sin x_3}{d_{11}d_{22} - d_{12}d_{21}} - \frac{p\sin x_3\left[(T_2 - d_{112})d_{11} - (T_1 - d_{111})d_{21}\right]}{(d_{11}d_{22} - d_{12}d_{21})^2} \tag{3.5.j}$$

All the above variables are shown in equation (3.4). Equation (3.5.a) is to be integrated simultaneously with the original nonlinear equation shown in equation (3.4). Based on the procedure outlined in Section 2.3.1, the Lyapunov Exponents for the two-link pendulum are defined as:

$$\lambda_i \approx \frac{1}{Kh}\sum_{k=1}^{K}\log_2\left\|u_i^k\right\| \qquad \text{where } i = 1,2,3,4 \tag{3.6}$$

$$\begin{aligned} u_1 &= \frac{v_1}{\|v_1\|} \\ u_2 &= \frac{v_2 - < v_2, u_1 > u_1}{\|v_2 - < v_2, u_1 > u_1\|} \\ u_3 &= \frac{v_3 - < v_3, u_2 > u_2 - < v_3, u_1 > u_1}{\|v_3 - < v_3, u_2 > u_2 - < v_3, u_1 > u_1\|} \\ u_4 &= \frac{v_4 - < v_4, u_3 > u_3 - < v_4, u_2 > u_2 - < v_4, u_1 > u_1}{\|v_4 - < v_4, u_3 > u_3 - < v_4, u_2 > u_2 - < v_4, u_1 > u_1\|} \end{aligned} \tag{3.7}$$

The vector v_i^k is equal to δx_i^k, and vector u_i^k is a normalized version of v_i^k.

For calculating the Lyapunov Exponents an important issue has to be discussed, specifically, the careful truncations of the adequate time period over which Lyapunov Exponents are calculated. Theoretically, Lyapunov Exponents should be calculated on an infinite time period. However, it has been found that the estimation of Lyapunov Exponents can be done in finite-time (Alligood et al., 1997). Recently, Grune (2000) found the finite

time exponential growth rates for some fixed time uniformly converge to the uniform exponential spectrum. Convergence is declared if these variations are significantly low. In this research, the Lyapunov Exponents are truncated when the largest variations of the Lyapunov Exponents are lower than 0.25%. The calculation time periods for stable and chaotic motion are 200 seconds and 500 seconds, respectively.

To improve the accuracy of the numerical integration, a higher order integration algorithm than Wolf's original method is employed, which calculates the Lyapunov Exponents from the mathematical model. For Wolf's method, a very small time step is required to get the accurate Lyapunov exponent. This is because it uses the first order Euler's Method for the numerical integration, which makes the calculation time longer and less accurate. In this research, the Runge-Kutta numerical integration is used to compare the results using the Euler's method in order to improve accuracy of the results and to reduce calculation time. Since the stable motion is of interest, the Lyapunov Exponents will be calculated for stable motion with a set point as an example to demonstrate the advantages of the Runge-Kutta algorithm.

Figure 3.8 shows the largest Lyapunov exponent from Euler's integration approach and the one from Runge-Kutta integration when integration time step is small ($h = 0.00001$). The calculation loop is 20000000 and the result $\lambda = -0.909$. Fig. 3.9 shows the Lyapunov exponent calculated with the time step $h = 0.01$ and the calculation loop is 20000. The result with a large integration step from the Runge-Kutta integration does not differ from the

one with a small integration step, as shown in Fig. 3.8. The exponent from the Euler algorithm however, changes significantly from the result with a small integration time step. Fig. 3.8 and 3.9 show that the Runge-Kutta algorithm is much more advantageous than the Euler algorithm for the calculation of the Lyapunov Exponents, due to the reduction of the calculation time while maintaining accuracy. Thus, the Runge-Kutta algorithm is applied in the numerical calculation method when calculating the Lyapunov Exponents in this thesis.

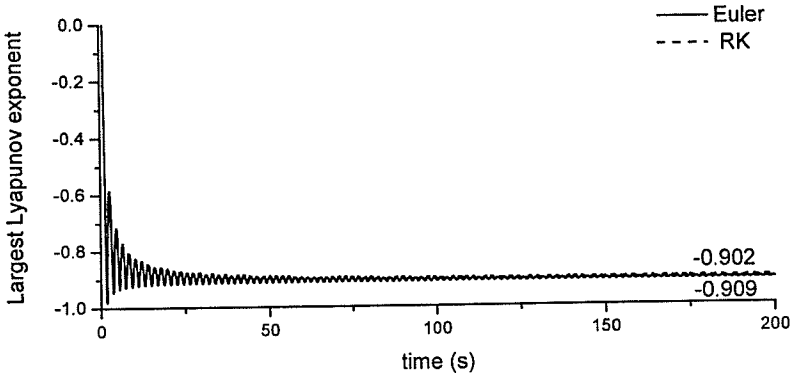

Fig 3.8 Largest Lyapunov Exponent (integration step-size $h = 0.00001(s)$)

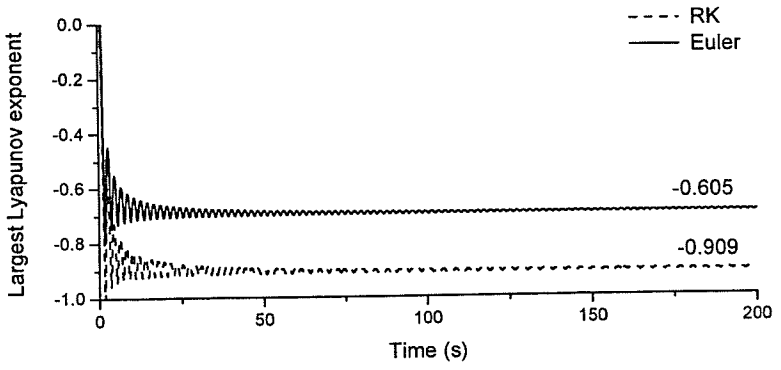

Fig. 3.9 Largest Lyapunov Exponent (integration step-size $h = 0.01(s)$)

3.3.1.1 Lyapunov Exponents for chaotic motion

In this section, the Lyapunov Exponents are calculated using Wolf's method based on the mathematical model for the two-link pendulum exhibiting chaotic motion as shown in section 3.2.1. The system is controlled by the PD controller shown in equation (3.3). The controller gain is $K_{p1} = K_{p2} = 50(N/rad)$ and $K_{v1} = K_{v2} = 1(N \bullet S/rad)$ in the simulation. The desired trajectories are $\theta_{d_1} = \frac{\pi}{2}\sin(2t)$ and $\theta_{d_2} = \frac{\pi}{4}\sin(2t)$. The simulation program is written in C++ language with the time step as $0.001(s)$. The calculation time will be truncated when Lyapunov Exponents change less than 0.25%. The initial condition is $\{0.0(rad), 0(rad/s), 0.0(rad), 0(rad/s)\}$

Such a chaotic control system is nonautonomous as shown in equation (3.4). Time, t, is taken as a new state which makes the state space model (3.4):

$$\begin{aligned}
\dot{x}_1 &= x_2 \\
\dot{x}_2 &= \frac{(T_1 - d_{111})d_{22} - (T_2 - d_{112})d_{12}}{d_{11}d_{22} - d_{12}d_{21}} \\
\dot{x}_3 &= x_4 \\
\dot{x}_4 &= \frac{(T_2 - d_{112})d_{11} - (T_1 - d_{111})d_{21}}{d_{11}d_{22} - d_{12}d_{21}} \\
\dot{x}_5 &= 1
\end{aligned} \tag{3.8}$$

where x_5 is one dimension of t in the state space model. Following the same procedure is shown in section 2.3.1. The Jacobian is:

$$F(t) = \begin{bmatrix}
0 & 0 & 0 & 0 & 0 \\
a_{21} & a_{22} & a_{23} & a_{24} & a_{25} \\
0 & 0 & 0 & 0 & 0 \\
a_{41} & a_{42} & a_{43} & a_{44} & a_{45} \\
0 & 0 & 0 & 0 & 0
\end{bmatrix} \tag{3.9}$$

where $a_{t1} = K_{p1}\pi\cos 2x_5 - K_{v1}2\pi\sin 2x_5$, $a_{t2} = K_{p2}\frac{\pi}{2}\cos s2x_5 - K_{v1}\pi\sin 2x_5$, a_{21}, a_{22}, a_{23}, a_{24}, a_{41}, a_{42}, a_{43}, a_{44} are defined from equation (3.5.b) to equation (3.5.j).

In Fig. 3.10, the Lyapunov Exponents for chaotic motion from the mathematic mode are shown with solid lines. All exponents converge to constants. The largest Lyapunov Exponent converges to 1.108 and the motion is indeed chaotic.

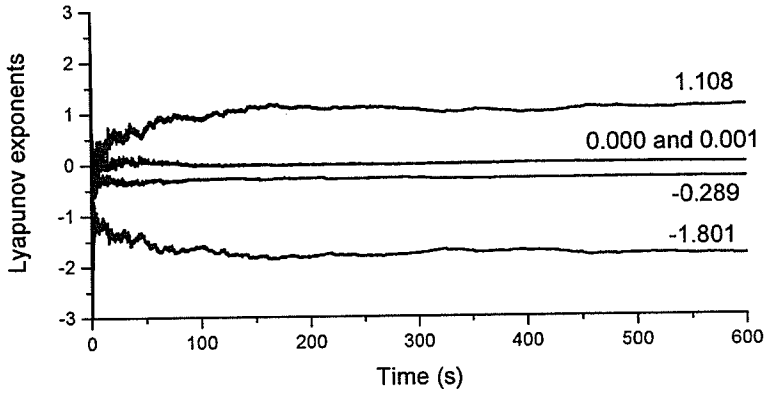

Fig. 3.10 Lyapunov Exponents for chaotic motion

3.3.1.2 Lyapunov Exponents for stable tracking motion

In this section the Lyapunov Exponents are calculated using Wolf's method based on the mathematical model for the two link pendulum tracking a desired trajectory as shown in section 3.2.2. The desired trajectory is set as the same sinusoid function $\theta_d^1 = 1.57\sin(2t)$ and $\theta_d^2 = \frac{1.57}{2}\sin(2t)$ and the system is controlled by the same PD controller as shown in the previous section. The control gains are set as $K_{p1} = K_{p2} = 50(N/rad)$ and $K_{v1} = K_{v2} = 20(N\bullet S/rad)$ in the simulations. Similar to the chaotic system discussed in the previous section, the mathematical model changes from 4-dimensional to 5-dimensional as

shown using equation (3.8). The simulation program is written in C++ language with a time step of $0.001(s)$. The calculation time will be truncated when Lyapunov Exponents change less than 0.25%. The initial condition is $\{0.0(rad), 0(rad/s), 0.0(rad), 0(rad/s)\}$

Similar to the chaotic motion, there is an extra zero exponent because of the time, t, which is taken as a new state. Fig. 3.11 shows there are one zero and four negative exponents for the stable tracking. The zero exponent is associated with the state x_5 (time). Four negative exponents indicate that the trajectories converge to the desired one.

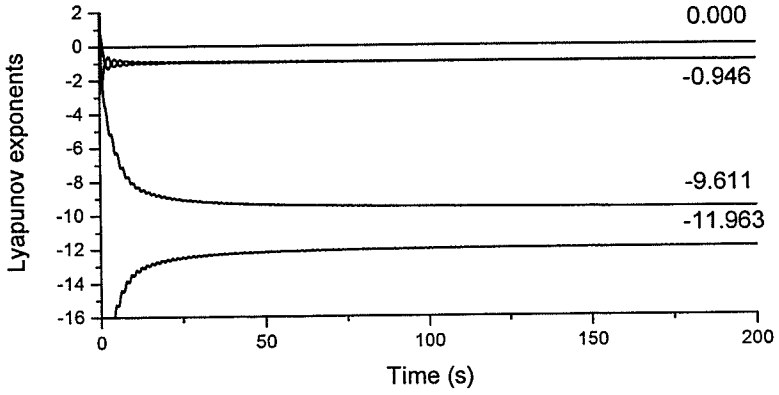

Fig. 3.11 Lyapunov Exponents for stable tracking motion

3.3.1.3 Lyapunov Exponents for stable motion with a set point

In this section the Lyapunov Exponents are calculated using Wolf's method based on the mathematical model for the two-link pendulum approaching the desired set position as shown in section 3.2.3. The control gains are set as $K_{p1} = K_{p2} = 20(N/rad)$ and $K_{v1} = K_{v2} = 5(N \bullet S/rad)$ in the simulations. The initial condition is $\{1(rad), 0(rad/s), 1(rad), 0(rad/s)\}$.

The Lyapunov Exponents for stable motion with a set point are shown in Fig. 3.12. The

vertical axis is the Lyapunov exponent and the horizontal axis is time. The first two exponents converge to -0.22 and the other two converge to -2.84.

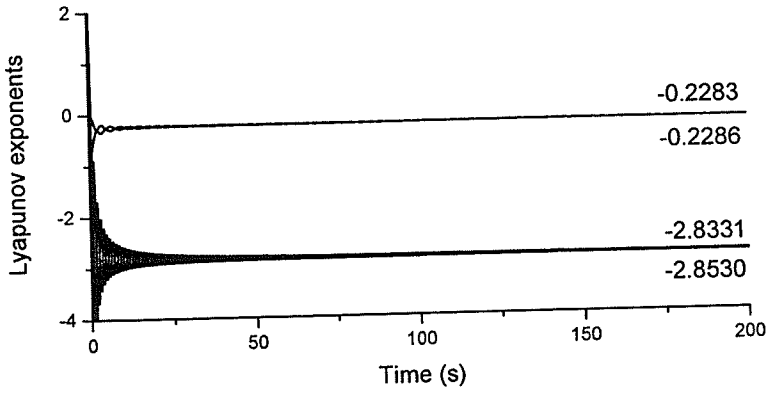

Fig. 3.12 Lyapunov Exponents from mathematic model for stable motion with a set point

The Lyapunov Exponents have been calculated using Wolf's method based on the mathematical models for the two-link pendulum with both chaotic motion and stable motion in this section. It is demonstrated that by using the Runge-Kutta algorithm, the accuracy of the Lyapunov exponent can be increased and the computing time significantly reduced. The calculated Lyapunov Exponents are used as the reference to be compared with those calculated from the time series.

3.3.2 The largest Lyapunov Exponent from time series data

Calculating the Lyapunov Exponent from a time series does not require the system's mathematical model. The calculation program in this research is developed based on Wolf's method (1985) where only the largest Lyapunov exponent can be calculated. Usually the method for calculating the Lyapunov Exponent from a time series is used for chaotic systems where the largest Lyapunov exponent is positive. In this research the possibility for applying

Wolf's method to potentially stable systems where the largest Lyapunov exponent is negative or zero, is explored.

In the calculation of the largest Lyapunov exponent from a time series, there are several parameters, as shown below, which need to be carefully determined. Unfortunately, there are no systematic methods to select these parameters:

The embedding dimension m: Following the discussion in section 2.3.2.1 and the Takens theory (1981), the embedding dimension is chosen as 9 for the two-link pendulum system since the original dimension is 4.

The delay time τ : In general, it is believed the selection of τ has a significant effect on the calculation of the largest Lyapunov Exponents from a time series. The largest Lyapunov exponent with a various time delay for the two-link pendulum with a stable set point case, is shown as the example in Fig. 3.13.

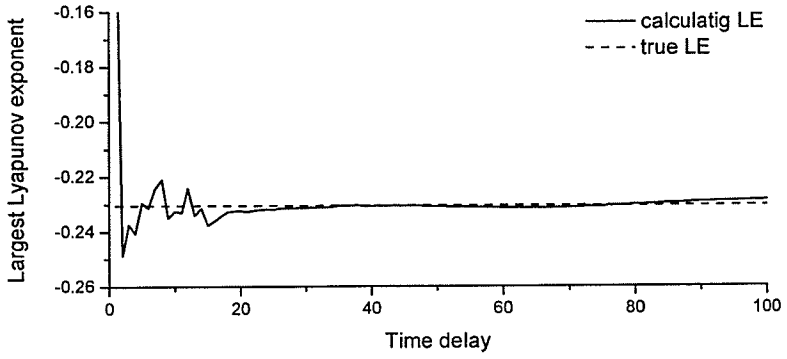

Fig. 3.13 Effect of time delay on the largest Lyapunov exponent

In Fig. 3.13 the horizontal axis is the time delay. The vertical axis is the largest Lyapunov exponent. Fig. 3.13 shows that as the time delay is chosen too low, the calculation

of Lyapunov Exponents shown in the solid curve is significantly different from the true exponent shown in the dash line. However, when the time delay is above 20, the calculated Lyapunov exponent does not change significantly. This indicates that the calculated Lyapunov exponent is not sensitive to the time delay for the two-link pendulum system with a set point for the special selected evolution time (30), the minimum and maximum cut-off lengths $(0.06(rad), 0.6(rad))$.

The evolution time between replacements: the largest Lyapunov exponent is calculated with the various evolution times for the same example in the Fig. 3.14

In Fig. 3.14 the horizontal axis is the evolution time, and the vertical axis is the largest Lyapunov exponent. Fig. 3.14 shows that the evolution time does not significantly affect the value of the largest Lyapunov exponent for the two-link pendulum with a stable set point for the selected the time delay (60), the minimum and maximum cut-off lengths $(0.06(rad), 0.6(rad))$.

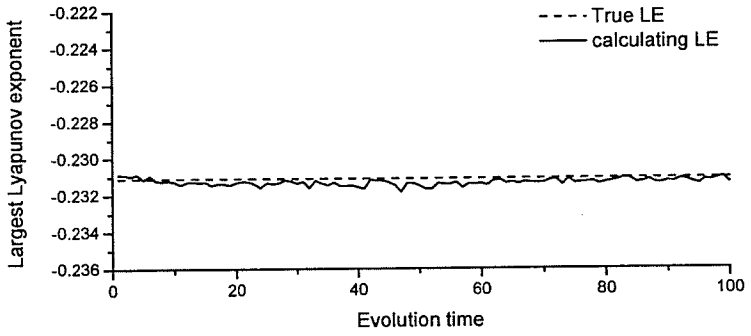

Fig. 3.14 Effect of evolution time on the largest Lyapunov exponent

The minimum and maximum cut-off length: Generally the minimum and maximum cut-off lengths are chosen arbitrarily in Wolf's method. In this research, after the emedding

dimension, time delay and evolution time are selected; the orientation length calculated in the first step is chosen to be minimum cut off length. The maximum orientation length is set to be 10 times that of the minimum orientation length. Fig. 3.15 and Fig. 3.16 show the effect of the minimum and maximum cut-off lengths on the calculation of the largest Lyapunov exponent when choosing the proper time delay and evolution time.

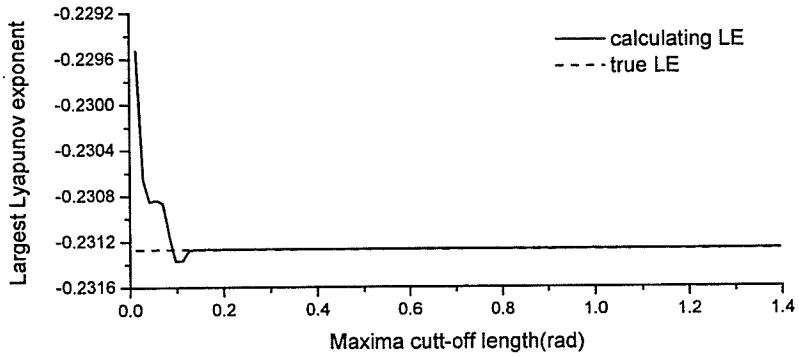

Fig. 3.15 Effect of maximum cut-off length on largest Lyapunov exponent

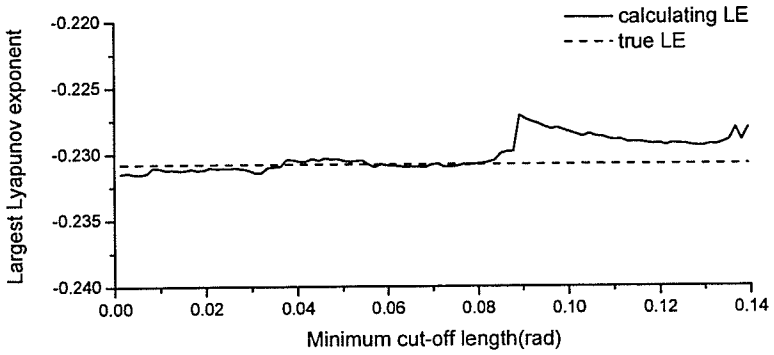

Fig. 3.16 Effect of minimum cut-off length on largest Lyapunov exponent

From Fig. 3.15, for the two-link pendulum system moving stably with a set point, it can be seen that as the maximum cut-off length is above 0.15, the calculated largest Lyapunov exponent is not sensitive to the changes in the maximum cut-off length. On the other hand, from Fig. 3.16, as the minimum cut-off length is below 0.08 (rad), the changes in the

minimum cut-off length have little effect on the largest Lyapunov exponent.

Normally, the embedding dimension, time delay, evolution time, maximum cut-off and minimum cut-off length are important for the calculation of the largest Lyapunov exponent using Wolf's method from a time series. The largest calculated Lyapunov exponent from time series is affected by the integrated actions of those five parameters. Since there are no methods available for such selections, different parameters are selected based on trial and error in this research. For the ranges of physical parameters shown in Fig. 3.13~3.16, the proper parameters are identified as: embedding dimension $m = 9$; time delay=60 and evolution time=30. The results of the largest Lyapunov Exponents are also determined with a wide range of time delay, evolution time and embedded dimensions to ensure that the results truly approximate the Lyapunov Exponents.

3.3.2.1 Calculation of the largest Lyapunov exponent for chaotic motion

Based on the procedure outlined in 2.3.2, the largest Lyapunov exponent for the two-link pendulum with chaotic motion can be calculated from any state time series of the system. The largest Lyapunov exponent is calculated using the time series of θ_1 and θ_2 and the result obtained from the mathematical model is shown below. Both of them have an error less than 8%, as compared with the result from the mathematical model which is shown in Table 3.2.

Table 3.2 Lyapunov exponent from the time series data and mathematical model

	Angular displacement of Link 1	Angular displacement of Link 2	Mathematical model
L. E.	1.0193	1.0343	1.108

Fig. 3.17 shows the largest Lyapunov exponent calculated from both angular displacements of the two-link pendulum. In Fig. 3.17, the horizontal axis is the time and vertical axis is the largest Lyapunov exponent. Both Lyapunov Exponents calculated from the time series converge. After 500 seconds, the difference of the two Lyapunov Exponents from time series reduces and is insignificant.

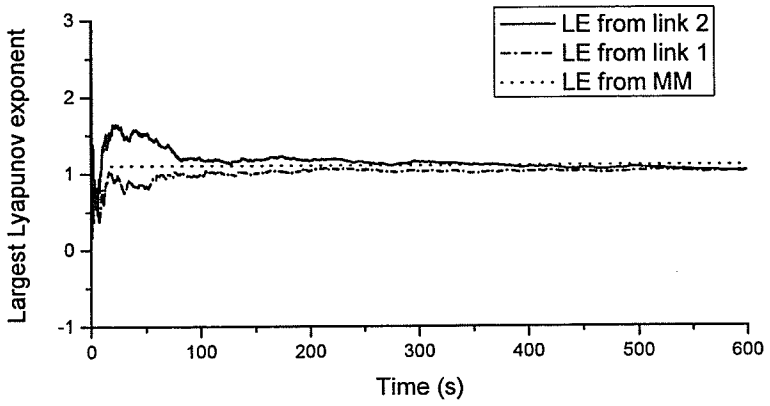

Fig. 3.17 Largest Lyapunov exponent calculated from time series data for chaotic motion

Time delay and evolution time are more important for calculating the largest Lyapunov exponent from a time series. The effects of the time delay and evolution time on the accuracy of the largest Lyapunov exponent are studied in Wolf's method using time series. The largest Lyapunov exponent was calculated with various time delays and evolution times, shown in Fig. 3.18.

In Fig. 3.18 the time delay and evolution time are the two horizontal axes and the vertical axis is the largest Lyapunov exponent. Fig. 3.18 shows that the largest Lyapunov exponent converges at 1.05 when the time delay and evolution time are chosen higher than 60 and

lower than 100. Fig. 3.18 also shows that the largest Lyapunov exponent does not change significantly with different evolution time at the same time delay which indicates that the time delay has a stronger effect on the largest Lyapunov exponent than evolution time. Thus Wolf's method for calculating the largest Lyapunov exponent offers a large range for selecting the proper time delay and evolution time for a two-link pendulum system.

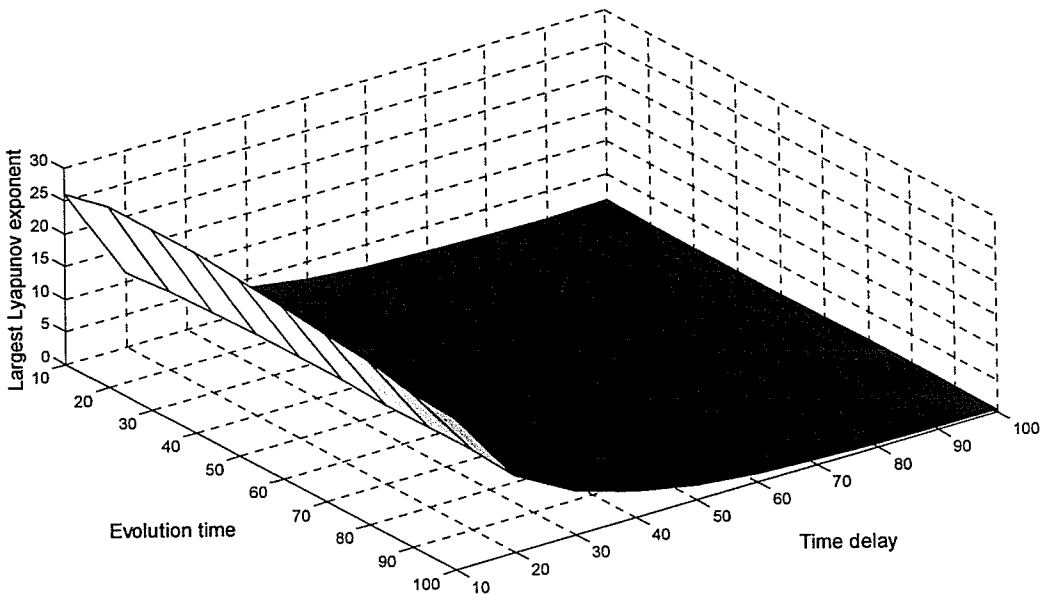

Fig. 3.18 Largest Lyapunov exponent with different time delay and evolution time

In this section Wolf's method for calculating the largest Lyapunov exponent from time series has been applied to the two-link pendulum system with chaotic motion. The effects of the important parameters in Wolf's method have been studied for the two-link pendulum system. The results of the largest Lyapunov exponent demonstrate that Wolf's method using time series works well for the two-link pendulum system. In the next section Wolf's method will be applied to the potentially stable two-link pendulum system.

3.3.2.2 Calculation of the largest Lyapunov exponent for the stable motion with a set point

Here, the possibility of applying Wolf's method for potentially stable systems is explored. Wolf's method using time series is not proved to be reliable for calculating negative and zero Lyapunov Exponents (Wolf e al., 1985). The objective of this section is to explore the possibility of applying Wolf's method based on a time series for calculating negative and zero Lyapunov Exponents. The two-link pendulum system with a stable set point is used as an example.

Table 3.3 shows the values of the largest exponents calculated from two states respectively, the largest one from the mathematical model. In Fig. 3.19, the largest Lyapunov exponent is calculated from the angular displacement of link 1 and link 2. The horizontal axis is the time and vertical axis is the largest Lyapunov exponent.

Table 3.3 The largest Lyapunov exponent calculated from the time series data and mathematical model

	Angle 1	Angle 2	Mathematical model
L. E.	-0.214	-0.233	-0.221

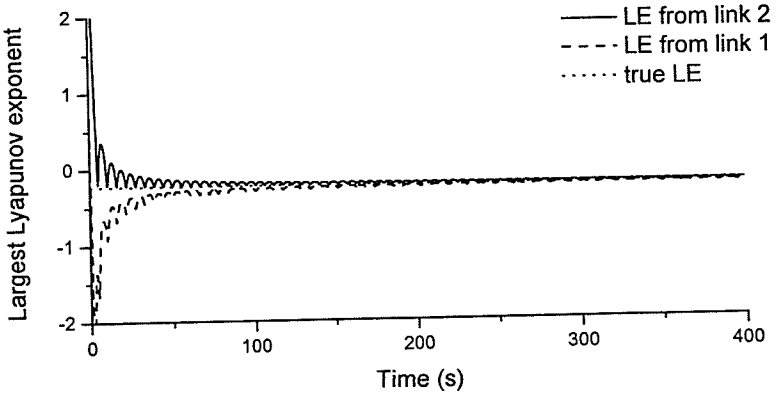

Fig. 3.19 The largest Lyapunov exponent calculated from both angle positions

In Fig. 3.19, both of the largest Lyapunov Exponents from time series converge to -0.22 after 200 seconds. Because the largest Lyapunov exponent is negative, all other exponents are also negative. The comparison made between the exponents calculated from the mathematical model the exponents calculated from the time series are very precise, about 4% error. Based on the concept of the Lyapunov exponent theory, the system is exponentially stable about the set point.

For studying the effects of time delay and evolution time on the Lyapunov exponent, the largest Lyapunov exponent is calculated and shown in Fig. 3.20 with various time delays and evolution times.

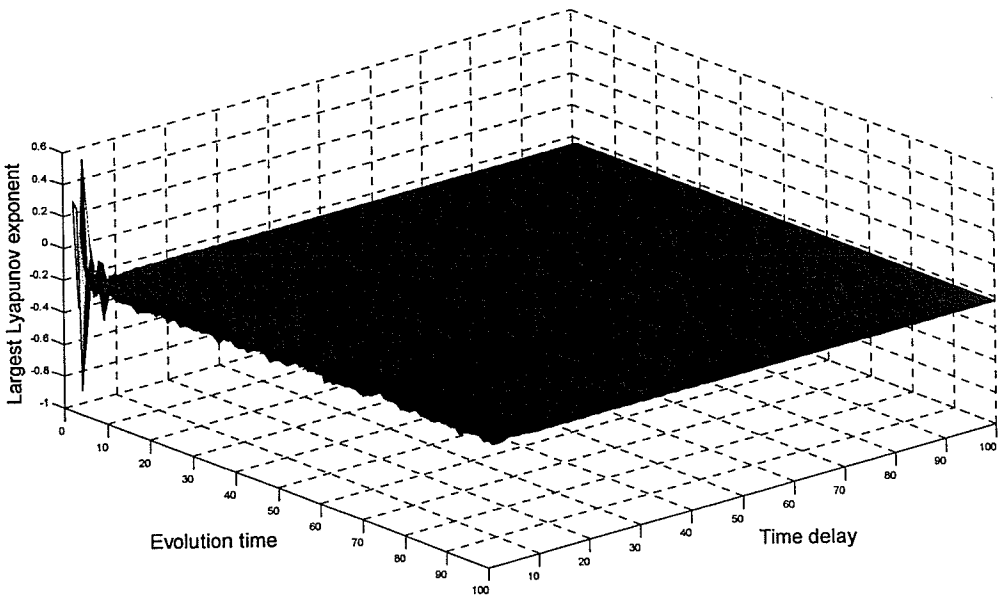

Fig. 3.20 Largest Lyapunov exponent with different time delay and evolution time

Fig. 3.20 shows that the largest Lyapunov exponent is not sensitive to different time delays or evolution times, except when the time delays and evolution times are selected

between 0 and 10. The time delay affects the largest Lyapunov exponent more than the evolution time. However, there is a good reason for choosing time delay and evolution time to calculate the largest Lyapunov exponent properly. At least for this low-link pendulum system, Wolf's method can calculate the largest Lyapunov exponent from time series of the stable motion with a set point.

3.3.2.3 Calculation of the largest Lyapunov exponent for stable tracking motion

In this section, the two-link pendulum system following the desired trajectory as shown in section 3.2.2 is used as an example for calculating the largest Lyapunov exponent using Wolf's method. The largest Lyapunov exponent is calculated based on the time series recorded in the simulations. Table 3.4 shows the largest Lyapunov exponent from the mathematical model and from the time series.

Table 3.4 The largest L.E. from the time and from the mathematical model

	Time series data	Mathematical model
L. E.	0.0006	0.0001

The largest Lyapunov exponent calculated from time series is shown as following:

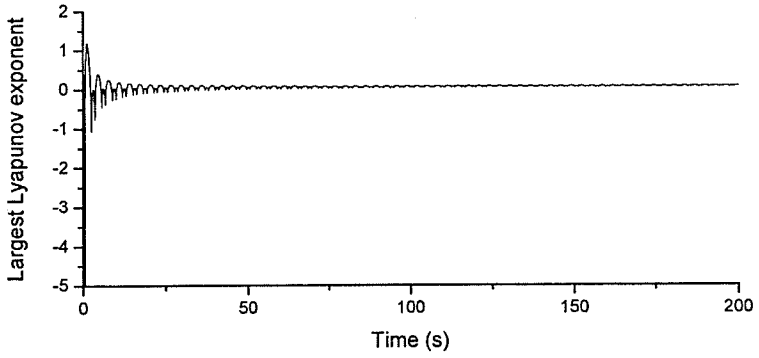

Fig. 3.21 Largest Lyapunov exponent calculated from time series data for stable tracking

The Lyapunov exponent calculated from a time series for the stable tracking has different indications as the largest exponent from the mathematical model. The zero Lyapunov exponent from the mathematical model corresponds to time as one dimension in the state space model. If the time series corresponds to periodic behavior, the Lyapunov exponent should be very small or zero, since the trajectory returns to exactly the same set of values. Hence, this trajectory method would reflect the fact that the Lyapunov exponent neither increases, nor decreases in its value. This result tells us that trajectory points on a periodic orbit neither converge nor diverge. However, the time series of values from the trajectory itself cannot tell us how nearby trajectories approach the attractor (Hilborn, 2004). Based on the above discussion, calculating zero exponents from the time series has a different meaning from that of the zero exponent calculated from the mathematical model and the stability of the system should be studied using the whole spectrum from the mathematical model.

In this section the largest Lyapunov Exponents have been calculated for two-link pendulum with chaotic motion, with a stable set-point and with stable tracking. It is documented that Wolf's method is valid for calculating the largest positive Lyapunov exponent (Wolf et al, 1985). By matching the largest Lyapunov exponent from a time series with the one from the mathematical model of the double pendulum system with a stable set point, it is found that Wolf's method (1985) for calculating the largest Lyapunov exponent from a time series has a potential for calculating the largest negative Lyapunov exponent. However, Wolf's method cannot be used for calculating zero Lyapunov Exponents.

3.4 Effects of noise on calculating Lyapunov Exponents

For the time series generated from experiments, the inevitable noise has its effects on the accuracy of the Lyapunov Exponents. In signal processing, noise is considered as data without providing meaningful information; that is, data that is not being used to transmit a signal, but is simply produced as an unwanted by-product of other activities. Normally as sensors transfer the signal to the receiver the noise is also transferred. After applying High-pass or Low-pass filters to reduce the noise, the Gaussian White noise (GWN) still remains. So GWN is selected as the noise sample to study the effects on the accuracy of the Lyapunov Exponents. White noise power density is defined as a constant over a finite frequency range. Gaussian White noise is a white noise with a normal distribution. In this thesis, GWN will be generated by a C++ program and added to the time series randomly.

The noise has its effects on the reconstruction of an attractor. Based on the discussion in sections 2.3.2 and 2.4.3, choosing the proper time delay can help reduce the noise effect on the reconstruction (Wolf et. al, 1985). However, the effects of the noise on the accuracy of Lyapunov Exponents have not been studied rigorously. In this section, the effects of the average power of GWN on the accuracy of the largest Lyapunov exponent using Wolf's method based on a time series are investigated. The Signal-to-Noise Ratio (SNR) is often used for studying the effects of the noise. It is defined as:

$$SNR = \frac{average \quad Power \quad of \quad Signal}{average \quad Power \quad of \quad Noise} \times 100\% \tag{3.10}$$

Because many signals have a wide dynamic range, SNR is usually expressed in terms of

the logarithmic decibel scale. In decibels, the SNR is by definition, 10 times the logarithm of the power ratio:

$$SNR(dB) = 10\log_{10}\left(\frac{average\ \ Power\ \ of\ \ Signal}{average\ \ Power\ \ of\ \ Noise}\right) \tag{3.11}$$

Based on the definition of SNR the average power of noise can not be zero. However, the noise effects on the calculation of the largest Lyapunov exponent are studied and compared with the results from the time series without noise. The Noise-to-Signal Ratio (NSR) is defined as

$$NSR = \frac{average\ \ Power\ \ of\ \ Noise}{average\ \ Power\ \ of\ \ Signal} \times 100\% \tag{3.12}$$

Under the above definition, the largest Lyapunov exponent can be calculated with NSR changing from 0 which indicate the time series without noise.

With the filtering technology improved, the white noise can usually be reduced to $SNR = 10dB$, which means the $NSR = 10\%$. In this research, 10% Gaussian White noise will be added to the original signal from the mathematical model of the 2-link pendulum system. In studying the noise effects, the largest Lyapunov exponent will be used for calculating such a time series. The Lyapunov exponent will then be calculated from the time series with the noise range from $NSR = 0$ to $NSR = 100\%$. The two-link pendulum system will be studied with the chaotic motion and stable motion with a set point.

3.4.1 The Chaotic motion

After applying the 10% NSR to the time series generated from the mathematical

model of the 2-link pendulum system with chaotic motion, the largest Lyapunov exponent is calculated from the time series and is shown in Fig. 3.22.

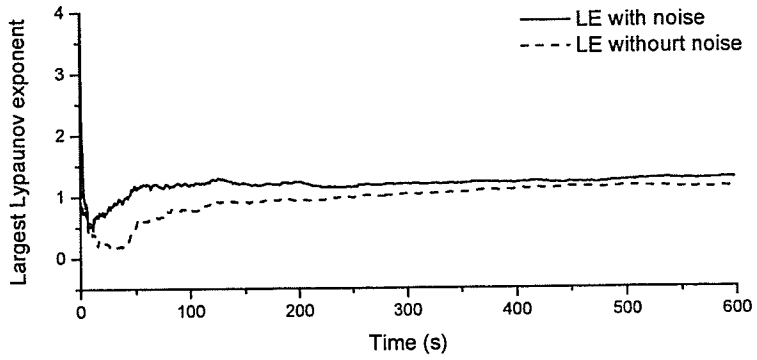

Fig. 3.22 Largest Lyapunov exponent from time series with noise for chaotic motion

In Fig. 3.22, the largest Lyapunov exponent calculated from the time series converges to 1.2 and has the 18% error as comparing with the largest Lyapunov exponent (1.108) calculated from time series without the noise.

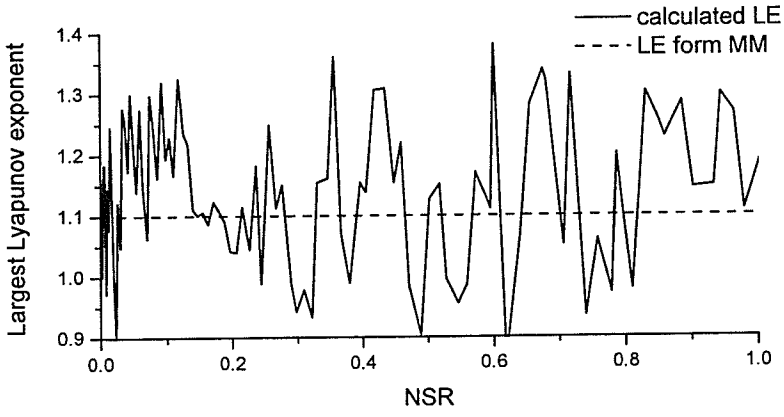

Fig. 3.23 Lyapunov exponent changed with the NSR

Fig. 3.23 shows the largest Lyapunov exponent for the chaotic motion calculated with NSR changing from 0 to 100%. It can be seen that the value of the Lyapunov exponent

does not show a trend in its accuracy with respect to the increase in noise, but oscillates about the largest Lyapunov exponent form the time series without noise in a rather random manner.

3.4.2 The stable motion with a set point

The largest Lyapunov exponent calculated is when the NSR=10%, as shown in Fig. 3.24. The changes in this exponent with various NSR are shown in Fig. 3.25.

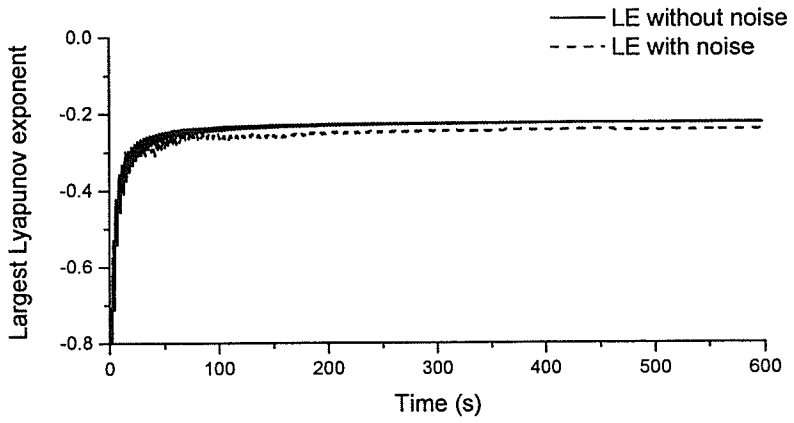

Fig. 3.24 Largest Lyapunov exponent calculated from the time series data with noise

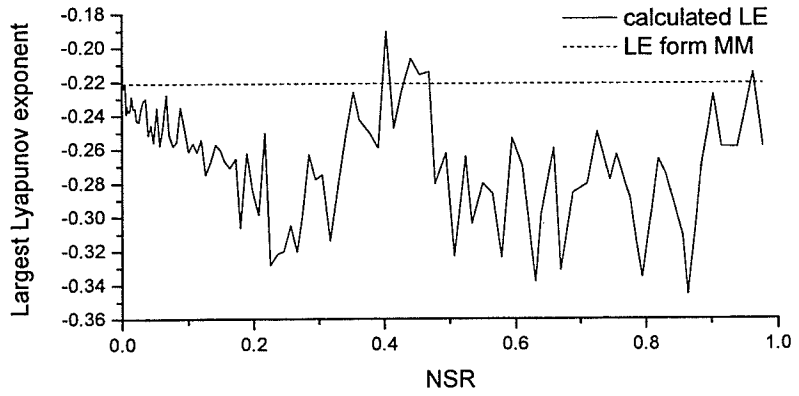

Fig. 3.25 Lyapunov exponents changed with the NSR

Fig. 3.24 shows that the largest Lyapunov exponent converges to the -0.24 and has the

7% error as compared to the largest exponent calculated without the noise. Fig. 3.25 shows that with NSR changing from 0 to 100%, the exponent oscillates about the largest Lyapunov exponent calculated from the mathematical model. No clear trend of accuracy is shown in the largest Lyapunov exponent with respect to the increase in NSR of Gaussian White noise.

3.5 Summary

In this chapter, the possibility of applying the Wolf's method for calculating the largest Lyapunov exponent based on the time series is explored for potentially stable systems. The two-link pendulum system is selected as an example. Since Wolf's method using the mathematical models of the system is believed valid for any systems (stable or chaotic), and that Wolf's method using a time series has been developed for the chaotic system, the two-link pendulum is controlled to show both chaotic and stable motions. First, the largest Lyapunov exponent is calculated from a time series for chaotic motion and is compared with the one calculated from the mathematical model to confirm validity of the program developed in this research. Then, for the two-link pendulum with stable motion, the largest Lyapunov exponent is studied in the same process as with chaotic motion. The effect of noise on the accuracy of the Lyapunov exponent is studied at the end of this chapter.

The error between the largest Lyapunov Exponents from a time series and the error from the mathematical model is below 6% for the 2-link pendulum system with a stable set-point. Thus, the results show that Wolf's method is adequate for calculating the largest negative Lyapunov exponent. For the 2-link pendulum system with stable tracking motion, zero

exponents have been calculated from both the mathematical model and the time series. However, the zero exponent from the time series and the one from the mathematical model have different indications. The zero Lyapunov exponent from the mathematical model responds to the extra dimension of time in state space. The zero Lyapunov exponent from the time series responds to the periodical orbit. The effects of GWN on the largest Lyapunov exponent are studied on the two-link pendulum system having chaotic motion or stable motion with a set-point. The largest Lyapunov exponent has been calculated with NSR increasing from 0 to 100%. The results show that the noise has significant effect on the calculation of the largest Lyapunov Exponents. This finding is consistent with previous findings from different systems (Wolf et. al, 1985). However, no clear trend has been found in the accuracy of the largest Lyapunov exponent with the increase in NSR.

Based on the results from this chapter, it is concluded that Wolf's method can be used for the system, of which the largest Lyapunov exponent is negative, i.e., the system is exponentially stable about a set-point. However, Wolf's method is not suitable for calculating zero Lyapunov Exponents, i.e., the system has a stable tracking motion. Noise, which is inevitable when the time series is collected during experimentation, has a significant effect on the accuracy of the largest Lyapunov exponent. With filter technology improving, the GWN usually can be reduced less than 10% NSR.

With the research done here, Wolf's method can be used to calculate the largest Lyapunov exponent from a time series when noise is reduced enough. It is imperative that

more research be conducted on how noise affects the accuracy of the Lyapunov exponent and on developing better methods, which are robust to the noisy time series.

Chapter 4

Calculation of Lyapunov Exponents for a stable pneumatic actuator system

In this chapter, a stable pneumatic servo-positioning actuator system will be used as an example for calculating Lyapunov Exponents. The exponents will be calculated from the dynamic model of the system and the largest Lyapunov exponent will be calculated using Wolf's method from a time series, which is via simulation of the pneumatic actuator system desired by the model. The objective is to understand if the Lyapunov Exponents calculated for such a highly nonlinear system produce meaningful results using these two methods.

4.1 Pneumatic system

4.1.1 Nonlinear model

The double-acting valve controlled pneumatic actuator is shown in Fig. 4.1. The schematic diagram of the pneumatic actuator is shown in Fig. 4.2. An electrical control signal applied to the valve spool allows movement of the control valve. The control valve produces a pressure differential between the sides of the piston creating an acting force, F_L.

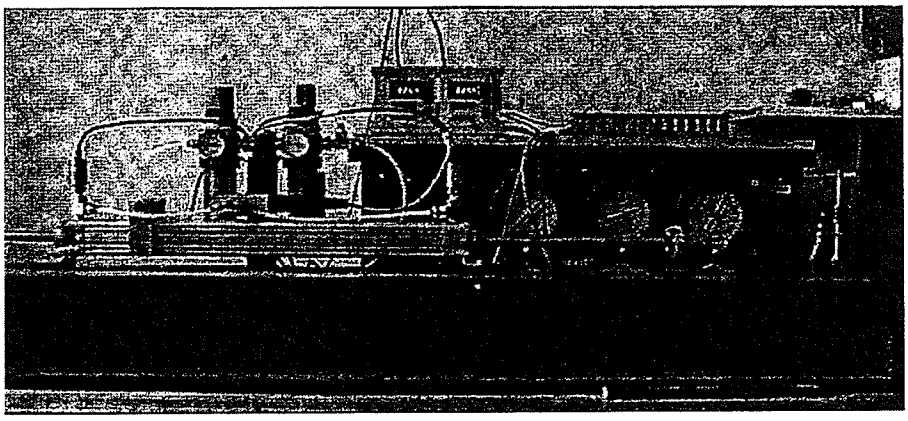

Fig. 4.1 Experimental test equipment

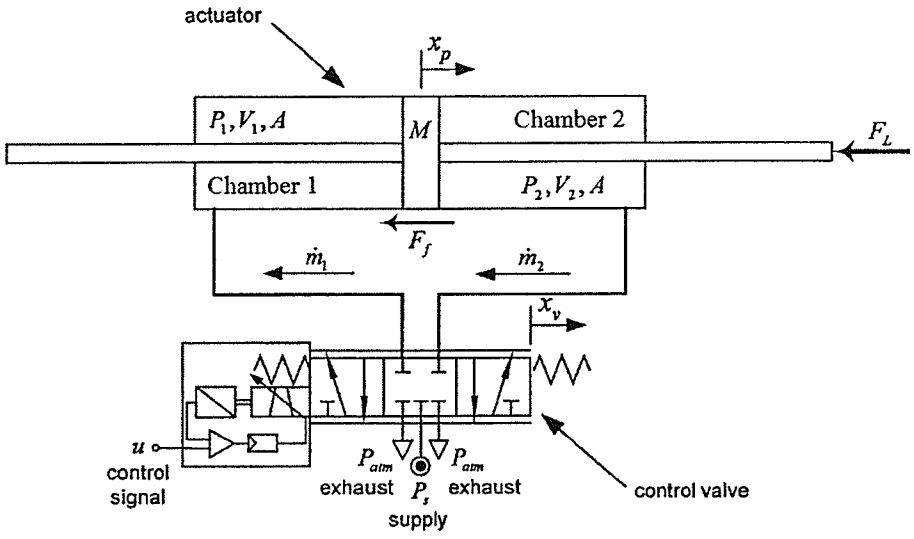

Fig. 4.2 Schematic plot of experimental pneumatic actuator

The equation of motion for the actuator and the load, F_L is:

$$M\ddot{x}_p + b\dot{x}_p = P_1A - P_2A - F_f - F_L \tag{4.1}$$

where x_p denotes the position of the piston. M is the combined mass of the piston-rod assembly and the external mass. P_1 and P_2 are the absolute pressure in each of the actuator chambers, A is the annulus area of the piston, b is the viscous friction coefficient, F_f represents dry friction force and F_L signifies the externally applied load.

The ideal gas law, the conservation of mass and the energy equation must be considered

simultaneously to model the control volumes defined by each of the actuator chambers. Assuming the gas is perfect and that the pressure and temperature is homogeneous in each chamber, the ideal gas law is written as

$$P = \rho RT \tag{4.2}$$

where ρ is the mass density of the working fluid and R is the ideal gas constant. P and T are the pressure and the temperature in the chamber of interest, respectively.

From conservation of mass, the continuity equation is established as

$$\dot{m} = \frac{d}{dt}(\rho V) = \dot{\rho} V + \rho \dot{V} \tag{4.3}$$

where $\dot{m}$ is the mass flow rate and V is the chamber volume.

Neglecting the kinetic and potential energy terms, the energy equation is:

$$\frac{d}{dt}(c_v \rho V T) = c_p \dot{m} T - P\dot{V} + \dot{Q} \tag{4.4}$$

where c_v is the specific heat at constant volume and c_p is the specific heat at constant pressure; $\dot{Q}$ is the rate of heat transfer across the cylinder wall. For the ideal gas, $\dot{Q} \approx 0$

Substituting equation (4.2) into the left hand of equation (4.4) gives

$$\frac{d}{dt}(c_v \rho V T) = \frac{c_v}{R}\frac{d}{dt}(PV) = \frac{c_v}{R}\left(\dot{P}V + P\dot{V}\right) \tag{4.5}$$

Then, the energy equation (4.4) becomes

$$\frac{c_v}{R}\left(\dot{P}V + P\dot{V}\right) = c_p \dot{m} T - P\dot{V} + \dot{Q} \tag{4.6}$$

Rearranging equation (4.6) and setting $\dot{Q} = 0$, the required rate of change in pressure is found to be

$$\dot{P} = \frac{c_p RT}{c_v V}\dot{m} - \frac{R}{c_v}\left(1 + \frac{c_v}{R}\right)\frac{P}{V}\dot{V} \tag{4.7}$$

Noting that $c_p - c_v = R$ and defining $\gamma = \frac{c_p}{c_v}$, equation (4.7) may be further simplified to

$$\dot{P} = \frac{\gamma RT}{V}\dot{m} - \frac{\gamma P}{V}\dot{V} \tag{4.8}$$

Assuming the initial piston position to be at the mid-point of the stroke, the volumes of the two chambers can be expressed as:

$$\begin{aligned} V_1(x_p) &= V_{o1} + A\left(\frac{L}{2} + x_p\right) \\ V_2(x_p) &= V_{o2} + A\left(\frac{L}{2} - x_p\right) \end{aligned} \tag{4.9}$$

Substituting equation (4.9) into (4.8), the differential equations that define the time derivatives of the chamber pressures are:

$$\begin{aligned} \dot{P}_1 &= \frac{\gamma RT}{V_{o1} + A\left(\frac{L}{2} + x_p\right)}\dot{m}_1 - \frac{\gamma P_1 A}{V_{o1} + A\left(\frac{L}{2} + x_p\right)}\dot{x}_p \\ \dot{P}_2 &= \frac{\gamma RT}{V_{o2} + A\left(\frac{L}{2} - x_p\right)}\dot{m}_2 - \frac{\gamma P_2 A}{V_{o2} + A\left(\frac{L}{2} - x_p\right)}\dot{x}_p \end{aligned} \tag{4.10}$$

The air mass flow rate through the valve orifice is given by Sanville (1971), who described that the complex internal geometries and the critical pressure ratio may be as low as 0.2 for air valves. Sanville (1971) proposed the following empirical relation for the mass flow rate through the valve orifice:

$$\dot{m} = \begin{cases} \dfrac{C_d A_v P_s}{\sqrt{T}}\sqrt{\dfrac{\gamma}{R}\left(\dfrac{2}{1+\gamma}\right)^{(\gamma+1)/(\gamma-1)}} & \dfrac{P_d}{P_s} \le P_{cr} \\ \dfrac{C_d A_v P_s}{\sqrt{T}}\sqrt{\dfrac{\gamma}{R}\left(\dfrac{2}{1+\gamma}\right)^{(\gamma+1)/(\gamma-1)}}\sqrt{1-\left(\dfrac{P_d/P_s - P_{cr}}{1-P_{cr}}\right)} & \dfrac{P_d}{P_s} > P_{cr} \end{cases} \tag{4.11}$$

where P_s is the supply pressure and P_d is the return pressure. The area of valve orifice,

A_v, is a function of the displacement of the valve spool, which is defined as a linear function of spool displacement:

$$A_v = wx_v \tag{4.12}$$

where x_v is the position of the control valve, controlled by the input voltage, u:

$$\mu\dot{x}_v + x_v = K_{valve}u \tag{4.13}$$

For Chambers 1 and 2, the air mass flow rates are different; as the air flows out one side of the cylinder and gets in the other side. For the side where the air comes in, the supply pressure is P_s and the return pressure is the pressure within the chamber. For the side where the air flows out, the supply pressure is the pressure within the chamber and the return pressure is the atmospheric pressure P_{atm}.

The nonlinear equations relating the control flows $\dot{m}_1$ and $\dot{m}_2$ to valve spool displacement are:

1) the supply port is connected to Chamber 1 and Chamber 2 is connected to the atmosphere:

$$\dot{m}_1 = \dot{m}_{i1} = \begin{cases} \dfrac{C_d w|x_1|P_s}{\sqrt{T}}\sqrt{\dfrac{\gamma}{R}\left(\dfrac{2}{\gamma+1}\right)^{(\gamma+1)/(\gamma-1)}} & \dfrac{x_2}{P_s} \le P_{cr} \\ \dfrac{C_d w|x_1|P_s}{\sqrt{T}}\sqrt{\dfrac{\gamma}{R}\left(\dfrac{2}{\gamma+1}\right)^{(\gamma+1)/(\gamma-1)}}\sqrt{1-\left(\dfrac{x_2/P_s - P_{cr}}{1-P_{cr}}\right)^2} & \dfrac{x_2}{P_s} > P_{cr} \end{cases}, \tag{4.14}$$

$$\dot{m}_2 = \dot{m}_{o2} = \begin{cases} \dfrac{C_d w|x_1|x_3}{\sqrt{T}}\sqrt{\dfrac{\gamma}{R}\left(\dfrac{2}{\gamma+1}\right)^{(\gamma+1)/(\gamma-1)}} & \dfrac{P_e}{x_3} \le P_{cr} \\ \dfrac{C_d w|x_1|x_3}{\sqrt{T}}\sqrt{\dfrac{\gamma}{R}\left(\dfrac{2}{\gamma+1}\right)^{(\gamma+1)/(\gamma-1)}}\sqrt{1-\left(\dfrac{P_e/x_3 - P_{cr}}{1-P_{cr}}\right)^2} & \dfrac{P_e}{x_3} > P_{cr} \end{cases}, \tag{4.15}$$

2) the supply port is connected to Chamber 2 and Chamber 1 is connected to the atmosphere:

$$\dot{m}_1 = \dot{m}_{o1} = \begin{cases} \dfrac{C_d w|x_1|x_2}{\sqrt{T}}\sqrt{\dfrac{\gamma}{R}\left(\dfrac{2}{\gamma+1}\right)^{(\gamma+1)/(\gamma-1)}} & \dfrac{P_e}{x_2} \le P_{cr} \\ \dfrac{C_d w|x_1|x_2}{\sqrt{T}}\sqrt{\dfrac{\gamma}{R}\left(\dfrac{2}{\gamma+1}\right)^{(\gamma+1)/(\gamma-1)}}\sqrt{1-\left(\dfrac{P_e/x_2 - P_{cr}}{1-P_{cr}}\right)^2} & \dfrac{P_e}{x_2} > P_{cr} \end{cases}, \quad (4.16)$$

$$\dot{m}_2 = \dot{m}_{i2} = \begin{cases} \dfrac{C_d w|x_1|P_s}{\sqrt{T}}\sqrt{\dfrac{\gamma}{R}\left(\dfrac{2}{\gamma+1}\right)^{(\gamma+1)/(\gamma-1)}} & \dfrac{x_3}{P_s} \le P_{cr} \\ \dfrac{C_d w|x_1|P_s}{\sqrt{T}}\sqrt{\dfrac{\gamma}{R}\left(\dfrac{2}{\gamma+1}\right)^{(\gamma+1)/(\gamma-1)}}\sqrt{1-\left(\dfrac{x_3/P_s - P_{cr}}{1-P_{cr}}\right)^2} & \dfrac{x_3}{P_s} > P_{cr} \end{cases}, \quad (4.17)$$

4.1.2 Friction model applied to pneumatic system

Friction is highly nonlinear and may result in steady state errors, limit cycles, and poor performance. It is therefore important, for control engineers to understand friction phenomena and to reduce its adverse effect on system performance.

Friction is the tangential reaction force between two surfaces in contact. Physically, the reaction forces are the result of many different mechanisms, which depend upon contact geometry and topology, properties of the bulk and surface materials of the bodies, displacement and relative velocity of the bodies and the presence of lubrication. Dynamic friction models have more advantage than conventional friction models' schemes based on static friction models (Olsson et. al., 1997). The dynamic friction model, LuGre model, is employed in this thesis. The LuGre model is continuous which makes it easy to calculate the Lyapunov exponent from the mathematical model. In the LuGre friction model, force is

modeled as the average deflection force of elastic springs. The tangential force applied to the bristles deflects them like springs, shown in Fig. 4.3. If the deflection is sufficiently large, the bristles start to slip. The average bristle deflection for a steady-state motion is determined by the velocity. It is lower at low velocities, which implies that the steady state deflection decreases with the increase in the velocity. The LuGre model is shown in Fig. 4.3.

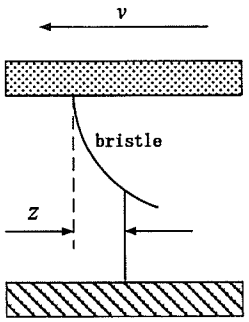

Fig. 4.3 LuGre friction model

The differential equations of LuGre model are shown in equation (4.14),

$$\begin{aligned} \frac{dz}{dt} &= v - \sigma_0 \frac{|v|}{g(v)} z \\ F_f &= \sigma_0 z + \sigma_1(v)\frac{dz}{dt} + f(v) \end{aligned} \tag{4.18}$$

where z is the bristle deflection which is considered as the extra state in the pneumatic system's mathematic model, $\sigma_1(v) = \sigma_1 e^{-(v/v_s)^2}$, $f(v) = bv$, $\alpha_0 = F_c$ and $\alpha_1 = F_s - F_c$. The parameter σ_0 is the stiffness of the bristles, and σ_1 is the damping. The function $g(v)$ models the Stribeck effect, and $f(v)$ is the viscous friction. A reasonable choice of $g(v)$ which gives a good approximation of the Stribeck effect, is

$$g(v) = \alpha_0 + \alpha_1 e^{-(v/v_s)^2} \tag{4.19}$$

The sum $\alpha_0 + \alpha_1$ then corresponds to stiction force and α_1 to Coulomb friction force. The

parameter v_s determines how $g(v)$ vary within its bounds $\alpha_0 < g(v) < \alpha_0 + \alpha_1$.

Although parameters σ_0 and σ_1 are hard to estimate, for the LuGre model the great advantage is the continuity, which is appealing for calculating Lyapunov Exponents towards the stability analysis of the pneumatic actuator system.

4.1.3 Control design

Sepehri et al. (1996, 1997) developed a number of nonlinear modifications to a conventional PI control scheme that significantly enhanced the tracking performance of industrial hydraulic manipulators. The goal was to overcome actuator stiction and flow deadband in the hydraulic valve, through the application of nonlinear conditioning to the integral term of the PI control. This modification can reduce the deadtime in the position response that arises from the control valve deadband and stiction through appropriate adjustment of the integral term of the PI controller.

For the integral part of the PI controller, the following algorithm is implemented:

$$I(t) = \begin{cases} \dfrac{-u_{lower} - K_p\left(x_{desired} - x_p\right)}{K_i} & \dot{e}_{deadband} > \varepsilon \;\&\; u(t) > -u_{lower} \\ I(t-\Delta t) + \left(x_{desired} - x_p\right)\Delta t & \left|\dot{e}_{deadband} \le \varepsilon\right| \\ \dfrac{u_{upper} - K_p\left(x_{desired} - x_p\right)}{K_i} & \dot{e}_{deadband} > \varepsilon \;\&\; u(t) < u_{up} \\ 0 & v_d(t) = 0 \;\&\; \left|e(t)\right| \le \tilde{\varepsilon} \end{cases} \tag{4.20}$$

It is observed that the largest error in the actuator deadband is the velocity error, $\dot{e} = v_{desired} - v$, while the smallest is the time integral, $\int (v_{desired} - v)dt$. This basic observation is used to construct a nonlinear filter that estimates the velocity error caused by the actuator deadband. The nonlinear filter is

$$\dot{e}_{deadband} = (v_{desired} - v)\frac{v_{desired}^2}{v_{desired}^2 + \beta v^2} \tag{4.21}$$

where $\dot{e}_{deadband}$ is an estimate of the velocity error caused by deadband and β is an experimental constant found though trial and error. When the $\dot{e}_{deadband}$ exceeds the threshold, ε, the controller with this modification will overcome the accumulate error of the deadband.

Thresholds u_{lower} and u_{up} are selected as the levels of controller output required to initiate the actuator motion. From the experimental results, the PI controller based on the velocity error, the triggered integral enhanced the performance of the actuator despite the effects of the control valve deadband and actuator friction. This PI controller will be used to control tracking of the pneumatic piston.

Combining equations (4.1), (4.10), (4.13) and (4.18); the nonlinear dynamic equations relating the position of the actuator, x_p, to the signal, u, can be written as follows:

$$\begin{aligned}
\dot{x}_p &= v_p \\
\dot{v}_p &= \frac{1}{M}\left(-bv_p + AP_1 - AP_2 - F_f - F_L\right) \\
\dot{P}_1 &= \frac{\gamma RT}{V_{o1} + A\left(\frac{L}{2} + x_p\right)}\dot{m}_1 - \frac{\gamma P_1 A}{V_{o1} + A\left(\frac{L}{2} + x_p\right)}\dot{x}_p \\
\dot{P}_2 &= \frac{\gamma RT}{V_{o2} + A\left(\frac{L}{2} - x_p\right)}\dot{m}_2 + \frac{\gamma P_2 A}{V_{o2} + A\left(\frac{L}{2} - x_p\right)}\dot{x}_p \\
\dot{x}_v &= -\frac{x_v}{\mu} + \frac{K_{valve}}{\mu}u \\
\dot{z} &= v_p - \sigma_0\frac{|v_p|}{\alpha_0 + \alpha_1 e^{-(v/v_s)^2}}z
\end{aligned} \tag{4.22}$$

where control signal $u = K_p(x_{desired} - x_p) + K_I I$, I was given by equation (4.20), $F_f = \sigma_0 z + \sigma_1 \dot{z} + bv_p$, $\alpha_0 = F_c$ and $\alpha_1 = F_s - F_c$. v_p is the velocity of the actuator. Mass

flows $\dot{m}_1$ and $\dot{m}_2$ are given either by equation (4.11) to (4.17). Rewriting the system's mathematic model in the state space based on equation (4.22):

$$\dot{x} = \begin{Bmatrix} \dot{x}_1 \\ \dot{x}_2 \\ \dot{x}_3 \\ \dot{x}_4 \\ \dot{x}_5 \\ \dot{x}_6 \end{Bmatrix} = f(x) = \begin{Bmatrix} -\frac{x_1}{\mu} + \frac{K_{valve}}{\mu} u \\ \frac{\gamma RT(\dot{m}_{i1} - \dot{m}_{o1}) - \gamma A x_4 x_2}{V_{o1} + A(\frac{L}{2} + x_5)} \\ \frac{\gamma RT(\dot{m}_{i2} - \dot{m}_{o2}) + \gamma A x_4 x_3}{V_{o1} + A(\frac{L}{2} - x_5)} \\ \frac{1}{M}\left(Ax_2 - Ax_3 - bx_4 - \left(\sigma_0 x_6 + \sigma_1 \dot{x}_6\right)\right) \\ x_4 \\ x_4 - \frac{\sigma_0 |x_4| x_6}{F_{sl} + (F_{st} - F_{sl}) e^{-(\frac{x_4}{v_s})^2}} \end{Bmatrix} \tag{4.23}$$

where x_1 denotes to the control valve position, x_2 and x_3 are the pressures in the actuator, x_4 is the piston's position, x_5 is the velocity of the piston and x_6 is the average bristle deflection in LuGre friction model, Mass flows $\dot{m}_{i1}$, $\dot{m}_{o1}$, $\dot{m}_{i2}$ and $\dot{m}_{o2}$ are given either by equation (4.11) to (4.17).

$$u = K_p(x_{desired} - x_5) + K_i I \tag{4.24}$$

$$I(t) = \begin{cases} \frac{-u_{lower} - K_p\left(x_{desired} - x_5\right)}{K_i} & \dot{e}_{deadband} > \varepsilon \;\&\; u(t) > -u_{lower} \\ I(t-\Delta t) + \left(x_{desired} - x_5\right)\Delta t & \left|\dot{e}_{deadband} \le \varepsilon\right| \\ \frac{u_{upper} - K_p\left(x_{desired} - x_5\right)}{K_i} & \dot{e}_{deadband} > \varepsilon \;\&\; u(t) < u_{up} \\ 0 & \dot{x}_{desired}(t) = 0 \;\&\; \left|\left(x_{desired} - x_5\right)\right| \le \tilde{\varepsilon} \end{cases} \tag{4.25}$$

where $\dot{e}_{deadband} = (v_{desired} - x_4)\frac{v_{desired}^2}{v_{desired}^2 + \beta x_4^2}$

In order to find the equilibrium points of the pneumatic system, the right hand side of

equation (4.22) is set to zero. Thus, the system has fixed values for the position (x_5), velocity ($x_4 = 0$) and control valve position ($x_1 = 0$) corresponding to the desired piston position in the control design. The values of Chamber 1 pressure (x_2), Chamber 2 pressure (x_3), the LuGre model variable (x_6) are not unique, i.e., there exist multiple values of pressures; with x_6 in the LuGre model corresponding to the controlled desired piston position. In other words, the system has a set of infinite non-isolated equilibrium points where three of the six variables of the system can have various values, two of which, x_2 and x_3, can arbitrarily change and the third one, x_6, is derived from the equation $Ax_2 - Ax_3 - \sigma_0 x_6 - F_L = 0$.

The parameters of the pneumatic actuator model studied in this work, are shown in Table 4.1, which are taken from previous work (Karpenko, 2003).

4.2 Simplified pneumatic actuator

4.2.1 Dynamic model

Due to the complication of the pneumatic system, a simplified pneumatic system will be developed to study Wolf's method calculating Lyapunov Exponents for a system with a set of equilibrium points. The control valve of the pneumatic system in Fig. 4.2 was removed and the chambers were closed. The simplified system is shown in Fig. 4.4.

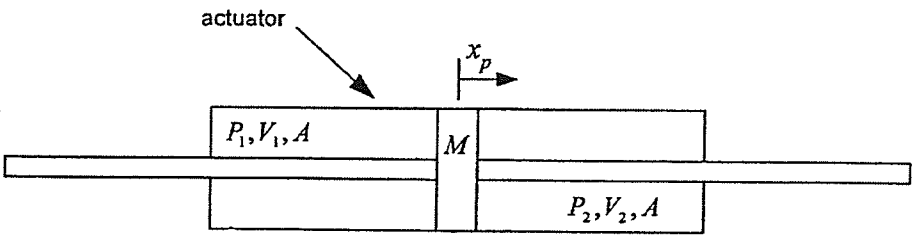

Fig. 4.4 Pneumatic actuator with valve closed

Table 4.1 Parameters of the pneumatic actuator model

Parameter	Symbol	Nominal Value
Supply pressure	P_s	5(bars)
Atmospheric pressure	P_{atm}	1(bar)
Total mass of piston, rods and load	M	1.91(kg)
Viscous damping coefficient	b	70 (N • sec/m)
Actuator stroke	L	500(mm)
Piston annulus area	A	10.6(cm^2)
Cylinder dead volume	V_{o1}, V_{o2}	5(mm^3)
Ideal gas constant	R	287(J/kg • K)
Temperature of air source	T	300(K)
Ratio of specific hearts	γ	1.4
Pressure-volume work correction factor	α	0.89
Valve coefficient of discharge	C_d	0.7
Valve orifice area gradient	w	22.6(mm^2/mm)
Min/Max valve spool displacement	$x_{v,\max} / x_{v,\min}$	+/— 1.25 (mm)
Valve deadband	—	4.7<u<5.6 (V)
Valve spool position gain	K_{valve}	0.25 (mm/V)
Valve first-order time constant	μ	4.2 (m • sec)
Valve critical pressure ratio	P_{cr}	0.2
Static friction	F_s	40 (N)
Coulomb friction	F_c	20 (N)
LuGre friction model pareameter	σ_0	200(N/m)
LuGre friction model parameter	σ_1	2(N/m)
Viscous velocity	v_s	0.0033 (m/s)
The velocity threshold	ε	0.005(m/s)
The position threshold	$\tilde{\varepsilon}$	0.004(m)

Because the chambers are closed, both $\dot{m}_1$ and $\dot{m}_2$ are zero. The control valve variable, x_v, and friction will be removed for simplicity. The volume of each chamber is calculated as follows:

$$\begin{aligned} V_1 &= A\left(\frac{L}{2}+x_p\right) \\ V_2 &= A\left(\frac{L}{2}-x_p\right) \end{aligned} \tag{4.26}$$

The dynamic model of the pneumatic system (equation (4.22)) is changed to:

$$\begin{aligned} \dot{x}_p &= v_p \\ \dot{v}_p &= \frac{1}{M}\left(-bv_p + AP_1 - AP_2\right) \\ \dot{P}_1 &= -\frac{\gamma P_1 A}{A\left(\frac{L}{2}+x_p\right)}\dot{x}_p \\ \dot{P}_2 &= \frac{\gamma P_2 A}{A\left(\frac{L}{2}-x_p\right)}\dot{x}_p \end{aligned} \tag{4.27}$$

where the parameters and variables are defined in Table 4.1.

Rewriting the dynamic model (equation (4.27)) in the state-space model as:

$$\begin{aligned} \dot{x}_1 &= \frac{-\gamma A x_1 x_3}{A\left(\frac{L}{2}+x_4\right)} \\ \dot{x}_2 &= \frac{\gamma A x_2 x_3}{A\left(\frac{L}{2}-x_4\right)} \\ \dot{x}_3 &= \frac{1}{M}(Ax_1 - Ax_2 - bx_3) \\ \dot{x}_4 &= x_3 \end{aligned} \tag{4.28}$$

where x_1 and x_2 denote the pressures (P_1 and P_1) in the actuator, x_3 denotes to the velocity of the piston and x_4 denotes to the piston's position.

With reference to Fig. 4.4, when there is a pressure difference between the two chambers (P_1 and P_2), the piston will move. If there is only viscous friction, the piston will stop after oscillating for a period of time. In the steady state, both pressures in the chambers are equal to each other. However, the values of the pressures are not unique. Given different initial pressures, the position of the piston will be different; but the velocity of the piston is zero. Thus, the system has a set of infinite non-isolated equilibrium points. In order to find the equilibrium points of the simplified pneumatic system, the equation (4.28) is set to equal zero. Thus, the system has fixed values for the position (x_4) and velocity ($x_3 = 0$). However, the values of the pressure (x_1) with Chamber 1 and the pressure (x_2) within Chamber 2 can be any value as long as $x_1 = x_2$. In other words, the system has a set of infinite non-isolated equilibrium points where two of the four variables of the system can have various values.

4.3 Calculation of Lyapunov Exponents for simplified pneumatic actuator

4.3.1 Calculation of Lyapunov Exponents from the mathematic model

In the simulation, the initial condition is first set as $\{2.5bar, 2.0bar, 0.0mm, 0.0mm/s\}$, where the piston moved to the right due to the pressure difference. The simulation results of the piston position, velocity and chamber pressures are shown in Fig.4.5. This figure shows, that the piston moves to the 55 mm and the velocity is zero at the steady state because of the viscous friction. The pressure of Chamber 1 decreases and the pressure of Chamber 2 increases. The two pressures equal each other (2.25 (bar)) at the steady state since there is no friction. Four Lyapunov Exponents calculated from the mathematic model are shown in Fig.

4.6. As shown, all of the Lyapunov Exponents converge. There are two zero exponents and two negative exponents. However, there is no limit cycle or torus in response.

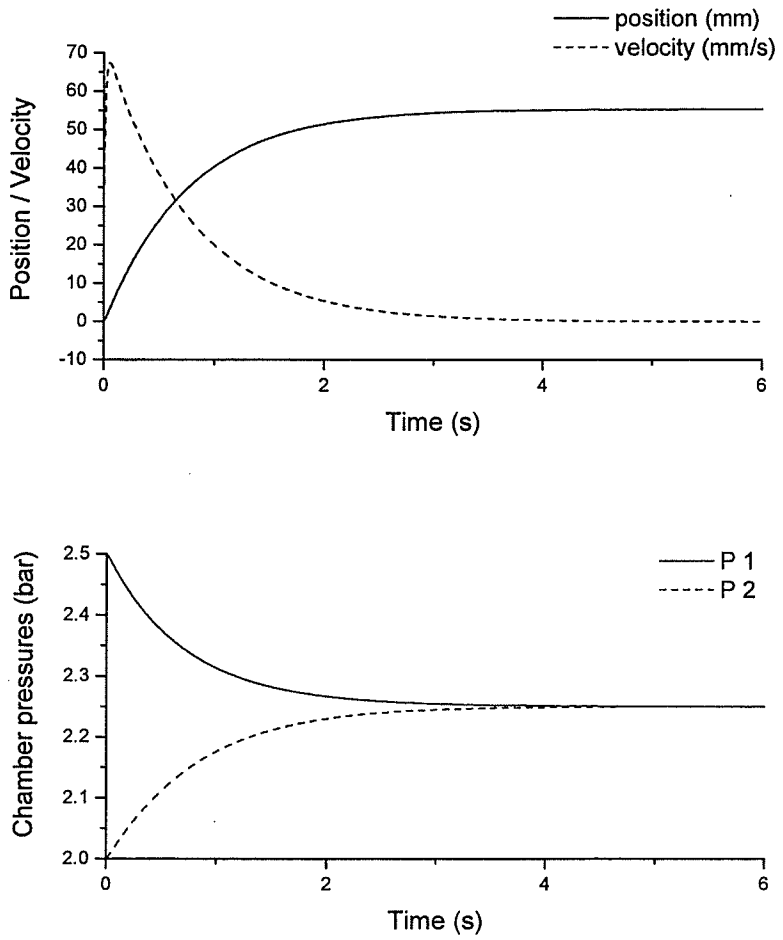

Fig. 4.5 Simulation results of position, velocity and pressures

Based on the procedure outlined in Section 2.3.1, the variation equation is as follows:

$$\dot{\psi}_t = F(t)\psi_t \tag{4.29}$$

The above equation should be integrated simultaneously with the original nonlinear equation (4.28). The initial conditions for numerical integrations are $\begin{Bmatrix} x(t_0) \\ \psi(t_0) \end{Bmatrix} = \begin{Bmatrix} x_0 \\ I \end{Bmatrix}$ where I is the identity matrix. The Lyapunov Exponents are calculated by following the evolution of the

area of the hyperellipsoid spanned by $\delta x_1, \delta x_2 ..., \delta x_n$ via separately following the evolutions of $\delta x_1, \delta x_2 ..., \delta x_n$ using any integration method. The Jacobian is:

$$F(t) = \begin{bmatrix} \frac{-\gamma A x_3}{A\left(\frac{L}{2}+x_4\right)} & 0 & \frac{-\gamma A x_1}{A\left(\frac{L}{2}+x_4\right)} & \frac{\gamma A x_1 x_3}{A\left(\frac{L}{2}+x_4\right)^2} \\ 0 & \frac{\gamma A x_3}{A\left(\frac{L}{2}-x_4\right)} & \frac{\gamma A x_2}{A\left(\frac{L}{2}-x_4\right)} & \frac{-\gamma A x_2 x_3}{A\left(\frac{L}{2}-x_4\right)^2} \\ \frac{A}{M} & -\frac{A}{M} & -\frac{b}{M} & 0 \\ 0 & 0 & 1 & 0 \end{bmatrix} \tag{4.30}$$

Based on the procedure outlined in 2.3.1, the Lyapunov Exponents for the pneumatic actuator are defined as:

$$\lambda_i \approx \frac{1}{Kh}\sum_{k=1}^{K}\log_2\left\|u_i^k\right\| \qquad \text{where } i = 1,2,3,4 \tag{4.31}$$

$$\begin{aligned} u_1 &= \frac{v_1}{\|v_1\|} \\ u_2 &= \frac{v_2 - < v_2, u_1 > u_1}{\|v_2 - < v_2, u_1 > u_1\|} \\ u_3 &= \frac{v_3 - < v_3, u_2 > u_2 - < v_3, u_1 > u_1}{\|v_3 - < v_3, u_2 > u_2 - < v_3, u_1 > u_1\|} \\ u_4 &= \frac{v_4 - < v_4, u_3 > u_3 - < v_4, u_2 > u_2 - < v_4, u_1 > u_1}{\|v_4 - < v_4, u_3 > u_3 - < v_4, u_2 > u_2 - < v_4, u_1 > u_1\|} \end{aligned} \tag{4.32}$$

The vector v_i^k is equal to δx_i^k, and vector u_i^k is a normalized version of v_i^k.

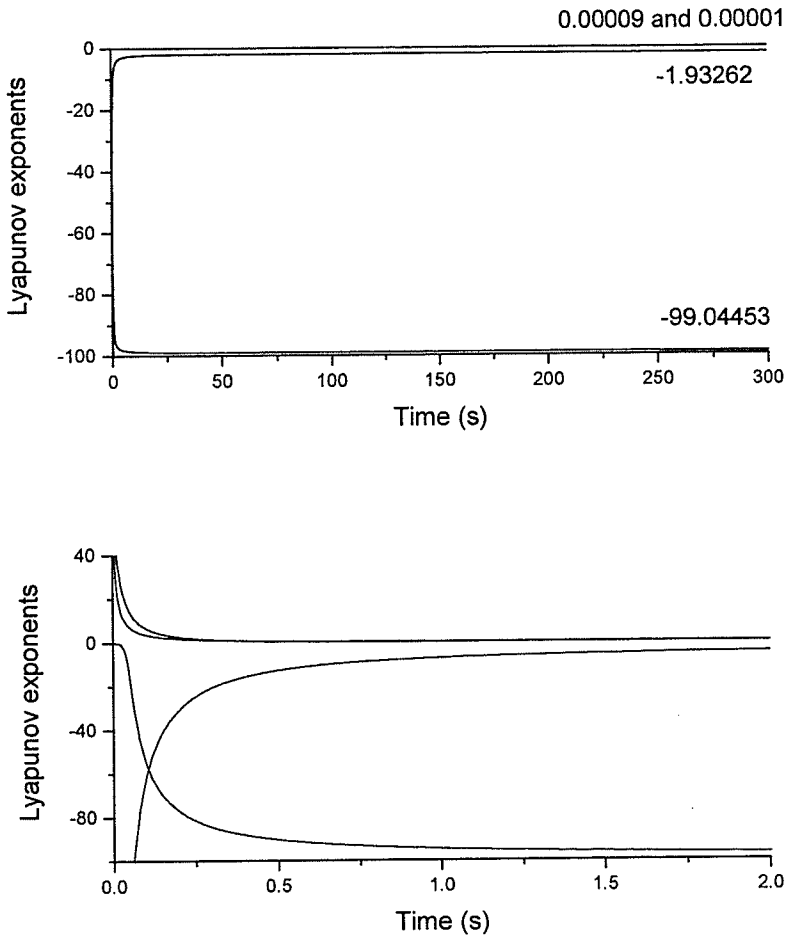

Fig. 4.6 Lyapunov Exponents using mathematical model and the close-up

In the second test, the initial condition was changed to $\{ 3.0bar , 2.5bar , 0.0mm, 0.0mm/s \}$, and the piston moved to the right due to the different pressures. The piston position and velocity as well as pressures are shown in Fig. 4.7. The position moves 100 mm and the velocity is zero at the steady state. The pressure of Chamber 1 decreases and the pressure of Chamber 2 increases. Both pressures are 2.5 (bar) at the steady state. The Lyapunov Exponents are calculated again from the mathematic model and are shown in Fig. 4.8.

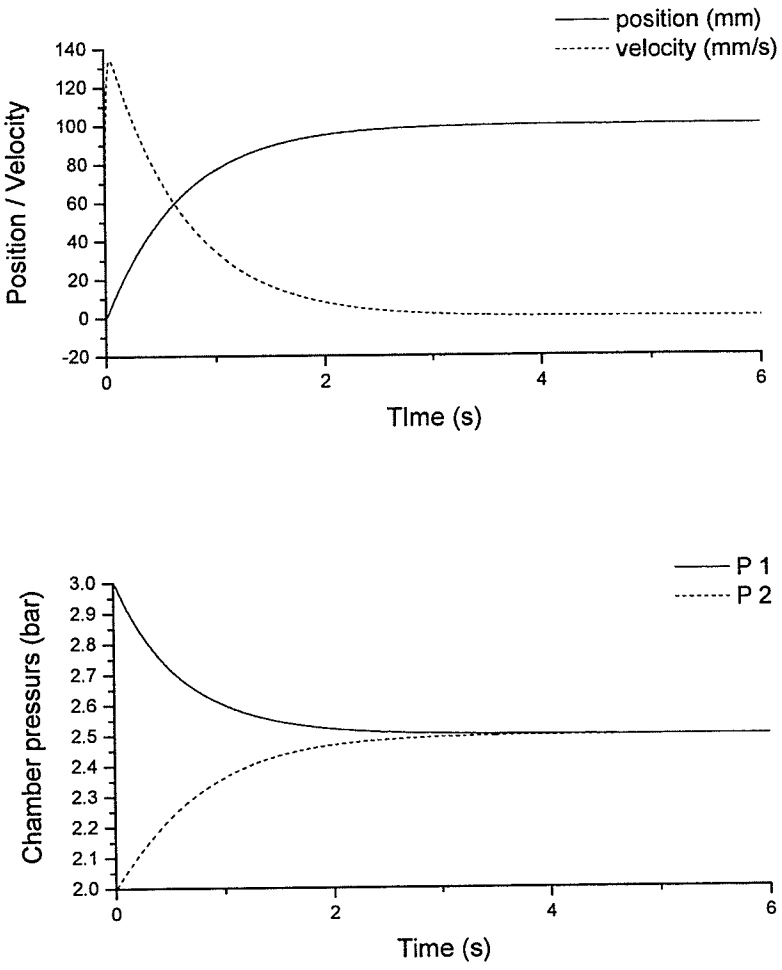

Fig. 4.7 Simulation results of position, velocity and pressures

Comparing the simulation results of Fig. 4.5 and Fig. 4.7, the position of the piston and both chambers pressure have different steady state values with different initial conditions. The results of the Lyapunov Exponents in Fig. 4.6 and Fig. 4.8 show, that there are two zero Exponents. The values of the negative Lyapunov Exponents do not change given different initial conditions. As in the original concept of the Lyapunov Exponents, the zero exponents indicate that the system is in some sort of steady state mode with some variables of the system having an attracting period orbit, i.e., the limit cycle. However, from the simulation

results it is observed that, in this case, there is no limit cycle or period orbit in the simplified pneumatic system. They are obtained because the simplified pneumatic system has a set of infinite non-isolated equilibrium points.

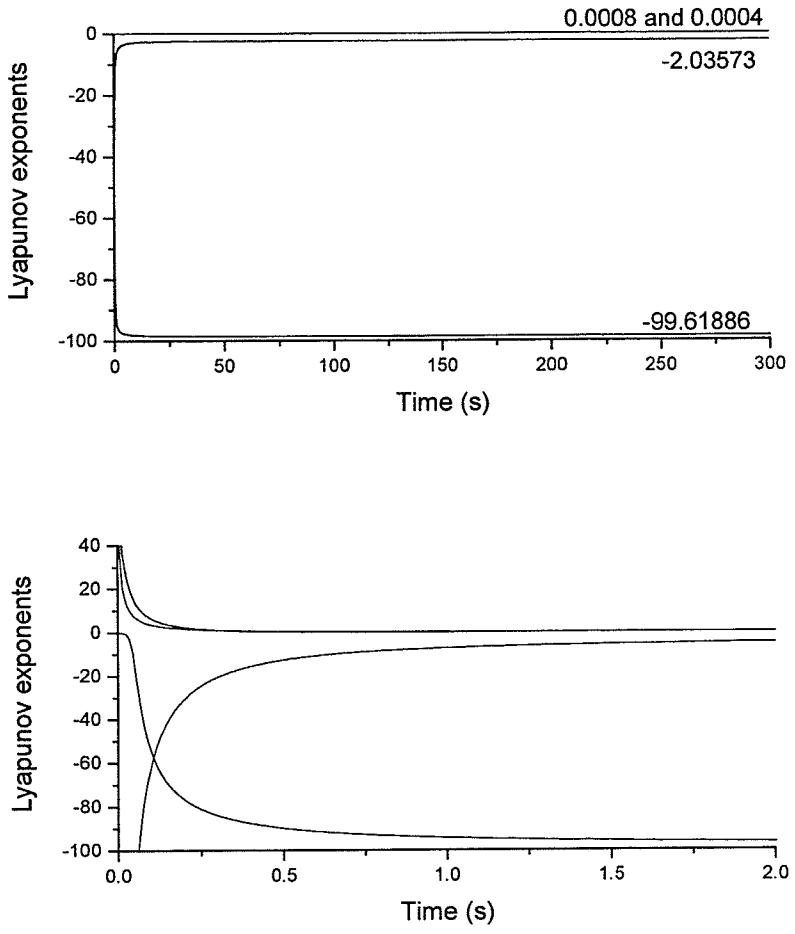

Fig. 4.8 Lyapunov Exponents using the mathematical model and the close-up

Note that the steady-state pressures of the two chambers can be different by setting different initial pressures, as long as the steady-state pressure differential is zero. If the initial condition of the pressures is changed, the position of the piston at the steady state will be different. This means that, only the velocity of the piston is fixed at the steady state. The

position and the two pressures will change with the initial condition.

4.3.2 Calculation of the largest Lyapunov exponent from time series

Given the initial condition $\{ 2.5bar , 2.0bar , 0.0mm , 0.0mm/s \}$, the largest Lyapunov exponent is calculated from the time series of the position of the piston and the pressure of Chamber 1 is recorded from the simulation, shown in Fig. 4.9 to 4.12.

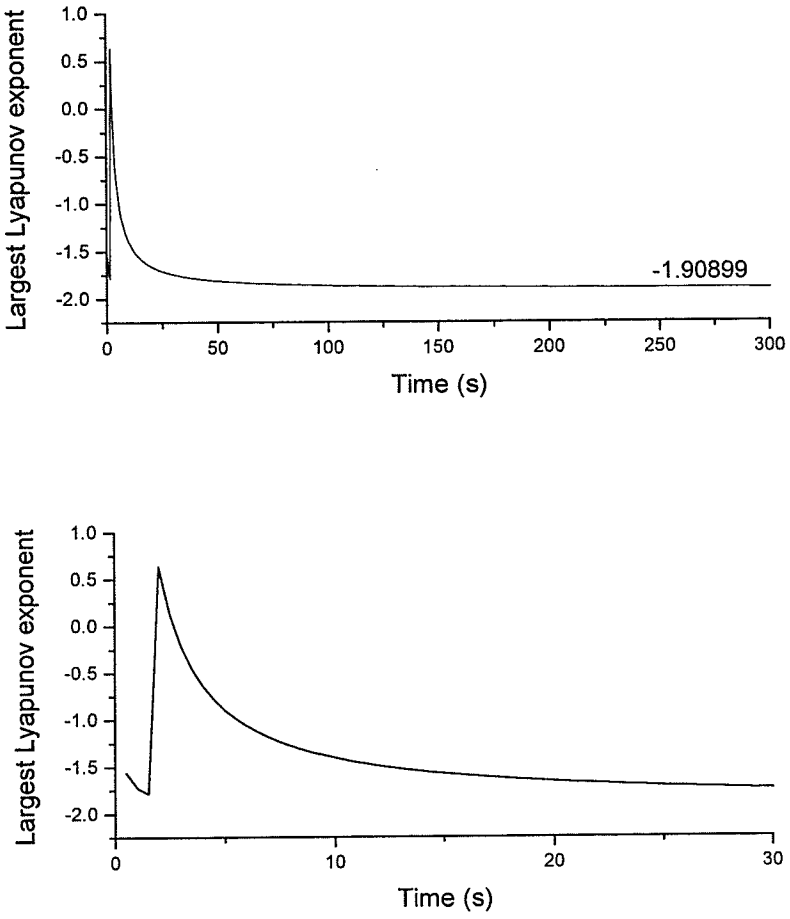

Fig. 4.9 Largest Lyapunov exponent from time series of position and the close-up

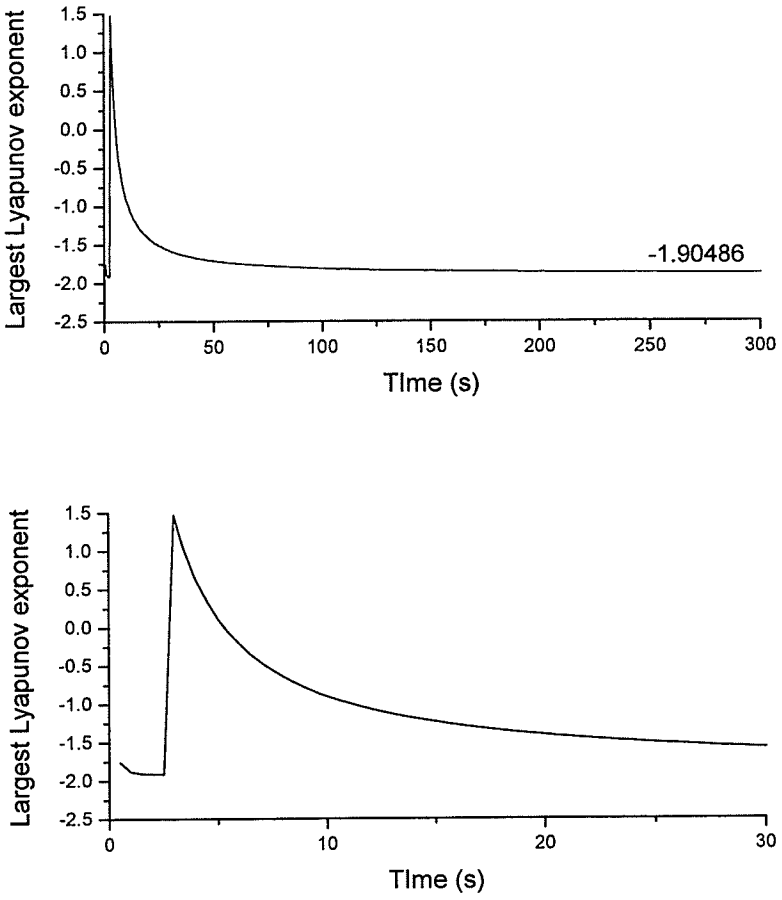

Fig. 4.10 Largest Lyapunov exponent from time series of Pressure 1 and the close-up

In the Fig. 4.9 and Fig. 4.10, both of the largest Lyapunov Exponents calculated from the time series of the piston position and the pressure of Chamber 1 converge to -1.9. The same largest Lyapunov exponent was obtained from the other variable recorded data of this system.

When the initial condition is $\{3.0(bar), 2.0(bar), 0.0(mm), 0.0(mm/s)\}$, the largest Lyapunov exponent is also calculated from the time series of the position of the piston and Pressure 1 recorded from the simulation.

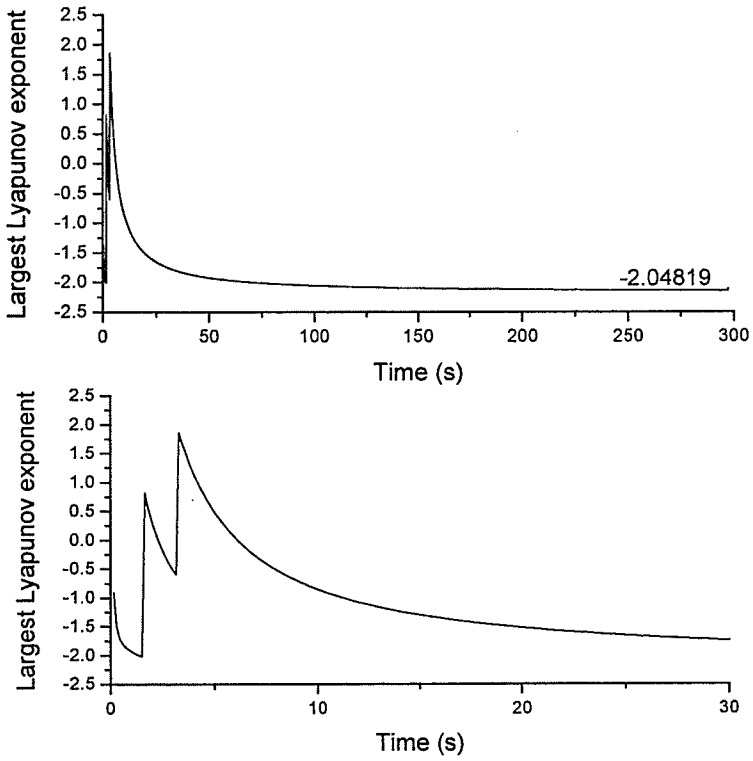

Fig. 4.11 Largest Lyapunov exponent from time series of the position and the close-up

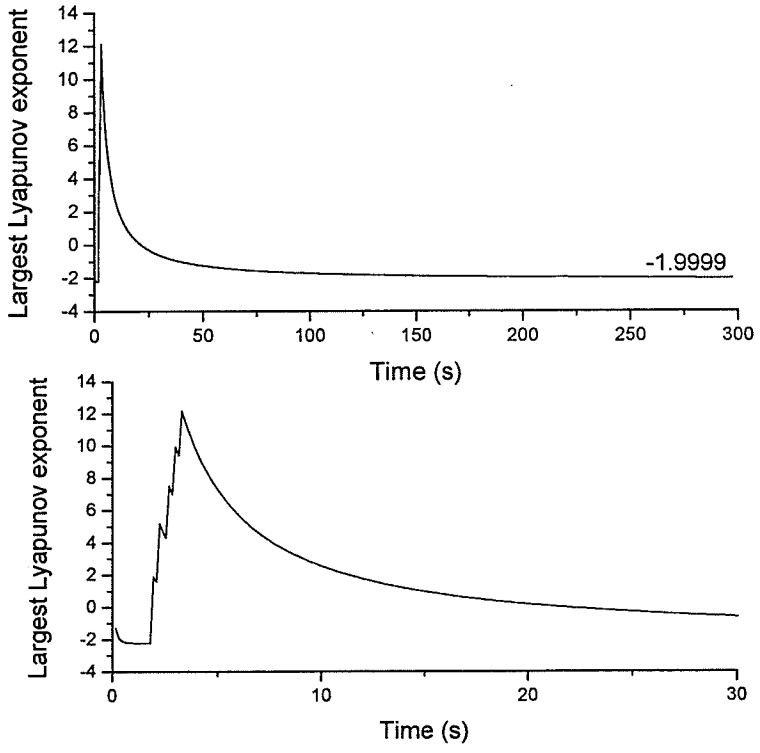

Fig. 4.12 Largest Lyapunov exponent from time series of Pressure 1 and the close-up

In the Fig. 4.11 and Fig. 4.12, both of the largest Lyapunov Exponents calculated from the time series of the piston position and the pressure of Chamber 1 converge to -2.0. The same largest Lyapunov exponent was obtained from the other variable recorded data of this system.

From Fig.4.9 to 4.12, it is seen that the largest Lyapunov exponent calculated from time series of different variable recorded data converges to about -1.95, which is significantly different from zero calculated from the mathematic model. This indicates that Wolf's method using time series can not be used to calculate the largest zero Lyapunov exponent for this simplified pneumatic system.

4.4 Calculation of Lyapunov Exponents for the complete pneumatic system

4.4.1 Calculation of Lyapunov Exponents using the mathematical model

In the simulation, the pneumatic system is controlled to move to a desired position or follow the desired trajectory tracking under a nonlinear PI controller described earlier. Lyapunov Exponents for the pneumatic control system under study are first calculated from the mathematic model. Based on the procedure outlined in Section 2.3.1, the variation equation is as follows:

$$\dot{\psi}_t = F(t)\psi_t \tag{4.33}$$

The above equation should be integrated simultaneously with the original nonlinear equation (4.22). The initial conditions for numerical integrations are $\begin{Bmatrix} x(t_0) \\ \psi(t_0) \end{Bmatrix} = \begin{Bmatrix} x_0 \\ I \end{Bmatrix}$ where I is the identity matrix. The Lyapunov Exponents are calculated by following the evolution of the

area of the hyperellipsoid spanned by $\delta x_1, \delta x_2 ..., \delta x_n$ via separately following the evolutions of $\delta x_1, \delta x_2 ..., \delta x_n$ using any integration method. The Jacobian is:

$$F(t) = \begin{bmatrix} a_{11} & a_{12} & a_{13} & a_{14} & a_{15} & a_{16} \\ a_{21} & a_{22} & a_{23} & a_{24} & a_{25} & a_{26} \\ a_{31} & a_{32} & a_{33} & a_{34} & a_{35} & a_{36} \\ a_{41} & a_{42} & a_{43} & a_{44} & a_{45} & a_{46} \\ a_{51} & a_{52} & a_{53} & a_{54} & a_{55} & a_{56} \\ a_{61} & a_{62} & a_{62} & a_{64} & a_{65} & a_{66} \end{bmatrix} \tag{4.34}$$

where

$$a_{11} = -\frac{1}{\mu}; \tag{4.35.a}$$

$$a_{12} = a_{13} = a_{14} = a_{16} = 0; \tag{4.35.b}$$

$$a_{15} = \frac{K_v\left(-K_p + K_i \dfrac{dI}{dx_5}\right)}{\mu}; \tag{4.35.c}$$

$$a_{21} = \frac{\gamma RT\left(\dfrac{dm_{i1}}{dx_1} - \dfrac{dm_{o1}}{dx_1}\right)}{V_{o1} + A\left(\dfrac{L}{2} + x_5\right)}; \tag{4.35.d}$$

$$a_{22} = \frac{\gamma RT\left(\dfrac{dm_{i1}}{dx_2} - \dfrac{dm_{o1}}{dx_2}\right) - \gamma A x_4}{V_{o1} + A\left(\dfrac{L}{2} + x_5\right)}; \tag{4.35.e}$$

$$a_{23} = a_{26} = 0; \tag{4.35.f}$$

$$a_{24} = \frac{-\gamma A x_2}{V_{o1} + A\left(\dfrac{L}{2} + x_5\right)}; \tag{4.35.g}$$

$$a_{32} = a_{36} = 0; \tag{4.35.h}$$

$$a_{25} = \frac{-A(\gamma RT(m_{i2} - m_{o2}) - \gamma A x_4 x_2)}{\left(V_{o1} + A\left(\frac{L}{2} + x_5\right)\right)^2}; \tag{4.35.i}$$

$$a_{31} = \frac{\gamma RT\left(\frac{dm_{i2}}{dx_1} - \frac{dm_{o2}}{dx_1}\right)}{V_{o2} + A\left(\frac{L}{2} - x_5\right)}; \tag{4.35.j}$$

$$a_{33} = \frac{\gamma RT\left(\frac{dm_{i2}}{dx_3} - \frac{dm_{o2}}{dx_3}\right) + \gamma A x_4}{V_{o1} + A\left(\frac{L}{2} - x_5\right)}; \tag{4.35.k}$$

$$a_{34} = \frac{\gamma A x_3}{V_{o2} + A\left(\frac{L}{2} - x_5\right)}; \tag{4.35.l}$$

$$a_{35} = \frac{A(\gamma RT(m_{i2} - m_{o2}) + \gamma A x_4 x_3)}{\left(V_{o1} + A\left(\frac{L}{2} - x_5\right)\right)^2}; \tag{4.35.m}$$

$$a_{41} = a_{45} = 0; \tag{4.35.n}$$

$$a_{42} = \frac{A}{M}; \tag{4.35.o}$$

$$a_{43} = -\frac{A}{M}; \tag{4.35.p}$$

$$a_{44} = -\frac{1}{M}\left(\beta + \frac{dF_f}{dx_4}\right); \tag{4.35.q}$$

$$a_{51} = a_{52} = a_{53} = a_{55} = a_{56} = a_{61} = a_{62} = a_{63} = a_{65} = 0; \tag{4.35.r}$$

$$a_{54} = 1; \tag{4.35.s}$$

$$a_{64} = 1 - \left(\frac{\sigma_0 dx_{4abs} x_6}{F_{sl} + (F_{st} - F_{sl}) e^{-\left(\frac{x_4}{V_x}\right)^2}} + \frac{2\sigma_0 |x_4| (F_{st} - F_{sl}) e^{-\left(\frac{x_4}{V_s}\right)^2} x_4 x_6}{v_s^2 \left(F_{sl} + (F_{st} - F_{sl}) e^{-\left(\frac{x_4}{V_s}\right)^2} \right)^2} \right) \tag{4.35.t}$$

where

$$\frac{dm_{i1}}{dx_1}=\begin{cases}\dfrac{C_d w P_s}{\sqrt{T}}\sqrt{\dfrac{\gamma}{R}\left(\dfrac{2}{\gamma+1}\right)^{(\gamma+1)/(\gamma-1)}} & \dfrac{x_2}{P_s}\le P_{cr}\\ \dfrac{C_d w P_s}{\sqrt{T}}\sqrt{\dfrac{\gamma}{R}\left(\dfrac{2}{\gamma+1}\right)^{(\gamma+1)/(\gamma-1)}}\sqrt{1-\left(\dfrac{x_2/P_s-P_{cr}}{1-P_{cr}}\right)^2} & \dfrac{x_2}{P_s}>P_{cr}\end{cases} \tag{4.36.a}$$

$$\frac{dm_{i1}}{dx_2}=\begin{cases}0 & \dfrac{x_2}{P_s}\le P_{cr}\\ -\dfrac{C_d|x_1|wP_s}{\sqrt{T}}\sqrt{\dfrac{\gamma}{R}\left(\dfrac{2}{\gamma+1}\right)^{(\gamma+1)/(\gamma-1)}}\dfrac{\left(\dfrac{x_2/P_s-P_{cr}}{1-P_{cr}}\right)}{P_s\sqrt{1-\left(\dfrac{x_2/P_s-P_{cr}}{1-P_{cr}}\right)^2}} & \dfrac{x_2}{P_s}>P_{cr}\end{cases} \tag{4.36.b}$$

$$\frac{dm_{o1}}{dx_1}=\begin{cases}-\dfrac{C_d w x_2}{\sqrt{T}}\sqrt{\dfrac{\gamma}{R}\left(\dfrac{2}{\gamma+1}\right)^{(\gamma+1)/(\gamma-1)}} & \dfrac{P_e}{x_2}\le P_{cr}\\ -\dfrac{C_d w x_2}{\sqrt{T}}\sqrt{\dfrac{\gamma}{R}\left(\dfrac{2}{\gamma+1}\right)^{(\gamma+1)/(\gamma-1)}}\sqrt{1-\left(\dfrac{P_e/x_2-P_{cr}}{1-P_{cr}}\right)^2} & \dfrac{P_e}{x_2}>P_{cr}\end{cases} \tag{4.36.c}$$

$$\frac{dm_{o1}}{dx_2}=\begin{cases}\dfrac{C_d w|x_1|}{\sqrt{T}}\sqrt{\dfrac{\gamma}{R}\left(\dfrac{2}{\gamma+1}\right)^{(\gamma+1)/(\gamma-1)}} & \dfrac{P_e}{x_2}\le P_{cr}\\ \dfrac{C_d w|x_1|}{\sqrt{T}}\sqrt{\dfrac{\gamma}{R}\left(\dfrac{2}{\gamma+1}\right)^{(\gamma+1)/(\gamma-1)}}\sqrt{1-\left(\dfrac{P_e/x_2-P_{cr}}{1-P_{cr}}\right)^2}+\dfrac{C_d|x_1|x_2 w}{\sqrt{T}}\sqrt{\dfrac{\gamma}{R}\left(\dfrac{2}{\gamma+1}\right)^{(\gamma+1)/(\gamma-1)}}\dfrac{P_e\dfrac{P_e/x_2-P_{cr}}{(1-P_{cr})^2}}{x_2^2\sqrt{1-\left(\dfrac{P_e/x_2-P_{cr}}{1-P_{cr}}\right)^2}} & \dfrac{P_e}{x_2}>P_{cr}\end{cases} \tag{4.36.d}$$

$$\frac{dm_{i2}}{dx_1}=\begin{cases}-\dfrac{C_d w P_s}{\sqrt{T}}\sqrt{\dfrac{\gamma}{R}\left(\dfrac{2}{\gamma+1}\right)^{(\gamma+1)/(\gamma-1)}} & \dfrac{x_3}{P_s}\le P_{cr}\\ -\dfrac{C_d w P_s}{\sqrt{T}}\sqrt{\dfrac{\gamma}{R}\left(\dfrac{2}{\gamma+1}\right)^{(\gamma+1)/(\gamma-1)}}\sqrt{1-\left(\dfrac{x_3/P_s-P_{cr}}{1-P_{cr}}\right)^2} & \dfrac{x_3}{P_s}\le P_{cr}\end{cases} \tag{4.36.e}$$

$$\frac{dm_{i2}}{dx_3}=\begin{cases}0 & \dfrac{x_3}{P_x}\le P_{cr}\\ -\dfrac{C_d|x_1|wP_s}{\sqrt{T}}\sqrt{\dfrac{\gamma}{R}\left(\dfrac{2}{\gamma+1}\right)^{(\gamma+1)/(\gamma-1)}}\dfrac{\dfrac{x_3/P_s-P_{cr}}{(1-P_{cr})^2}}{P_s\sqrt{1-\left(\dfrac{x_3/P_s-P_{cr}}{1-P_{cr}}\right)^2}} & \dfrac{x_3}{P_x}>P_{cr}\end{cases} \tag{4.36.f}$$

$$\frac{dm_{o2}}{dx_1}=\begin{cases}\dfrac{C_d w x_3}{\sqrt{T}}\sqrt{\dfrac{\gamma}{R}\left(\dfrac{2}{\gamma+1}\right)^{(\gamma+1)/(\gamma-1)}} & \dfrac{P_e}{x_3}\le P_{cr}\\ \dfrac{C_d w x_3}{\sqrt{T}}\sqrt{\dfrac{\gamma}{R}\left(\dfrac{2}{\gamma+1}\right)^{(\gamma+1)/(\gamma-1)}}\sqrt{1-\left(\dfrac{P_e/x_3-P_{cr}}{1-P_{cr}}\right)^2} & \dfrac{P_e}{x_3}>P_{cr}\end{cases} \tag{4.36.g}$$

$$\frac{dm_{o2}}{dx_3}=\begin{cases}\dfrac{C_d w|x_1|}{\sqrt{T}}\sqrt{\dfrac{\gamma}{R}\left(\dfrac{2}{\gamma+1}\right)^{(\gamma+1)/(\gamma-1)}} & \dfrac{P_e}{x_3}\le P_{cr}\\ \dfrac{C_d w|x_1|}{\sqrt{T}}\sqrt{\dfrac{\gamma}{R}\left(\dfrac{2}{\gamma+1}\right)^{(\gamma+1)/(\gamma-1)}}\sqrt{1-\left(\dfrac{P_e/x_3-P_{cr}}{1-P_{cr}}\right)^2}+\dfrac{C_d w|x_1|x_3}{\sqrt{T}}\sqrt{\dfrac{\gamma}{R}\left(\dfrac{2}{\gamma+1}\right)^{(\gamma+1)/(\gamma-1)}}\dfrac{P_e\dfrac{P_e/x_3-P_{cr}}{(1-P_{cr})^2}}{x_3^2\sqrt{1-\left(\dfrac{P_e/x_3-P_{cr}}{1-P_{cr}}\right)^2}} & \dfrac{P_e}{x_3}>P_{cr}\end{cases} \tag{4.36.h}$$

$$\frac{dF_f}{dx_4}=\sigma_1-\sigma_1\left(\frac{\sigma_0 dx_{4abs}x_6}{F_{sl}+(F_{st}-F_{sl})e^{-\left(\frac{x_4}{V_x}\right)^2}}+\frac{2\sigma_0|x_4|(F_{st}-F_{sl})e^{-\left(\frac{x_4}{v_s}\right)^2}x_4x_6}{v_s^2\left(F_{sl}+(F_{st}-F_{sl})e^{-\left(\frac{x_4}{v_s}\right)^2}\right)^2}\right) \tag{4.36.i}$$

$$dx_{4abs}=\begin{cases}1 & x_4>0\\ -1 & x_4<0\end{cases} \tag{4.36.j}$$

$$\frac{dI}{dx_5}=\begin{cases}\dfrac{K_p}{K_i} & \dot{e}_{deadband}>\varepsilon\ \&\ u(t)>-u_{lower}\\ -\Delta t & \left|\dot{e}_{deadband}\le\dot{e}_{\min}\right|\\ \dfrac{K_p}{K_i} & \dot{e}_{deadband}>\varepsilon\ \&\ u(t)<u_{up}\\ 0 & \dot{x}_{desired}(t)=0\ \&\left|\left(x_{desired}-x_5\right)\right|\le\tilde{\varepsilon}\end{cases} \tag{4.36.k}$$

In the calculation, there are non-smooth terms in the mathematic model. At the instants of switching points due to the discontinuity, the linearized equations are evaluated using the indicator function, $h(x)$ and the transition function, $g(x)$, both defined based on the physical behavior of the system. The non-smooth parts come from $|x_4|$ and $I(t)$ in the mathematical model (equation (4.22)) of the pneumatic system.

- At $t=t_1$, $x_4=0$ and $|x_4|$ changes from $-x_4$ to x_4

The indicator function is $$h_1 = -x_4 - x_4 = 0 \tag{4.37}$$

Jacobian of the indicator function is

$$H_1 = \left[\frac{\partial h_1}{\partial x_1} \quad \frac{\partial h_1}{\partial x_2} \quad \frac{\partial h_1}{\partial x_3} \quad \frac{\partial h_1}{\partial x_4} \quad \frac{\partial h_1}{\partial x_5} \quad \frac{\partial h_1}{\partial x_6}\right] = \begin{bmatrix} h_{11} & h_{12} & h_{13} & h_{14} & h_{15} & h_{16} \end{bmatrix} \tag{4.38}$$

Jacobian of the transition condition is $$G_1 = \begin{bmatrix} 1 & 0 & 0 & 0 & 0 & 0 \\ 0 & 1 & 0 & 0 & 0 & 0 \\ 0 & 0 & 1 & 0 & 0 & 0 \\ 0 & 0 & 0 & 1 & 0 & 0 \\ 0 & 0 & 0 & 0 & 1 & 0 \\ 0 & 0 & 0 & 0 & 0 & 1 \end{bmatrix} \tag{4.39}$$

Following the guideline in Section 2.3.1.2 and equation (2.17), the new value of variation equation $\psi_{t=t_1^+}$ is given below:

$$\delta x\left(t_1^+\right) = G_1\left(x^-\right)\delta x\left(t_1^-\right) - \left[G_1\left(x^-\right) f_1\left(x\left(t_1^-\right)\right) - f_2\left(x\left(t_1^+\right)\right)\right]\frac{H_1\left(x^-\right)\delta x\left(t_1^-\right)}{H_1\left(x^-\right) f_1\left(x\left(t_1^-\right)\right)} \tag{4.40}$$

where "+" and "—" denote just after and before switch instants t_1. Rewriting equation (4.40),

$$\begin{bmatrix} x_7^{new} & x_8^{new} & x_9^{new} & x_{10}^{new} & x_{11}^{new} & x_{12}^{new} \\ x_{13}^{new} & x_{14}^{new} & x_{15}^{new} & x_{16}^{new} & x_{17}^{new} & x_{18}^{new} \\ x_{19}^{new} & x_{20}^{new} & x_{21}^{new} & x_{22}^{new} & x_{23}^{new} & x_{24}^{new} \\ x_{25}^{new} & x_{26}^{new} & x_{27}^{new} & x_{28}^{new} & x_{29}^{new} & x_{30}^{new} \\ x_{31}^{new} & x_{32}^{new} & x_{33}^{new} & x_{34}^{new} & x_{35}^{new} & x_{36}^{new} \\ x_{37}^{new} & x_{38}^{new} & x_{39}^{new} & x_{40}^{new} & x_{41}^{new} & x_{42}^{new} \end{bmatrix} = \begin{bmatrix} 1 & 0 & 0 & 0 & 0 & 0 \\ 0 & 1 & 0 & 0 & 0 & 0 \\ 0 & 0 & 1 & 0 & 0 & 0 \\ 0 & 0 & 0 & 1 & 0 & 0 \\ 0 & 0 & 0 & 0 & 1 & 0 \\ 0 & 0 & 0 & 0 & 0 & 1 \end{bmatrix} \begin{bmatrix} x_7 & x_8 & x_9 & x_{10} & x_{11} & x_{12} \\ x_{13} & x_{14} & x_{15} & x_{16} & x_{17} & x_{18} \\ x_{19} & x_{20} & x_{21} & x_{22} & x_{23} & x_{24} \\ x_{25} & x_{26} & x_{27} & x_{28} & x_{29} & x_{30} \\ x_{31} & x_{32} & x_{33} & x_{34} & x_{35} & x_{36} \\ x_{37} & x_{38} & x_{39} & x_{40} & x_{41} & x_{42} \end{bmatrix}$$

$$- \left\{ \begin{bmatrix} 1 & 0 & 0 & 0 & 0 & 0 \\ 0 & 1 & 0 & 0 & 0 & 0 \\ 0 & 0 & 1 & 0 & 0 & 0 \\ 0 & 0 & 0 & 1 & 0 & 0 \\ 0 & 0 & 0 & 0 & 1 & 0 \\ 0 & 0 & 0 & 0 & 0 & 1 \end{bmatrix} \begin{bmatrix} f_{11} \\ f_{12} \\ f_{13} \\ f_{14} \\ f_{15} \\ f_{16} \end{bmatrix} - \begin{bmatrix} f_{21} \\ f_{22} \\ f_{23} \\ f_{24} \\ f_{25} \\ f_{26} \end{bmatrix} \right\} \frac{\begin{bmatrix} h_{11} & h_{12} & h_{13} & h_{14} & h_{15} & h_{16} \end{bmatrix} \begin{bmatrix} x_7 & x_8 & x_9 & x_{10} & x_{11} & x_{12} \\ x_{13} & x_{14} & x_{15} & x_{16} & x_{17} & x_{18} \\ x_{19} & x_{20} & x_{21} & x_{22} & x_{23} & x_{24} \\ x_{25} & x_{26} & x_{27} & x_{28} & x_{29} & x_{30} \\ x_{31} & x_{32} & x_{33} & x_{34} & x_{35} & x_{36} \\ x_{37} & x_{38} & x_{39} & x_{40} & x_{41} & x_{42} \end{bmatrix}}{\begin{bmatrix} h_{11} & h_{12} & h_{13} & h_{14} & h_{15} & h_{16} \end{bmatrix} \begin{bmatrix} f_{11} \\ f_{12} \\ f_{13} \\ f_{14} \\ f_{15} \\ f_{16} \end{bmatrix}} \tag{4.41}$$

where $f_1\left(x\left(t_1^-\right)\right)$ denotes the $f(x)$ in equation (4.22) when $x_4<0$ and $f_2\left(x\left(t_1^+\right)\right)$ denotes the $f(x)$ in equation (4.22) when $x_4>0$.

- At $t=t_2$, $x_4=0$ and $|x_4|$ change from x_4 to $-x_4$

The indicator function is $$h_1=x_4+x_4=0 \tag{4.42}$$

Jacobian of the indicator function is

$$H_2=\left[\frac{\partial h_2}{\partial x_1}\ \frac{\partial h_2}{\partial x_2}\ \frac{\partial h_2}{\partial x_3}\ \frac{\partial h_2}{\partial x_4}\ \frac{\partial h_2}{\partial x_5}\ \frac{\partial h_2}{\partial x_6}\right]=\left[h_{21}\ \ h_{22}\ \ h_{23}\ \ h_{24}\ \ h_{25}\ \ h_{26}\right] \tag{4.43}$$

Jacobian of the transition condition is $$G_2=\begin{bmatrix}1&0&0&0&0&0\\0&1&0&0&0&0\\0&0&1&0&0&0\\0&0&0&1&0&0\\0&0&0&0&1&0\\0&0&0&0&0&1\end{bmatrix} \tag{4.44}$$

Following the guideline in section 2.3.1.2 and equation (2.17), the new value of variation equation $\psi_{t=t_2^+}$ is as follows:

$$\delta x\left(t_2^+\right)=G_2\left(x^-\right)\delta x\left(t_2^-\right)-\left[G_2\left(x^-\right)f_2\left(x\left(t_2^-\right)\right)-f_1\left(x\left(t_2^+\right)\right)\right]\frac{H_2\left(x^-\right)\delta x\left(t_2^-\right)}{H_2\left(x^-\right)f_2\left(x\left(t_2^-\right)\right)} \tag{4.45}$$

where "+" and "—" denote the time just after and before switch instants t_2. Rewriting equation (4.45),

$$\begin{bmatrix}x_7^{new}&x_8^{new}&x_9^{new}&x_{10}^{new}&x_{11}^{new}&x_{12}^{new}\\x_{13}^{new}&x_{14}^{new}&x_{15}^{new}&x_{16}^{new}&x_{17}^{new}&x_{18}^{new}\\x_{19}^{new}&x_{20}^{new}&x_{21}^{new}&x_{22}^{new}&x_{23}^{new}&x_{24}^{new}\\x_{25}^{new}&x_{26}^{new}&x_{27}^{new}&x_{28}^{new}&x_{29}^{new}&x_{30}^{new}\\x_{31}^{new}&x_{32}^{new}&x_{33}^{new}&x_{34}^{new}&x_{35}^{new}&x_{36}^{new}\\x_{37}^{new}&x_{38}^{new}&x_{39}^{new}&x_{40}^{new}&x_{41}^{new}&x_{42}^{new}\end{bmatrix}=\begin{bmatrix}1&0&0&0&0&0\\0&1&0&0&0&0\\0&0&1&0&0&0\\0&0&0&1&0&0\\0&0&0&0&1&0\\0&0&0&0&0&1\end{bmatrix}\begin{bmatrix}x_7&x_8&x_9&x_{10}&x_{11}&x_{12}\\x_{13}&x_{14}&x_{15}&x_{16}&x_{17}&x_{18}\\x_{19}&x_{20}&x_{21}&x_{22}&x_{23}&x_{24}\\x_{25}&x_{26}&x_{27}&x_{28}&x_{29}&x_{30}\\x_{31}&x_{32}&x_{33}&x_{34}&x_{35}&x_{36}\\x_{37}&x_{38}&x_{39}&x_{40}&x_{41}&x_{42}\end{bmatrix}$$

$$-\left\{\begin{bmatrix}1&0&0&0&0&0\\0&1&0&0&0&0\\0&0&1&0&0&0\\0&0&0&1&0&0\\0&0&0&0&1&0\\0&0&0&0&0&1\end{bmatrix}\begin{bmatrix}f_{21}\\f_{22}\\f_{23}\\f_{24}\\f_{25}\\f_{26}\end{bmatrix}-\begin{bmatrix}f_{11}\\f_{12}\\f_{13}\\f_{14}\\f_{15}\\f_{16}\end{bmatrix}\right\}\frac{\begin{bmatrix}h_{21}&h_{22}&h_{23}&h_{24}&h_{25}&h_{26}\end{bmatrix}\begin{bmatrix}x_7&x_8&x_9&x_{10}&x_{11}&x_{12}\\x_{13}&x_{14}&x_{15}&x_{16}&x_{17}&x_{18}\\x_{19}&x_{20}&x_{21}&x_{22}&x_{23}&x_{24}\\x_{25}&x_{26}&x_{27}&x_{28}&x_{29}&x_{30}\\x_{31}&x_{32}&x_{33}&x_{34}&x_{35}&x_{36}\\x_{37}&x_{38}&x_{39}&x_{40}&x_{41}&x_{42}\end{bmatrix}}{\begin{bmatrix}h_{21}&h_{22}&h_{23}&h_{24}&h_{25}&h_{26}\end{bmatrix}\begin{bmatrix}f_{21}\\f_{22}\\f_{23}\\f_{24}\\f_{25}\\f_{26}\end{bmatrix}} \tag{4.46}$$

where $f_2\left(x\left(t_2^-\right)\right)$ denotes the $f(x)$ in equation (4.22) when $x_4>0$ and $f_1\left(x\left(t_2^+\right)\right)$ denotes the $f(x)$ in equation (4.22) when $x_4<0$.

- At $t=t_3$, $I(t)$ changes from $\dfrac{-u_{lower}-K_p e(t)}{K_i}$ to $I(t-\Delta t)+e(t)\Delta t$

The indicator function is $$h_3=\frac{-u_{lower}-K_p e(t)}{K_i}-\left(I(t-\Delta t)+e(t)\Delta t\right)=0 \tag{4.47}$$

Jacobian of the indicator function is

$$H_3=\begin{bmatrix}\dfrac{\partial h_3}{\partial x_1}&\dfrac{\partial h_3}{\partial x_2}&\dfrac{\partial h_3}{\partial x_3}&\dfrac{\partial h_3}{\partial x_4}&\dfrac{\partial h_3}{\partial x_5}&\dfrac{\partial h_3}{\partial x_6}\end{bmatrix}=\begin{bmatrix}h_{31}&h_{32}&h_{33}&h_{34}&h_{35}&h_{36}\end{bmatrix} \tag{4.48}$$

Jacobian of the transition condition is $$G_3=\begin{bmatrix}1&0&0&0&0&0\\0&1&0&0&0&0\\0&0&1&0&0&0\\0&0&0&1&0&0\\0&0&0&0&1&0\\0&0&0&0&0&1\end{bmatrix} \tag{4.49}$$

Following the guideline in section 2.3.1.2 and equation (2.17), the new value of variation equation $\psi_{t=t_3^+}$ is as follows:

$$\delta x\left(t_3^+\right)=G_3\left(x^-\right)\delta x\left(t_3^-\right)-\left[G_3\left(x^-\right)f_3\left(x\left(t_3^-\right)\right)-f_4\left(x\left(t_3^+\right)\right)\right]\frac{H_3\left(x^-\right)\delta x\left(t_3^-\right)}{H_3\left(x^-\right)f_3\left(x\left(t_3^-\right)\right)} \tag{4.50}$$

where "+" and "—" denote the time just after and before switch instants t_3. Rewriting equation (4.50),

$$\begin{bmatrix} x_7^{new} & x_8^{new} & x_9^{new} & x_{10}^{new} & x_{11}^{new} & x_{12}^{new} \\ x_{13}^{new} & x_{14}^{new} & x_{15}^{new} & x_{16}^{new} & x_{17}^{new} & x_{18}^{new} \\ x_{19}^{new} & x_{20}^{new} & x_{21}^{new} & x_{22}^{new} & x_{23}^{new} & x_{24}^{new} \\ x_{25}^{new} & x_{26}^{new} & x_{27}^{new} & x_{28}^{new} & x_{29}^{new} & x_{30}^{new} \\ x_{31}^{new} & x_{32}^{new} & x_{33}^{new} & x_{34}^{new} & x_{35}^{new} & x_{36}^{new} \\ x_{37}^{new} & x_{38}^{new} & x_{39}^{new} & x_{40}^{new} & x_{41}^{new} & x_{42}^{new} \end{bmatrix} = \begin{bmatrix} 1 & 0 & 0 & 0 & 0 & 0 \\ 0 & 1 & 0 & 0 & 0 & 0 \\ 0 & 0 & 1 & 0 & 0 & 0 \\ 0 & 0 & 0 & 1 & 0 & 0 \\ 0 & 0 & 0 & 0 & 1 & 0 \\ 0 & 0 & 0 & 0 & 0 & 1 \end{bmatrix} \begin{bmatrix} x_7 & x_8 & x_9 & x_{10} & x_{11} & x_{12} \\ x_{13} & x_{14} & x_{15} & x_{16} & x_{17} & x_{18} \\ x_{19} & x_{20} & x_{21} & x_{22} & x_{23} & x_{24} \\ x_{25} & x_{26} & x_{27} & x_{28} & x_{29} & x_{30} \\ x_{31} & x_{32} & x_{33} & x_{34} & x_{35} & x_{36} \\ x_{37} & x_{38} & x_{39} & x_{40} & x_{41} & x_{42} \end{bmatrix}$$

$$- \left\{ \begin{bmatrix} 1 & 0 & 0 & 0 & 0 & 0 \\ 0 & 1 & 0 & 0 & 0 & 0 \\ 0 & 0 & 1 & 0 & 0 & 0 \\ 0 & 0 & 0 & 1 & 0 & 0 \\ 0 & 0 & 0 & 0 & 1 & 0 \\ 0 & 0 & 0 & 0 & 0 & 1 \end{bmatrix} \begin{bmatrix} f_{31} \\ f_{32} \\ f_{33} \\ f_{34} \\ f_{35} \\ f_{36} \end{bmatrix} - \begin{bmatrix} f_{41} \\ f_{42} \\ f_{43} \\ f_{44} \\ f_{45} \\ f_{46} \end{bmatrix} \right\} \frac{\begin{bmatrix} h_{31} & h_{32} & h_{33} & h_{34} & h_{35} & h_{36} \end{bmatrix} \begin{bmatrix} x_7 & x_8 & x_9 & x_{10} & x_{11} & x_{12} \\ x_{13} & x_{14} & x_{15} & x_{16} & x_{17} & x_{18} \\ x_{19} & x_{20} & x_{21} & x_{22} & x_{23} & x_{24} \\ x_{25} & x_{26} & x_{27} & x_{28} & x_{29} & x_{30} \\ x_{31} & x_{32} & x_{33} & x_{34} & x_{35} & x_{36} \\ x_{37} & x_{38} & x_{39} & x_{40} & x_{41} & x_{42} \end{bmatrix}}{\begin{bmatrix} h_{31} & h_{32} & h_{33} & h_{34} & h_{35} & h_{36} \end{bmatrix} \begin{bmatrix} f_{31} \\ f_{32} \\ f_{33} \\ f_{34} \\ f_{35} \\ f_{36} \end{bmatrix}} \tag{4.51}$$

where $f_3\left(x\left(t_3^-\right)\right)$ denotes the $f(x)$ in equation (4.22) when $I(t) = \dfrac{-u_{lower} - K_p e(t)}{K_i}$ and $f_4\left(x\left(t_3^+\right)\right)$ denotes the $f(x)$ in equation (4.22) when $I(t) = I(t-\Delta t) + e(t)\Delta t$.

- At $t = t_4$, $I(t)$ change from $I(t-\Delta t) + e(t)\Delta t$ to $\dfrac{-u_{lower} - K_p e(t)}{K_i}$ 39

The indicator function is

$$h_4 = \left(I(t-\Delta t) + e(t)\Delta t\right) - \frac{-u_{lower} - K_p e(t)}{K_i} = 0 \tag{4.52}$$

Jacobian of the indicator function is

$$H_4 = \left[\frac{\partial h_4}{\partial x_1} \quad \frac{\partial h_4}{\partial x_2} \quad \frac{\partial h_4}{\partial x_3} \quad \frac{\partial h_4}{\partial x_4} \quad \frac{\partial h_4}{\partial x_5} \quad \frac{\partial h_4}{\partial x_6}\right] = \begin{bmatrix} h_{41} & h_{42} & h_{43} & h_{44} & h_{45} & h_{46} \end{bmatrix} \tag{4.53}$$

Jacobian of the transition condition is $G_4 = \begin{bmatrix} 1 & 0 & 0 & 0 & 0 & 0 \\ 0 & 1 & 0 & 0 & 0 & 0 \\ 0 & 0 & 1 & 0 & 0 & 0 \\ 0 & 0 & 0 & 1 & 0 & 0 \\ 0 & 0 & 0 & 0 & 1 & 0 \\ 0 & 0 & 0 & 0 & 0 & 1 \end{bmatrix}$ (4.54)

Following the guideline in section 2.3.1.2 and equation (2.17), the new value of variation equation $\psi_{t=t_4^+}$ is as follows:

$$\delta x\left(t_4^+\right) = G_4\left(x^-\right)\delta x\left(t_4^-\right) - \left[G_4\left(x^-\right) f_4\left(x\left(t_4^-\right)\right) - f_3\left(x\left(t_4^+\right)\right)\right] \frac{H_4\left(x^-\right)\delta x\left(t_4^-\right)}{H_4\left(x^-\right) f_4\left(x\left(t_4^-\right)\right)} \tag{4.55}$$

where "+" and "—" denote the time just after and before switch instants t_4. Rewriting equation (4.55),

$$\begin{bmatrix} x_7^{new} & x_8^{new} & x_9^{new} & x_{10}^{new} & x_{11}^{new} & x_{12}^{new} \\ x_{13}^{new} & x_{14}^{new} & x_{15}^{new} & x_{16}^{new} & x_{17}^{new} & x_{18}^{new} \\ x_{19}^{new} & x_{20}^{new} & x_{21}^{new} & x_{22}^{new} & x_{23}^{new} & x_{24}^{new} \\ x_{25}^{new} & x_{26}^{new} & x_{27}^{new} & x_{28}^{new} & x_{29}^{new} & x_{30}^{new} \\ x_{31}^{new} & x_{32}^{new} & x_{33}^{new} & x_{34}^{new} & x_{35}^{new} & x_{36}^{new} \\ x_{37}^{new} & x_{38}^{new} & x_{39}^{new} & x_{40}^{new} & x_{41}^{new} & x_{42}^{new} \end{bmatrix} = \begin{bmatrix} 1 & 0 & 0 & 0 & 0 & 0 \\ 0 & 1 & 0 & 0 & 0 & 0 \\ 0 & 0 & 1 & 0 & 0 & 0 \\ 0 & 0 & 0 & 1 & 0 & 0 \\ 0 & 0 & 0 & 0 & 1 & 0 \\ 0 & 0 & 0 & 0 & 0 & 1 \end{bmatrix} \begin{bmatrix} x_7 & x_8 & x_9 & x_{10} & x_{11} & x_{12} \\ x_{13} & x_{14} & x_{15} & x_{16} & x_{17} & x_{18} \\ x_{19} & x_{20} & x_{21} & x_{22} & x_{23} & x_{24} \\ x_{25} & x_{26} & x_{27} & x_{28} & x_{29} & x_{30} \\ x_{31} & x_{32} & x_{33} & x_{34} & x_{35} & x_{36} \\ x_{37} & x_{38} & x_{39} & x_{40} & x_{41} & x_{42} \end{bmatrix} \tag{4.56}$$

$$- \left\{ \begin{bmatrix} 1 & 0 & 0 & 0 & 0 & 0 \\ 0 & 1 & 0 & 0 & 0 & 0 \\ 0 & 0 & 1 & 0 & 0 & 0 \\ 0 & 0 & 0 & 1 & 0 & 0 \\ 0 & 0 & 0 & 0 & 1 & 0 \\ 0 & 0 & 0 & 0 & 0 & 1 \end{bmatrix} \begin{bmatrix} f_{41} \\ f_{42} \\ f_{43} \\ f_{44} \\ f_{45} \\ f_{46} \end{bmatrix} - \begin{bmatrix} f_{31} \\ f_{32} \\ f_{33} \\ f_{34} \\ f_{35} \\ f_{36} \end{bmatrix} \right\} \frac{\begin{bmatrix} h_{41} & h_{42} & h_{43} & h_{44} & h_{45} & h_{46} \end{bmatrix} \begin{bmatrix} x_7 & x_8 & x_9 & x_{10} & x_{11} & x_{12} \\ x_{13} & x_{14} & x_{15} & x_{16} & x_{17} & x_{18} \\ x_{19} & x_{20} & x_{21} & x_{22} & x_{23} & x_{24} \\ x_{25} & x_{26} & x_{27} & x_{28} & x_{29} & x_{30} \\ x_{31} & x_{32} & x_{33} & x_{34} & x_{35} & x_{36} \\ x_{37} & x_{38} & x_{39} & x_{40} & x_{41} & x_{42} \end{bmatrix}}{\begin{bmatrix} h_{41} & h_{42} & h_{43} & h_{44} & h_{45} & h_{46} \end{bmatrix} \begin{bmatrix} f_{41} \\ f_{42} \\ f_{43} \\ f_{44} \\ f_{45} \\ f_{46} \end{bmatrix}}$$

where $f_4\left(x\left(t_4^-\right)\right)$ denotes the $f(x)$ in equation (4.22) when $I(t) = I(t-\Delta t) + e(t)\Delta t$ and

$f_3\left(x\left(t_4^+\right)\right)$ denotes the $f(x)$ in equation (4.22) when $I(t)=\dfrac{-u_{lower}-K_p e(t)}{K_i}$.

- At $t=t_5$, $I(t)$ change from $I(t-\Delta t)+e(t)\Delta t$ to $\dfrac{u_{upper}-K_p e(t)}{K_i}$

The indicator function is $$h_5=\left(I(t-\Delta t)+e(t)\Delta t\right)-\frac{u_{upper}-K_p e(t)}{K_i}=0 \tag{4.57}$$

Jacobian of the indicator function is

$$H_5=\left[\frac{\partial h_5}{\partial x_1}\ \frac{\partial h_5}{\partial x_2}\ \frac{\partial h_5}{\partial x_3}\ \frac{\partial h_5}{\partial x_4}\ \frac{\partial h_5}{\partial x_5}\ \frac{\partial h_5}{\partial x_6}\right]=\left[h_{51}\ \ h_{52}\ \ h_{53}\ \ h_{54}\ \ h_{55}\ \ h_{56}\right] \tag{4.58}$$

Jacobian of the transition condition is $$G_5=\begin{bmatrix}1&0&0&0&0&0\\0&1&0&0&0&0\\0&0&1&0&0&0\\0&0&0&1&0&0\\0&0&0&0&1&0\\0&0&0&0&0&1\end{bmatrix} \tag{4.59}$$

Following the guideline in section 2.3.1.2 and equation (2.17), the new value of variation equation $\psi_{t=t_5^+}$ is as follows:

$$\delta x\left(t_5^+\right)=G_5\left(x^-\right)\delta x\left(t_5^-\right)-\left[G_5\left(x^-\right)f_4\left(x\left(t_5^-\right)\right)-f_5\left(x\left(t_5^+\right)\right)\right]\frac{H_5\left(x^-\right)\delta x\left(t_5^-\right)}{H_5\left(x^-\right)f_4\left(x\left(t_5^-\right)\right)} \tag{4.60}$$

where "+" and "—" denote the time just after and before switch instants t_5. Rewriting equation (4.60),

$$\begin{bmatrix}x_7^{new}&x_8^{new}&x_9^{new}&x_{10}^{new}&x_{11}^{new}&x_{12}^{new}\\x_{13}^{new}&x_{14}^{new}&x_{15}^{new}&x_{16}^{new}&x_{17}^{new}&x_{18}^{new}\\x_{19}^{new}&x_{20}^{new}&x_{21}^{new}&x_{22}^{new}&x_{23}^{new}&x_{24}^{new}\\x_{25}^{new}&x_{26}^{new}&x_{27}^{new}&x_{28}^{new}&x_{29}^{new}&x_{30}^{new}\\x_{31}^{new}&x_{32}^{new}&x_{33}^{new}&x_{34}^{new}&x_{35}^{new}&x_{36}^{new}\\x_{37}^{new}&x_{38}^{new}&x_{39}^{new}&x_{40}^{new}&x_{41}^{new}&x_{42}^{new}\end{bmatrix}=\begin{bmatrix}1&0&0&0&0&0\\0&1&0&0&0&0\\0&0&1&0&0&0\\0&0&0&1&0&0\\0&0&0&0&1&0\\0&0&0&0&0&1\end{bmatrix}\begin{bmatrix}x_7&x_8&x_9&x_{10}&x_{11}&x_{12}\\x_{13}&x_{14}&x_{15}&x_{16}&x_{17}&x_{18}\\x_{19}&x_{20}&x_{21}&x_{22}&x_{23}&x_{24}\\x_{25}&x_{26}&x_{27}&x_{28}&x_{29}&x_{30}\\x_{31}&x_{32}&x_{33}&x_{34}&x_{35}&x_{36}\\x_{37}&x_{38}&x_{39}&x_{40}&x_{41}&x_{42}\end{bmatrix}$$

$$-\left\{\begin{bmatrix}1&0&0&0&0&0\\0&1&0&0&0&0\\0&0&1&0&0&0\\0&0&0&1&0&0\\0&0&0&0&1&0\\0&0&0&0&0&1\end{bmatrix}\begin{bmatrix}f_{41}\\f_{42}\\f_{43}\\f_{44}\\f_{45}\\f_{46}\end{bmatrix}-\begin{bmatrix}f_{51}\\f_{52}\\f_{53}\\f_{54}\\f_{55}\\f_{56}\end{bmatrix}\right\}\frac{\begin{bmatrix}h_{51}&h_{52}&h_{53}&h_{54}&h_{55}&h_{56}\end{bmatrix}\begin{bmatrix}x_7&x_8&x_9&x_{10}&x_{11}&x_{12}\\x_{13}&x_{14}&x_{15}&x_{16}&x_{17}&x_{18}\\x_{19}&x_{20}&x_{21}&x_{22}&x_{23}&x_{24}\\x_{25}&x_{26}&x_{27}&x_{28}&x_{29}&x_{30}\\x_{31}&x_{32}&x_{33}&x_{34}&x_{35}&x_{36}\\x_{37}&x_{38}&x_{39}&x_{40}&x_{41}&x_{42}\end{bmatrix}}{\begin{bmatrix}h_{51}&h_{52}&h_{53}&h_{54}&h_{55}&h_{56}\end{bmatrix}\begin{bmatrix}f_{41}\\f_{42}\\f_{43}\\f_{44}\\f_{45}\\f_{46}\end{bmatrix}} \quad (4.61)$$

where $f_4\left(x\left(t_5^-\right)\right)$ denotes the $f(x)$ in equation (4.22) when $I(t)=I(t-\Delta t)+e(t)\Delta t$ and $f_5\left(x\left(t_5^+\right)\right)$ denotes the $f(x)$ in equation (4.22) when $I(t)=\dfrac{u_{upper}-K_p e(t)}{K_i}$.

- At $t=t_6$, $I(t)$ change from $\dfrac{u_{upper}-K_p e(t)}{K_i}$ to $I(t-\Delta t)+e(t)\Delta t$

The indicator function is $h_6=\dfrac{u_{upper}-K_p e(t)}{K_i}-\left(I(t-\Delta t)+e(t)\Delta t\right)=0$ (4.62)

Jacobian of the indicator function is

$$H_6=\left[\frac{\partial h_6}{\partial x_1}\quad\frac{\partial h_6}{\partial x_2}\quad\frac{\partial h_6}{\partial x_3}\quad\frac{\partial h_6}{\partial x_4}\quad\frac{\partial h_6}{\partial x_5}\quad\frac{\partial h_6}{\partial x_6}\right]=\begin{bmatrix}h_{61}&h_{62}&h_{63}&h_{64}&h_{65}&h_{66}\end{bmatrix} \quad (4.63)$$

Jacobian of the transition condition is $G_6=\begin{bmatrix}1&0&0&0&0&0\\0&1&0&0&0&0\\0&0&1&0&0&0\\0&0&0&1&0&0\\0&0&0&0&1&0\\0&0&0&0&0&1\end{bmatrix}$ (4.64)

Following the guideline in section 2.3.1.2 and equation (2.17), the new value of variation equation $\psi_{t=t_6^+}$ is as follows:

$$\delta x\left(t_6^+\right)=G_6\left(x^-\right)\delta x\left(t_6^-\right)-\left[G_6\left(x^-\right)f_5\left(x\left(t_6^-\right)\right)-f_4\left(x\left(t_6^+\right)\right)\right]\frac{H_6\left(x^-\right)\delta x\left(t_6^-\right)}{H_6\left(x^-\right)f_5\left(x\left(t_6^-\right)\right)} \tag{4.65}$$

where "+" and "—" denote the time just after and before switch instants t_6. Rewriting equation (4.65),

$$\begin{bmatrix} x_7^{new} & x_8^{new} & x_9^{new} & x_{10}^{new} & x_{11}^{new} & x_{12}^{new} \\ x_{13}^{new} & x_{14}^{new} & x_{15}^{new} & x_{16}^{new} & x_{17}^{new} & x_{18}^{new} \\ x_{19}^{new} & x_{20}^{new} & x_{21}^{new} & x_{22}^{new} & x_{23}^{new} & x_{24}^{new} \\ x_{25}^{new} & x_{26}^{new} & x_{27}^{new} & x_{28}^{new} & x_{29}^{new} & x_{30}^{new} \\ x_{31}^{new} & x_{32}^{new} & x_{33}^{new} & x_{34}^{new} & x_{35}^{new} & x_{36}^{new} \\ x_{37}^{new} & x_{38}^{new} & x_{39}^{new} & x_{40}^{new} & x_{41}^{new} & x_{42}^{new} \end{bmatrix} = \begin{bmatrix} 1 & 0 & 0 & 0 & 0 & 0 \\ 0 & 1 & 0 & 0 & 0 & 0 \\ 0 & 0 & 1 & 0 & 0 & 0 \\ 0 & 0 & 0 & 1 & 0 & 0 \\ 0 & 0 & 0 & 0 & 1 & 0 \\ 0 & 0 & 0 & 0 & 0 & 1 \end{bmatrix} \begin{bmatrix} x_7 & x_8 & x_9 & x_{10} & x_{11} & x_{12} \\ x_{13} & x_{14} & x_{15} & x_{16} & x_{17} & x_{18} \\ x_{19} & x_{20} & x_{21} & x_{22} & x_{23} & x_{24} \\ x_{25} & x_{26} & x_{27} & x_{28} & x_{29} & x_{30} \\ x_{31} & x_{32} & x_{33} & x_{34} & x_{35} & x_{36} \\ x_{37} & x_{38} & x_{39} & x_{40} & x_{41} & x_{42} \end{bmatrix}$$

$$-\left\{\begin{bmatrix} 1 & 0 & 0 & 0 & 0 & 0 \\ 0 & 1 & 0 & 0 & 0 & 0 \\ 0 & 0 & 1 & 0 & 0 & 0 \\ 0 & 0 & 0 & 1 & 0 & 0 \\ 0 & 0 & 0 & 0 & 1 & 0 \\ 0 & 0 & 0 & 0 & 0 & 1 \end{bmatrix} \begin{bmatrix} f_{51} \\ f_{52} \\ f_{53} \\ f_{54} \\ f_{55} \\ f_{56} \end{bmatrix} - \begin{bmatrix} f_{41} \\ f_{42} \\ f_{43} \\ f_{44} \\ f_{45} \\ f_{46} \end{bmatrix}\right\} \frac{\begin{bmatrix} h_{61} & h_{62} & h_{63} & h_{64} & h_{65} & h_{66} \end{bmatrix} \begin{bmatrix} x_7 & x_8 & x_9 & x_{10} & x_{11} & x_{12} \\ x_{13} & x_{14} & x_{15} & x_{16} & x_{17} & x_{18} \\ x_{19} & x_{20} & x_{21} & x_{22} & x_{23} & x_{24} \\ x_{25} & x_{26} & x_{27} & x_{28} & x_{29} & x_{30} \\ x_{31} & x_{32} & x_{33} & x_{34} & x_{35} & x_{36} \\ x_{37} & x_{38} & x_{39} & x_{40} & x_{41} & x_{42} \end{bmatrix}}{\begin{bmatrix} h_{61} & h_{62} & h_{63} & h_{64} & h_{65} & h_{66} \end{bmatrix} \begin{bmatrix} f_{51} \\ f_{52} \\ f_{53} \\ f_{54} \\ f_{55} \\ f_{56} \end{bmatrix}} \tag{4.66}$$

where $f_4\left(x\left(t_5^-\right)\right)$ denotes the $f(x)$ in equation (4.22) when $I(t)=I(t-\Delta t)+e(t)\Delta t$ and $f_5\left(x\left(t_5^+\right)\right)$ denotes the $f(x)$ in equation (4.22) when $I(t)=\dfrac{u_{upper}-K_p e(t)}{K_i}$.

4.4.1.1 Lyapunov Exponents for stable motion with a set point

Under the controller shown in equation (4.24), the piston is controlled to move to the desired position. The desired actuator piston position is $x_{desired}=0.2m$, the control gains are given in Table 4.2.

Table 4.2 Control gains of the pneumatic system

Parameters	K_p (V/m)	K_i (V/ms)	U_{lower}(V)	U_{upper}(V)	$\dot{e}_{\min}$ (m/s)	ε	β
values	10	26	0.65	0.65	0.005	0.004	50

The method introduced in Section 2.3.1 which calculates Lyapunov Exponents, is adapted to the pneumatic system. The piston displacement is shown in Fig. 4.13. Fig. 4.14 shows the pressures of the two chambers in steady-state..

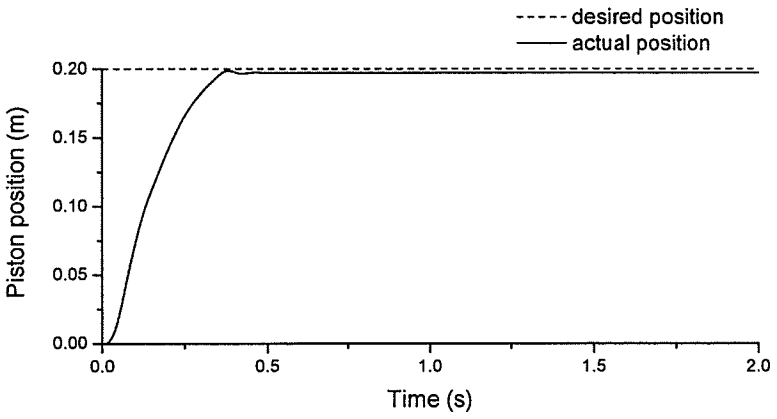

Fig. 4.13 Close-loop position response of the piston

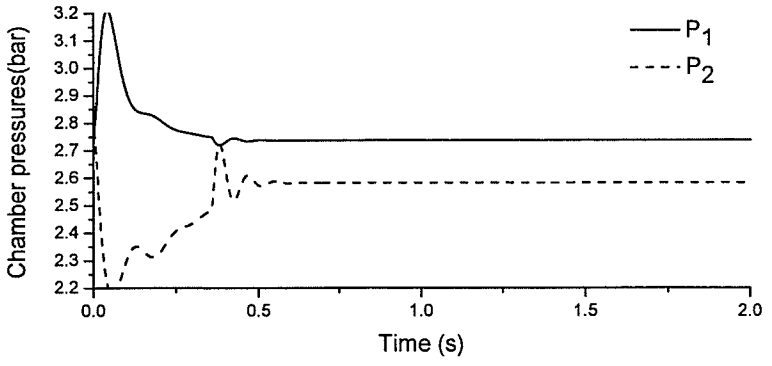

Fig. 4.14 Chamber pressures

Figure 4.13 shows that the system has the steady state error because of the PI controller

and friction. When $\dot{x}_{desired}(t)=0$ and $\left|(x_{desired}-x_5)\right|\le\tilde{\varepsilon}$, the integral part, I, is zero. When the velocity error is too small, the control signal generated by the PI controller is zero and the control valve does not move. The piston will stop there. In Fig. 4.14, the two pressures go to different values at the steady state, due to the friction in the system. The difference in pressures between the chambers generates a net force to balance the friction.

The time history of the Lyapunov Exponents for the pneumatic control system understudy is calculated using the mathematical model. The spectrum is shown in Fig. 4.15. The whole Lyapunov Exponents' spectrum is shown in Table 4.3.

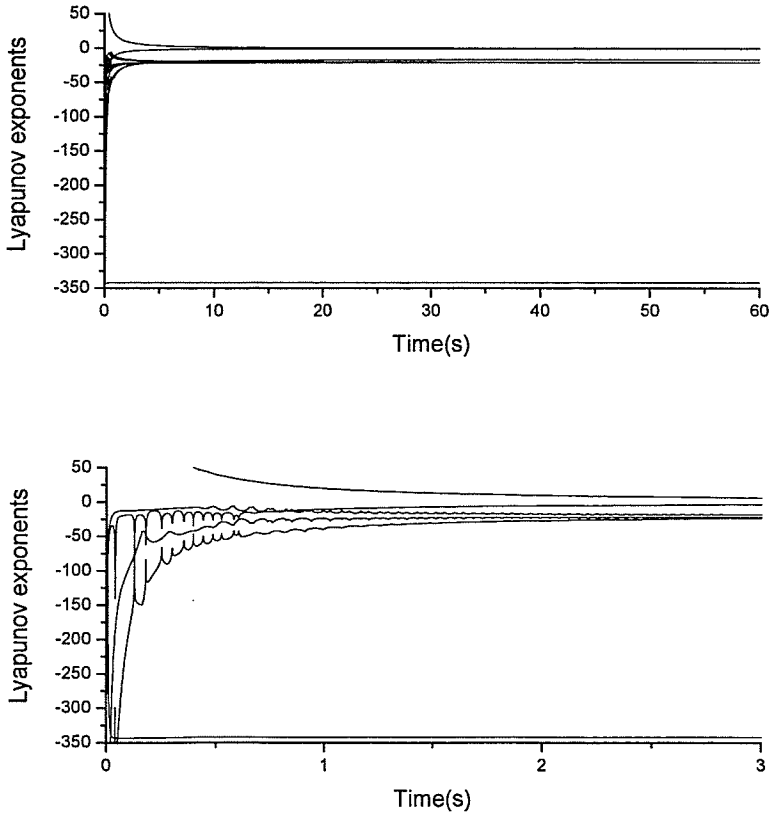

Fig. 4.15 Lyapunov Exponents and the close-up of the pneumatic system

Table 4.3 Lyapunov Exponents of the pneumatic system

λ_1	λ_2	λ_3	λ_4	λ_5	λ_6
0.0	0.0	-16.13	-20.35	-20.20	-341.87

With reference to Fig. 4.15, there are two zero exponents and four negative exponents. As in the original concept of Lyapunov Exponents, zero and negative exponents indicate the system is in some sort of steady state mode with some variables of the system having an attracting period orbit. However, the pneumatic control system does not have a limit cycle or torus and each variable converges to a fixed point. In order to interpret the physical meaning of the results, the system's mathematic model i.e., equation (4.19) is restudied. The controller was designed for the desired piston position and velocity. No requirements of other states of the system were imposed. Different initial chamber pressures may cause the trajectories to converge to two different equilibrium points belonging to the system's equilibrium points. Consequently, the steady-state lengths of $\|x_i(t)\|$ in two directions as $t \to \infty$ stays at a constant non-zero value leading to zero Lyapunov Exponents. Thus, the new interpretation of the zero Lyapunov Exponents is that for the system with a set of non-isolated equilibrium points, zero exponents do not imply the existence of limit cycle or torus. Rather, it indicates that the separation of two trajectories initiated from two different initial conditions remain constants in two directions. The largest distance is within the set of the equilibrium points. The remaining negative Lyapunov Exponents indicate that the trajectories converge on each other in all other directions.

4.4.1.2 Lyapunov Exponents for stable tracking motion

In this section, the piston moves back and forth under the control signal. The desired trajectory is a sinusoid function. Since time t shows up in the controller which makes the systems non-autonomous, another dimension has to be added to the dynamic model. The mathematic model becomes:

$$\begin{aligned}
\dot{t} &= 1 \\
\dot{x}_p &= v_p \\
\dot{v}_p &= \frac{1}{M}\left(-bv_p + AP_1 - AP_2 - F_f - F_L\right) \\
\dot{P}_1 &= \frac{\gamma RT}{V_{o1} + A\left(\frac{L}{2} + x_p\right)}\dot{m}_1 - \frac{\gamma P_1 A}{V_{o1} + A\left(\frac{L}{2} + x_p\right)}\dot{x}_p \\
\dot{P}_2 &= \frac{\gamma RT}{V_{o2} + A\left(\frac{L}{2} - x_p\right)}\dot{m}_2 + \frac{\gamma P_2 A}{V_{o2} + A\left(\frac{L}{2} - x_p\right)}\dot{x}_p \\
\dot{x}_v &= -\frac{x_v}{\mu} + \frac{K_{valve}}{\mu}u
\end{aligned} \tag{4.67}$$

In the simulations, the pneumatic system follows the desired trajectory. The desired trajectory is described as $0.2\cos(1.57t)$ (m). The controller gains are the same as those in the stable motion with a set point.

The initial condition of the system is chosen at $x_p = 0(m)$, $v_p = 0(m/s)$, $P_1 = P_2 = 2.77(bar)$ and $x_v = 0(m)$. The displacement of the piston is shown in Fig. 4.8. It can be seen that the actual displacement of the piston approaches the desired trajectory very well, with slight overshoots at the point with maximum and minimum displacements.

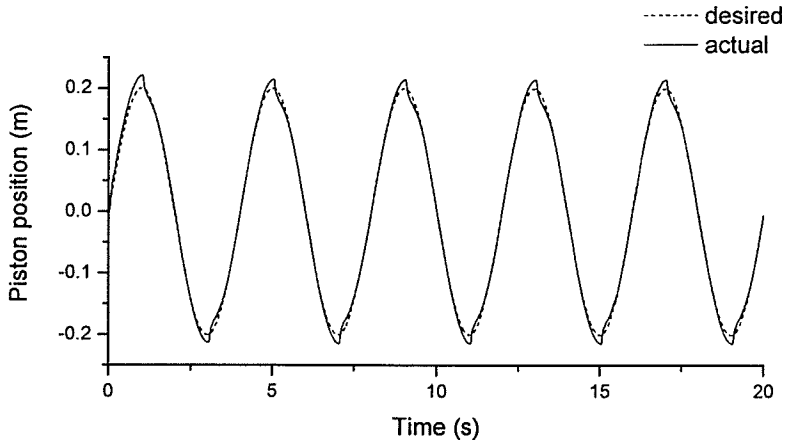

Fig. 4.16 Piston tracking response

The Lyapunov spectrum is shown in Fig. 4.14. All the Lyapunov Exponents converge to the steady value rapidly. The final values of Lyapunov Exponents are shown in Table 4.5. The zero Lyapunov exponent comes from the t dimension.

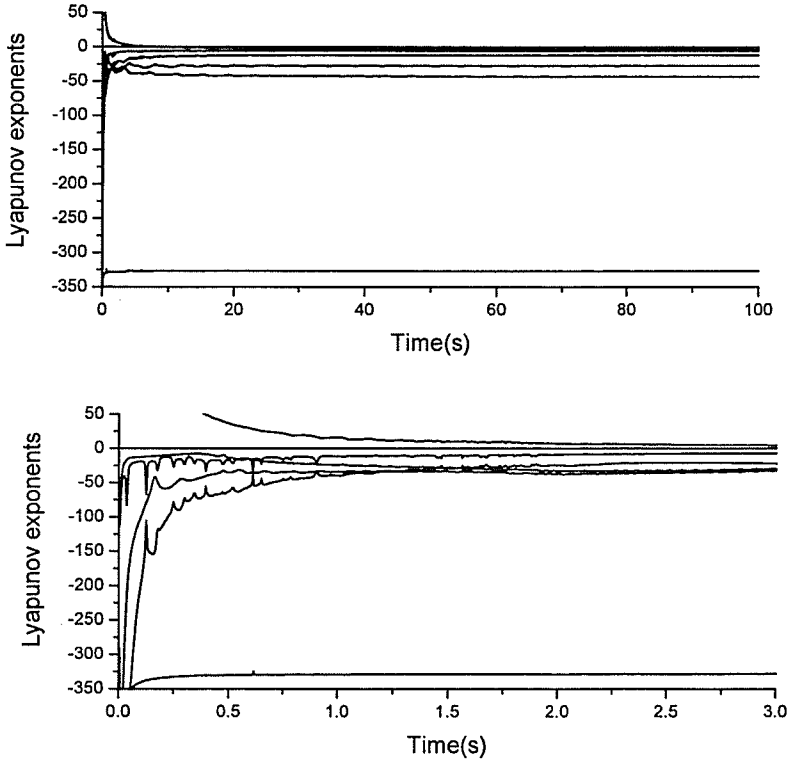

Fig 4.17 Lyapunov exponents and the close-up of the pneumatic system

Table 4.4 Lyapunov Exponents of the pneumatic system

λ_1	λ_2	λ_3	λ_4	λ_5	λ_6	λ_7
0.000	-2.361	-5.946	-10.106	-26.686	-42.501	-341.650

4.4.2 Calculation of the Largest Lyapunov exponent from a time series

4.4.2.1 Stable motion with a set point

For the same system as discussed in Section 4.1, the largest Lyapunov exponent is calculated and presented in this section. In Fig. 4.16 the largest Lyapunov exponent is calculated from the time series of recorded position data. The program calculates the largest Lyapunov exponent with the time step 0.001 and 600,000 points. The values of the largest Lyapunov Exponents from both the time series and the mathematical model, are shown in Table 4.4.

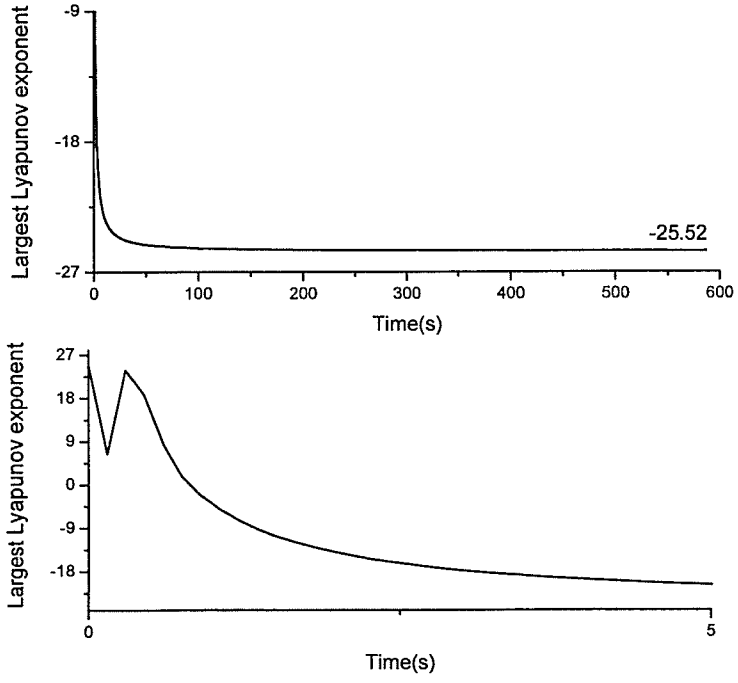

Fig 4.18 Largest Lyapunov exponent and the close-up from the time series

Table 4.5 Largest Lyapunov exponent from the time series and mathematic model

	Time series	Mathematic model
Lyapunov exponent	-25.52	0.000

The largest Lyapunov exponent calculated from the time series can not match the exponent from the mathematic model. To ensure that the poorly calculated largest Lyapunov exponent is not the artifact of inadequate selection of time delay and evolve time, the largest Lyapunov exponent was also calculated with different time delays and evolution times as shown in Fig. 4.17. To demonstrate that although the largest Lyapunov Exponents calculated from the time series changes with the key parameters of time delay and evolve time, all the largest Lyapunov exponent are below -20.

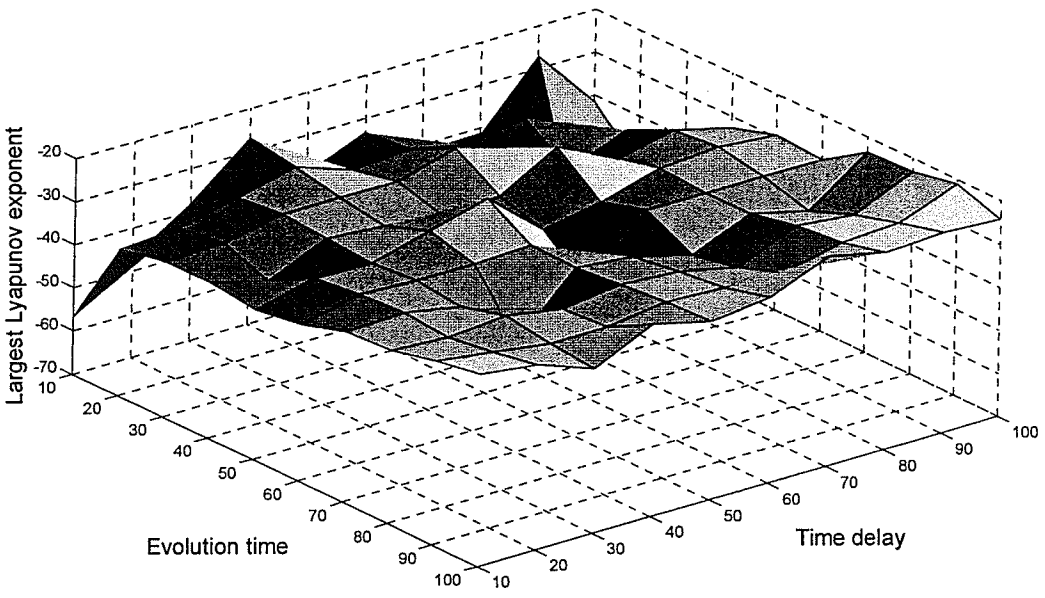

Fig. 4.19 Largest Lyapunov exponent with different time delay and evolution time

Thus, the largest Lyapunov exponent calculated using Wolf's method for the pneumatic

system with a stable set point cannot match the one determined using the mathematical model. The problem comes from the reconstruction of the attractor. The reconstruction is based on a series of data. As the system has a set of infinite non-isolated equilibrium points, the reconstruction of the phase space cannot be carried out based on Taken's theory. Therefore, Wolf's method for calculating the largest Lyapunov exponent from time series does not work for the systems with a set of infinite non-isolated equilibrium points.

4.4.2.2 Stable tracking motion

The time series of the position of the system is recorded from the simulation result. The time delay is 0.001 and the total data are 600,000. The largest Lyapunov exponent is calculated from time series for tracking motion and shown in Fig. 4.20.

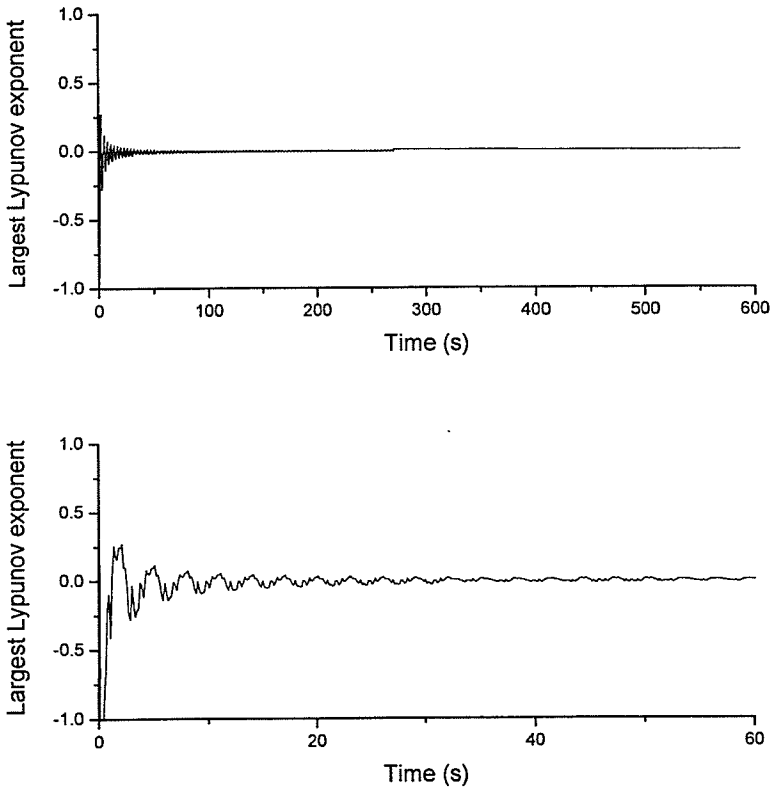

Fig 4.20 Largest Lyapunov exponent and the close-up for tracking response

Table 4.6 Lyapunov exponent calculated from the time series data compared to the result from the mathematic model

	Time series	Mathematic model
L. E.	0.0003	0.000

Although the largest Lyapunov exponent calculated from time series is zero, it has different indications from the mathematic model. The zero Lyapunov exponent from the mathematic model is caused by treating t as another dimension. The zero Lyapunov exponent from the time series shows that the system is stable for a periodic orbit. Furthermore, as discussed in Section 3.3.2.3, if the time series corresponds to periodic behavior, the Lyapunov exponent should be very small or zero as the trajectory returns to exactly the same set of values. However, it does not indicate the convergence or the divergence of nearby trajectories. Hence, this trajectory method reflects the fact that the Lyapunov exponent neither increases nor decreases in its value.

4.5 Summary

In this chapter, Wolf's method was employed to calculate the Lyapunov Exponents from both the mathematic model and a time series for the pneumatic system. For the stable motion with a set of infinite non-isolated equilibrium points, as the pneumatic system studied in this work, the new interpretation of zero exponents with other negative exponents calculated from the mathematical model is presented. This is in line with numerical calculation of the exponents shown in Table 4.3. It is concluded that the whole spectrum of Lyapunov Exponents determined from the mathematical model can still be used to analyze system stability. Some simple examples were presented and discussed in Appendix II to further

support the above explanations.

In this research the largest Lyapunov exponent from a time series of a system with infinite non-isolated equilibrium points was found to significantly differ using the one from the dynamic model. The reason is believed to the set of infinite non-isolated equilibrium points, which cause reconstruction of the phase space being invalid. Thus, the limitation of Wolf's method calculating the largest Lyapunov exponent from time series is demonstrated. It is concluded that Wolf's method cannot be used for calculating the largest Lyapunov exponent for systems with a set of infinite non-isolated equilibrium points. Further studies for a different system with similar properties should be conducted. For the case of pneumatic system tracking desired trajectories, the finding is similar to the one of the two-link pendulum systems in that zero exponents have been calculated from both the mathematical model and the time series. However, the zero exponent from the time series and the one from the mathematical model have different indications. The zero Lyapunov exponent from the mathematical model responds to the extra dimension of time in state space. The zero Lyapunov exponent from the time series responds to the periodical orbit.

Chapter 5

Conclusions

For complex nonlinear systems, it is extremely difficult to derive a Lyapunov function for stability analysis. It is impossible to do the stability analysis in the context of Lyapunov's stability theory when only a set of time series recorded from the experiment is available. The concept of Lyapunov Exponents provides a possible way to analyze the stability of a system. The Lyapunov Exponents can be calculated from either the mathematical model of the system or a time series, which are independent from the initial conditions and can characterize the system's stability provided that the numerical artifact is under control. However, the concept of Lyapunov exponent is usually used for analyzing chaotic systems, where at least one Lyapunov exponent is positive. The methods for calculating Lyapunov Exponents using a time series have been considered unreliable for calculating negative and zero exponents.

In this thesis the possibility of using Wolf's method (1985) to calculate the largest Lyapunov exponent from a time series is studied and applied to the potentially stable systems

where the largest Lyapunov exponent is negative. Two robotic systems, namely a two-link pendulum system and a pneumatic actuator, have been used as examples. The Lyapunov exponent spectrums have been first calculated from the mathematical models, which serve as the reference for comparisons. The time series of each system is generated from the mathematical model and the largest Lyapunov exponent has been calculated using Wolf's method. Note that, in calculating Lyapunov Exponents based on a time series, three key parameters, such as the time-lag, the evolving-time and the embedding dimension for reconstruction of the state space have significant effects on the calculated Lyapunov Exponents. The question of proper selections of the above parameters still remains open. In this work, since the dimensions of the systems are known, large ranges of the parameters for both the time-lag and evolving time are used. The following conclusions have been drawn:

1) Wolf's method has been successfully applied to the stable two-link pendulum system moving to a desired point, *i.e.*, the system has a unique stable equilibrium point. This is evidenced by the fact that the largest negative Lyapunov exponent calculated using Wolf's method is very close to the one calculated from the mathematical model.
2) For the two-link pendulum system under study, the calculated Lyapunov Exponents are not sensitive to the time-lag and time-evolve provided that the time delay is not too low.
3) For both simplified and complete stable pneumatic systems moving to the desire position, there exists a set of infinite non-isolated equilibrium points. Two zero exponents and three negative exponents have been determined from both

mathematical models, which contradicts the conventional concept of Lyapunov Exponents. Such zero exponents indicate the existence of a set of infinite non-isolated equilibrium points rather than a limit cycle or a torus. The causes of such a zero exponent have been discussed. It has been further demonstrated that such phenomena (the system with a set of infinite non-isolated equilibrium points) can occur in robotic systems frequently.

4) The largest Lyapunov exponent calculated using Wolf's method for pneumatic system does not match the one from the mathematical model when a set of infinite non-isolated equilibrium points exists. Thus, Wolf's method based on a time series can not be used for such a system.

5) For systems track the desired trajectories. Zero exponents have been calculated from both the mathematical model and the time series. However, the zero exponent from the time series and the one from the mathematical model have different indications. The zero Lyapunov exponent from the mathematical model responds to the extra dimension of time in state space. The zero Lyapunov exponent from the time series responds to the periodical orbit.

6) The effects of GWN on the largest Lyapunov exponent are studied on the two-link pendulum system having chaotic motion or stable motion with a set-point. The results show that the noise has significant effect on the calculation of the largest Lyapunov Exponents. However, no clear trend has been found in the accuracy of the largest Lyapunov exponent with the increase in NSR.

Overall, based on this research, Wolf's method which calculates the largest Lyapunov exponent from the time series can be applied to stable mechanical systems which possess isolated equilibrium points. The calculated Lyapunov Exponents are not sensitive to the parameters of time-lag and evolve-time. If the systems possess infinite and non-isolated equilibrium points, the method calculating Lyapunov Exponents from the mathematical model is still reliable and the new indication of the zero exponents has been developed. However, the largest Lyapunov exponent calculated from a time series is not reliable and should not be used. More research on calculating the Lyapunov Exponents using a time series for systems with a set of infinite non-isolated equilibrium points should be performed.

Appendix A

Development of the Mathematical Model of Two-link Pendulum System

In this appendix, the dynamic model of the two-link pendulum used in this work, is developed. The two-link pendulum model is shown in Fig. A1.1. The system consists of two rigid links with length l_1 and l_2. The base of Link 1 is fixed at point O. m_1 and m_2 are the masses of the two links. r_1 and r_2 are the locations of the mass centers of the two links. θ_1 and θ_2 are the joint angles which are positive in the clockwise direction. τ_1 and τ_2 are the control torques applied at both joints which are positive in the counter clockwise direction.

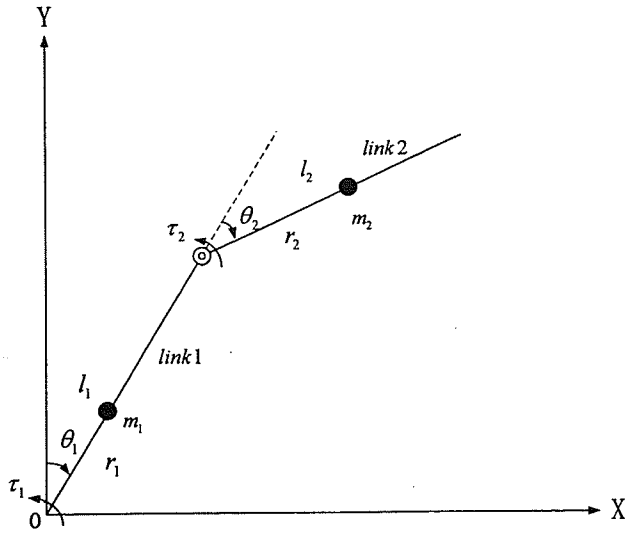

Fig A1.1 Two-link pendulum model

The dynamic equations can be derived from the Lagrangian formulation. In this thesis the two-link pendulum is assumed to move in a horizontal plane.

For Link 1:

The position of the mass center of Link 1 is:

$$\begin{aligned} x &= r_1 \sin\theta_1 \\ y &= r_1 \cos\theta_1 \end{aligned} \tag{A1.1}$$

The velocity of the mass center of Link 1 is:

$$\begin{aligned} \dot{x} &= r_1\dot{\theta}_1 \cos\theta_1 \\ \dot{y} &= -r_1\dot{\theta}_1 \sin\theta_1 \end{aligned} \tag{A1.2}$$

The kinetic energy of Link 1 is as follows:

$$K_1 = \frac{1}{2}m_1 v_1^2 + \frac{1}{2}I_1\dot{\theta}_1^2 = \frac{1}{2}m_1(\dot{x}_1^2 + \dot{y}_1^2) + \frac{1}{2}I_1\dot{\theta}_1^2 \tag{A1.3}$$

Substituting equation (A1.2) into equation (A1.3), we have:

$$K_1 = \frac{1}{2}m_1 r_1^2\dot{\theta}_1^2 + \frac{1}{2}I_1\dot{\theta}_1^2 \tag{A1.4}$$

The potential energy of Link 1 is 0 since the two-link pendulum moves in the horizontal plane.

For Link 2:

The position of the mass center of Link 2 is:

$$\begin{aligned} x &= l_1 \sin\theta_1 + r_2 \sin(\theta_1 + \theta_2) \\ y &= l_1 \cos\theta_1 + r_2 \cos(\theta_1 + \theta_2) \end{aligned} \tag{A1.5}$$

Then the velocity of the mass center of Link 2 is:

$$\begin{aligned} \dot{x} &= l_1\dot{\theta}_1 \cos\theta_1 + r_2(\dot{\theta}_1 + \dot{\theta}_2)\cos(\theta_1 + \theta_2) \\ y &= -l_1\dot{\theta}_1 \sin\theta_1 - r_2(\dot{\theta}_1 + \dot{\theta}_2)\sin(\theta_1 + \theta_2) \end{aligned} \tag{A1.6}$$

The kinetic energy of Link 2 is as follows:

$$K_2 = \frac{1}{2} m_2 v_2^2 + \frac{1}{2} I_2 \dot{\theta}_2^2 = \frac{1}{2} m_2 (\dot{x}_2^2 + \dot{y}_2^2) + \frac{1}{2} I_2 \dot{\theta}_2^2 \tag{A1.7}$$

Substituting equation (A1.6) into equation (A1.7), we have:

$$K_2 = \frac{1}{2} m_2 l_1^2 \dot{\theta}_1^2 + \frac{1}{2} m_2 r_2^2 (\dot{\theta}_1 + \dot{\theta}_2)^2 + m_2 l_1 r_2 (\dot{\theta}_1^2 + \dot{\theta}_1 \dot{\theta}_2) \cos\theta_2 + \frac{1}{2} I_2 (\dot{\theta}_1 + \dot{\theta}_2)^2 \tag{A1.8}$$

The potential energy of Link 2 is 0.

The Lagrangian function of the two-link pendulum is:

$$L = K - P = K_1 + K_2 \tag{A1.9}$$

$$= \frac{1}{2} m_1 r_1^2 \dot{\theta}_1^2 + \frac{1}{2} I_1 \dot{\theta}_1^2 + \frac{1}{2} m_2 l_1^2 \dot{\theta}_1^2 + \frac{1}{2} m_2 r_2^2 (\dot{\theta}_1 + \dot{\theta}_2)^2 + m_2 l_1 r_2 (\dot{\theta}_1^2 + \dot{\theta}_1 \dot{\theta}_2) \cos\theta_2 + \frac{1}{2} I_2 (\dot{\theta}_1 + \dot{\theta}_2)^2$$

Based on the Lagrangian formulation:

$$\tau_i = \frac{d}{dt}\left(\frac{\partial L}{\partial \dot{\theta}_i}\right) - \frac{\partial L}{\partial \theta_i} \tag{A1.10}$$

we have

$$\tau_1 = \left(m_1 r_1^2 + I_1 + m_2 l_1^2 + m_2 r_2^2 + I_2 + 2 m_2 l_1 r_2\right) \ddot{\theta}_1 \tag{A1.11}$$

$$+ \left(m_2 r_2^2 + I_2 + m_2 l_1 r_2 \cos\theta_2\right) \ddot{\theta}_2 - m_2 l_1 r_2 \left(\dot{\theta}_2^2 + 2\dot{\theta}_1 \dot{\theta}_2\right) \sin\theta_2$$

$$\tau_2 = \left(I_2 + m_2 r_2^2 + m_2 l_1 r_2 \cos\theta_2\right) \ddot{\theta}_1 + \left(m_2 r_2^2 + I_2\right) \ddot{\theta}_2 + m_2 l_1 r_2 \dot{\theta}_1^2 \sin\theta_2 \tag{A1.12}$$

Let $J_1 = I_1 + m_1 r_1^2 + m_2 l_1^2$, $J_2 = I_2 + m_2 r_2^2$, $p = m_2 l_1 r_2$

Equations (A1.11) and (A1.12) become:

$$\tau_1 = \left(J_1 + J_2 + 2p\cos\theta_2\right) \ddot{\theta}_1 + \left(J_2 + p\cos\theta_2\right) \ddot{\theta}_2 - p(2\theta_1 \dot{\theta}_2 + \dot{\theta}_2^2) \sin\theta_2 \tag{A1.13}$$

$$\tau_2 = \left(J_2 + p\cos\theta_2\right) \ddot{\theta}_1 + J_2 \ddot{\theta}_2 + p\dot{\theta}_1^2 \sin\theta_2 \tag{A1.14}$$

The dynamic equations can be written in the following matrix form:

$$M(\theta)\ddot{\theta} + C(\theta, \dot{\theta}) = T \tag{A1.15}$$

where

$$M = \begin{bmatrix} d_{11} & d_{12} \\ d_{21} & d_{22} \end{bmatrix} = \begin{bmatrix} J_1 + J_2 + 2p\cos\theta_2 & J_2 + p\cos\theta_2 \\ J_2 + p\cos\theta_2 & J_2 \end{bmatrix}$$

$$C = \begin{bmatrix} d_{111} \\ d_{112} \end{bmatrix} = \begin{bmatrix} -p(\theta_1\dot{\theta}_2 + \dot{\theta}_2^2)\sin\theta_2 \\ p\dot{\theta}_1^2 \sin\theta_2 \end{bmatrix}$$

$$T = \begin{bmatrix} \tau_1 \\ \tau_2 \end{bmatrix}$$

Appendix B

Calculation of Lyapunov Exponents for a Stable Spring Mass System

To support the explanation of the results on Lyapunov Exponents of the pneumatic system in Chapter 4, the spring mass system is studied as a different example. This is a simple system with a set of infinite non-isolated equilibrium points which make the largest Lyapunov exponent zero. The spring mass system's model is shown in Fig. B.1.

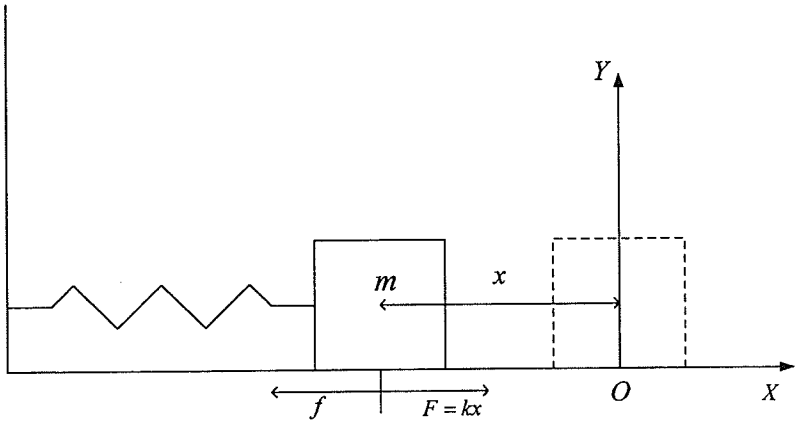

Fig. B.1 Spring mass model

In Fig. B.1, the initial condition is x away from the static position, where the spring has no deformation. The spring force ($F = kx$) is positive in the X axes direction. The friction is positive

in opposite direction as the velocity of the mass. After releasing the mass it oscillates around the balance position. In the research the LuGre model is used.

The dynamic model of the spring mass model is:

$$m\ddot{x} = kx - f \tag{B2.1}$$

Rewriting the dynamic model in the state space model is:

$$\begin{aligned} \dot{x}_1 &= x_2 \\ \dot{x}_2 &= \frac{k}{m}x_1 - \frac{f}{m} \\ \dot{x}_3 &= x_2 - \frac{\sigma_0 |x_2| x_3}{F_{sl} + (F_{st} - F_{sl}) e^{-(\frac{x_2}{V_s})^2}} \end{aligned} \tag{B2.2}$$

where $f = \sigma_0 x_3 + \sigma_1 \dot{x}_3 + b x_2$, x_1 is the position, x_2 is the velocity and x_3 is the variable for LuGre friction model. The parameters of the spring mass system are shown in Table B.1.

Table B.1 The parameters in the spring-mass system

Parameter	Symbol	Nominal Value
The Spring Constant	$k(N/m)$	5
Static friction	$F_s(N)$	4
Coulomb friction	$F_c(N)$	2
LuGre friction model parameter	$\sigma_0(N/m)$	0.15
LuGre friction model parameter	$\sigma_1(N \cdot s/m)$	0.8
Viscous velocity	$v_s(m/s)$	0.1
Damping parameter	$b(N \cdot s/m)$	2.0

In the simulation, the initial condition is set as $\{-1.0(m), 0.0(m/s)\}$, and the mass will oscillate and then stop because of the friction. However, the end positions change with different

initial conditions. This means that, there is a set of infinite non-isolated equilibrium points for the system. As the intial condition is set to overcome the static friction, the mass will move until the force generated by the spring equals the frction. The simulation results of mass position and friction are shown below:

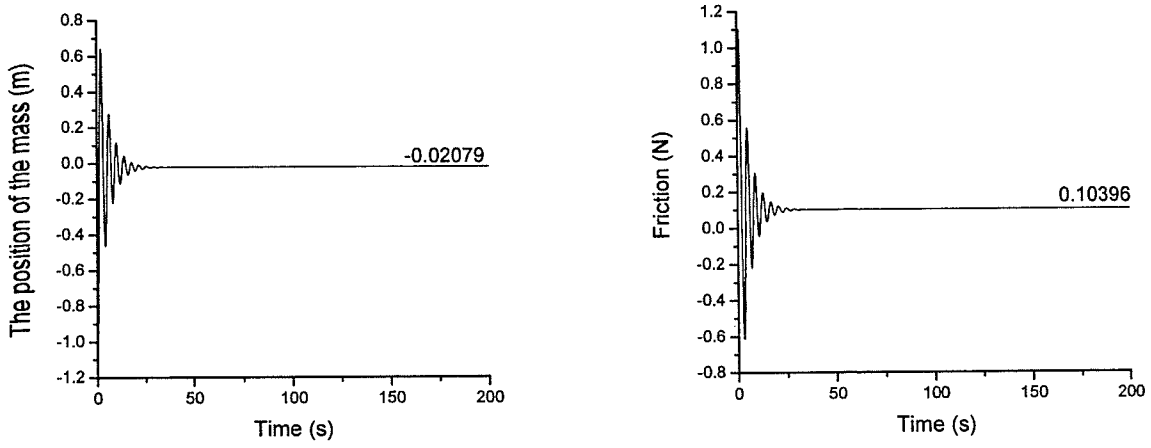

Fig B.2 Position of the mass and the end friction

Then the initial condition is changed as $\{2.0(m), 0.0(m/s)\}$, the simulation results of position and friction are shown in Fig. B.3.

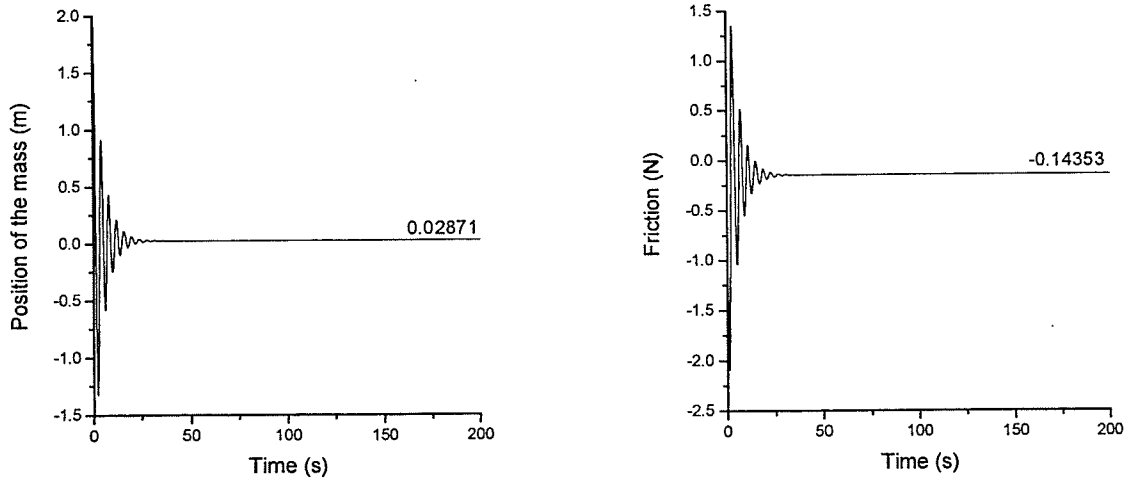

Fig B.3 Position of the mass and the friction

The Lyapunov Exponents are calculated from the mathematic model and shown in Fig. B.4, where three exponents are obtained. Based on the discussion in Chapter 4, the largest zero exponents respond to multi-equilibrium points of the system. The Lyapunov spectrum is in Table B.2.

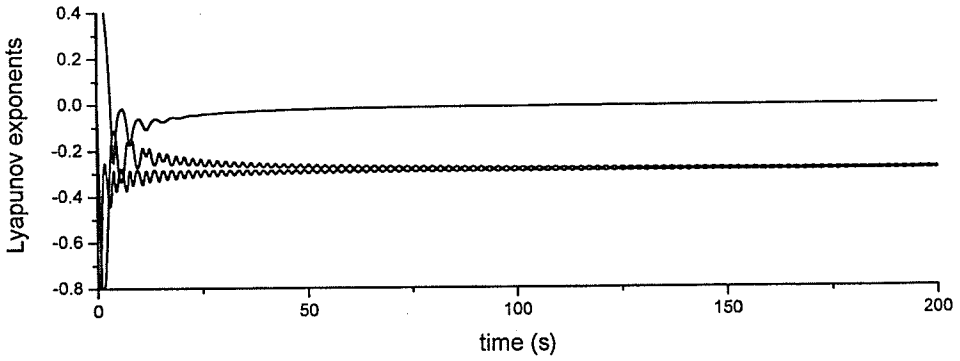

Fig B.4 Lyapunov Exponents from the mathematic model

Table B.2 Lyapunov spectrum

λ_1	λ_2	λ_3
0.00	-0.276	-0.291

Then the largest Lyapunov exponent is calculated from the time series, which is shown in Fig. B.5. In the calculation, the time delay is chosen as 60 and evolution time is chosen as 30. The largest Lyapunov Exponents for the same mass-spring system calculated with a large range of key parameters (time lag and evolve time) are shown in Fig. B.6. In Fig. B.6, the time delay and evolution time are the two horizontal axes and the vertical axis is the largest Lyapunov exponent. Fig. B.6, shows that the largest Lyapunov exponent converges to the -0.29 when the time delay is chosen higher than 40 and lower than 310. With the different simulation parameters, the largest

Lyapunov exponent from time series does not vary significantly. However, it can not match the largest Lyapunov exponent (0.00) from mathematic model. Similar findings are shown in Chapter4.

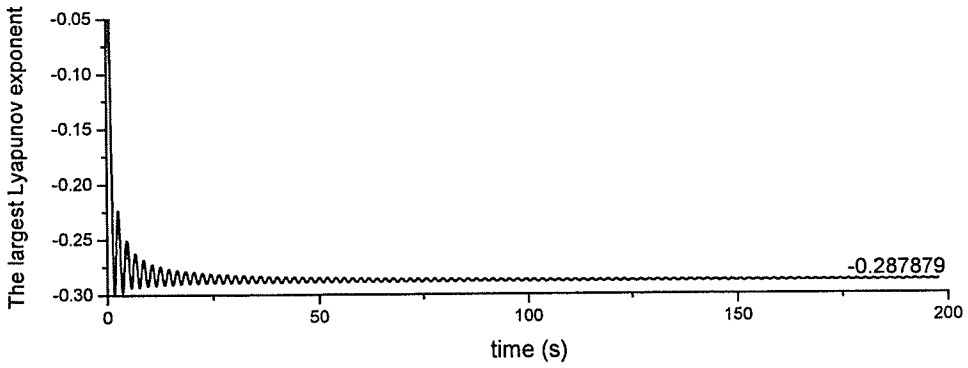

Fig B.5 Lyapunov Exponents from the time series

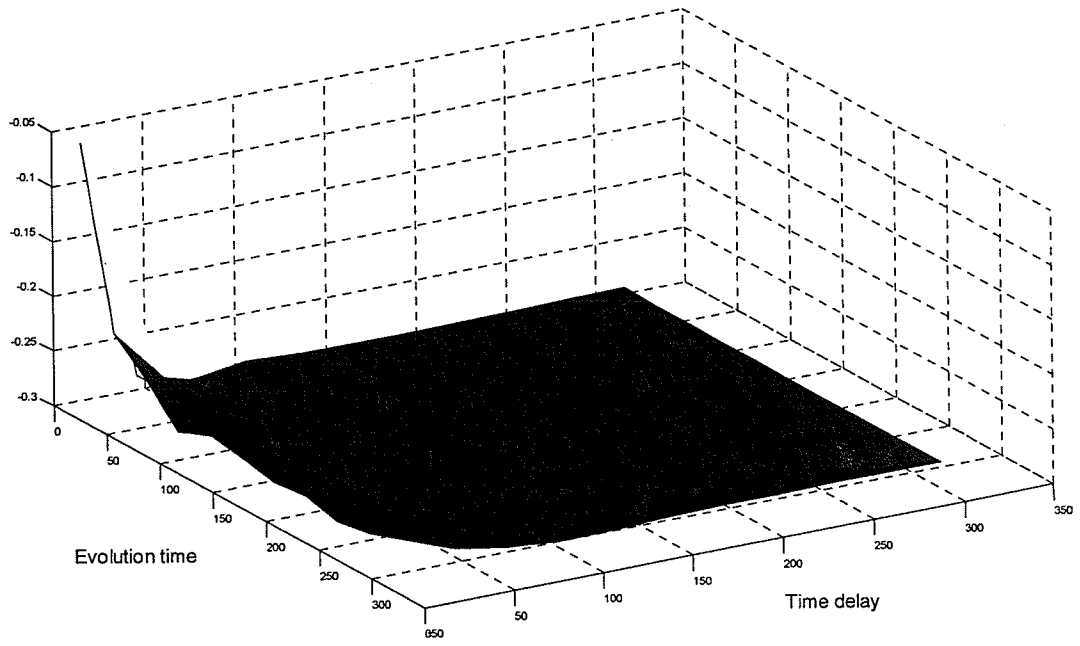

Fig B.6 Largest Lyapunov exponent with different time delay and evolution time

References

Abarbanel, H.D.I., Brown, R., and Kennel, M,B., "Variation of Lyapunov Exponents on a Strange Attractor", *Journal of Nonlinear Science* 1, 175- 199 (1991)

Abarbanel, H.D.I., Brown, R., and Kennel, MB., "Local Lyapunov Exponents Computed from Observed Data", *Journal of Nonlinear Science* 2, 343-365 (1992)

Abarbanel, H.D.I., Analysis of Observed Chaotic Data, Springer, New York, (1996)

Abarbanel, H.D.I., Gilpin, M.E. and Rotenberg, M., "Analysis of Observed Chaotic Data", *Springer*, New York, (1997)

Alvarez, J. and Verduzco, V., "Bifurcations and chaos in a PD-controlled pendulum", *Journal of Dynamic Systems, Measurement, and Control* 120(1), 146–149, (1998)

Amin, J., Friendland, Harnoy, A., "Implementation of a friction estimation and compensation technique", *IEEE Control Systems Magazine*, 17(4):71-76, (1997)

Asada H., Slotline J.J.E., "Robot Analysis and Control", (1986)

Armstrong-Hélouvry, B., "Control of Machines with Friction", *Kluwer Academic Publishers*, Boston, Ma., (1991)

Badii, R. and Politi, A., "Dimensions and Entropies in chaotic systems", G. Mayer-Kress, Ed., *Berlin: Springer*, p. 67 (1989)

Ballance, D.J., and Gawthrop, P.J., "Control Systems Design Via a QFT Approach," *Procs. Control* 91, pp. 476-481, (1991)

Brandstater, A., J. Swift, H.L. Swinney, A. Wolf, J.D. Farmer, E. Jen and J.P. Crutchfield, "Low-dimensional chaos in a hydrodynamic system", *Phys. Rev. Lett.* 51, (1983)

Banbrook, M., Ushaw, G., and McLaughlin, S., "Lyapunov exponents from a time series: A noise robust extraction algorithm", *Chaos Solutions Fractals*, vol. 7, pp. 973–976, (1996)

Banbrook, M., Ushaw, G. and McLaughlin, S., "How to Extract Lyapunov Exponents from Short and Noisy Time Series", *IEEE*, (1997)

Berge F., Pomeau Y., and Vidal C., "Order within chaos", *Wiley*, (1984)

Benettin, G., Galgani, L., Giorgilli, A., and Strelcyn, J. M., "Lyapunov characteristic exponents for smooth dynamical systems and for Hamiltonian systems; A method for computing all of them", *Theory, Meccanica*, 15(1):9-20 (1980)

Berglund, C. N., "A Note on Power-Law Devices and Their Effect on Signal-to-Noise Ratio", *IEEE Transactions on Information Theory,* (1964)
Bowden, F. P. and Tabor, D., "The friction and Lubrication of Solids", *Oxford Univ. Press*, Oxford, (1950)

Bryant, P., Brown, R. and Abarbanel, H.D.I., "Lyapunov Exponents form Observed Time Series", *Physics Review Letter* 65, 1523 (1990)

Broomhead D. S. and King G. P., "On the qualitative analysis of experimental dynamical systems in 'Nonlinear Phenomena and Chaos (edited by S. sarkar)'", *Adam Hilger: Bristol*, 113-142,(1985)

Butcher, J. C., "Numerical Methods for Ordinary Differential Equations", *Wiley*, New York, 2003.

Buzug, Th. M., Reimers, T. and Pfister, G., "Nonlinear Evolution of Spatio-Temporal Structures in Dissipative Continuous Systems", F.H. Busse and L. Kramer, Eds., New York, *Plenum Press*, p. 7 (1990)

Canudas de Wit, C., Olsson, H., Åström, K. J. and Lischinsky, P., "A new model for control of systems with friction", 40H3I, (1995)

Chandra Shekara Bhat, C., Kaimal, M R and Ramamohan, T R, "Application of chaotic noise reduction techniques to chaotic data trained by ANN", *Sadhana*, Vol. 26, Part 5, pp. 485–494, (2001)

Canudas de Wit, C., Olsson, H., Astrom, K. J., and Lischinsky, P., "A new model for control of systems with friction", *IEEE Transactions on Automatic Control*, 40(3):419-425(1995)

Chen, G. and Lai, D., "Making a Dynamical System Chaotic: Feedback Control of Lyapunov Exponents for Discrete-Time Dynamical Systems," *IEEE Transactions on Circuits and Systems*, vol. 44, No. 3, (1997)

Chin, P.S.M., "A Genera Method to derive Lyapunov Function for Non-linear Systems", *In. J. Control* 44, 381-393 (1986)

Chin, P.S.M., "Stability of Non-linear systems via the Intrinsic Method", *In. J. Control* 48, 1561-1567 (1988)

Chin, P.S.M., "Stability Results for the solutions of Certain Fourth-order Autonomous

Darbyshire A.G. and Broomhead D.S., "Calculation of Lyapunov exponents from experimental data submitted for publication", (1994)

Darbyshire, A.G., "Calculating Lyapunov Exponents from a Time Series", *IEEE*, (1994)

Differential Equations", *In. J. Control* 49, 1163-1173 (1989)

Eckmann J.P. and Ruelle D., "Ergodic theory of chaos and strange attractors", *Rev. Mod. Phys.*, 57, 617-657, (1985)

Eckmann, J.-P., Kamphorst, S.O., Ruelle, D., and Ciliberto, S., "Lyapunov Exponents from Time Series", *Physics Review A* 34, 4971 (1986)

Eker, J. and Astrom, K. J., "A nonlinear observer for the inverted pendulum", *IEEE conference on Control Application*, (1996)

Farmer, J.D., Hart, J. and Weidman, P., "A phase space analysis of a baroclinic flow", *Phys. Lett*, 91A , (1982)

Filippov, A. F., "On the approximate computation of solutions of ordinary differential equations with discontinuous right-hand sides", *Moscow University Computational Mathematics and Cybernetics*, 2:19-21(2001)

Friedland, B. and Park, Y.-J. "On adaptive friction compensation", *In Proceedings of the IEEE Conference on Decision and Control*, pages 2899–2902, (1991)

Furuta, K., Kobayashi, S., and Nishimura, M., "A new inverted pendulum apparatus for eduction", *Prepeints IFAC Conference on Advances in Control Educations*, pages 191–196, (1991)

Ganseman, C., Swevers, J. and Al-Bender, F., "An integrated friction model with improved presliding behavior", *In 5th IFAC Symposium on Robot Control,* Nantes, France, 1997.

Green, A & Sasiadek, J. Z., "Fuzzy and Optimal Control of a Two-Link Flexible Manipulator", *IEEE/ASME International Conference on Advanced Intelligent Mechatronics Proceedings*, (2001)

Grassberger, P. and Procaccia, I., "Characterization of strange attractors", *Physical Review Letters, Vol. 50, No. 5*, pp. 346 (1983)

Hemami, H. and Golliday, C. Jr., "The Inverted Pendulum and Biped Stability", Mathematical Bioscience 34, 95-110 (1997a)

Hemami, H. and Cvetkovic, V.S., "Postural Stability of Two biped Models via Lyapunov Second Method", *IEEE Transactions on Automatic Control* 22, 66-70 (1997b)

Holzfuss, J and Lauterborn, W., "Lyapunov Exponents from a Time Series of Acoustic Chaos", *Phsical Review* 1 39(4), 2146-2152(1989)

Kantz, H., and Schreiber, T., Nonlinear Time Series Analysis, Cambridge, UK: *Cambridge Univ. Press.* (2004), 2nd Edition

Khosla, P. K., "Real-Time control and identification of Direct-Drive manipulators", *Ph. D. Thesis*, Dept. of Electrical and Computer Engg., Carnegie Mellon University, USA, (1986)

Kinsner, W., Fractal and Chaos Engineering, Lecture notes. Winnipeg, MB: Dept. Electrical computer eng., Univ. Manitoba, 1996, 760pp

Kinsner, W., "Characterizing Chaos through Lyapunov Metrics", *Proceedings of the Second IEEE International Conference on Cognitive Informatics*, (2003), pp. 189-201

Kunze, M., "On Lyapunov Exponents for Non- Smooth Dynamical Systems with an Application to a Pendulum with Dry Friction", *Journal of Dynamics and Differential Equations* 12(1), 31-116 (2000)

Kuo, A.D., "An optimal Control Model for Analyzing Human Posture Balance", *IEEE Transactions on Biomedical Engineering* 42, 87-101 (1995)

Lankalapalli, S. and Ghosal, A., "Possible chaotic motions in a feedback controlled 2R robot", *IEEE, International Conference on Robotics and Automation* (1996)

Lankalapalli, S. and Ghosal, A., "Possible chaotic motion in a feedback controlled 2R robot", *in Proceedings of the 1996 IEEE International Conference on Robotics and Automation*, Minneapolis, MN, April, N. Caplan and T. J. Tarn (eds.), IEEE Press, New York, pp. 1241–1246, (1996)

Lankalapalli, S. and Ghosal, A., "Chaos in robot control equations", *International Journal of Bifurcation and Chaos 7(3)*, 707–720, (1997)

Liu, W.D., Ren, K.F., Meunier-Guttin-Cluzel, S. and Gouesbet, G., "Global Vector-Field Reconstruction of Nonlinear Dynamical Systems form a Time Series with SVD Method and Validation with Lyapunov Exponents", *Chinese Physics* 12(12), 1366-1373 (2003)

Lyapunov, A.M., 1892, "The General Problem of the Stability of Motion", Translated by Fuller, *A.T. International Journal of Control* 52, 531-773; also (London: Taylor & Francis, 1992)

Mahout, V., Lopez, P., Carcassés, J. P., and Mira, C., "Complex behaviors of a two-revolute joints robot: Harmonic, subharmonic, higher harmonic, fractional harmonic, chaotic responses", *in Proceedings of the IEEE Systems, Man & Cybernetics '93 Conference*, Le Touquet, France, pp. 201–205, (1993)

Merrit, H.E., "Hydraulic control system", New York, (1967)

Mickens, R.E. and Gumel, A.B., "Construction and Analysis of a Nonstandard Finite Difference Scheme for the Burgers-Fisher Equation", *Journal of Sound and Vibration* 257, 791-797 (2002)

Miksovsky, J. and Raidl, A., "Multivariate Phase Space Reconstruction of Meteorological Systems", *Geophysical Research Abstracts* 5, 01916 (2003)

Miksovsky, J., "On some Meteorological Applications of Nonlinear Time Series Methods", Extended Abstract of Doctoral Thesis, Charles University, Prague, (2004)
Most, T., Bucher, C. and Schorling, Y., "Dynamic Stability Analysis of Non-Linear Structures with Geometrical Imperfections under Random Loading", *Journal of Sound and Vibration* 276, 381-400 (2004)

Mu, X. and Wu, Q., "Development of a complete dynamic Model of a Planar Five-Link Biped and Sliding Mode Control of its Locomotion during the Double Support Phase", *International Journal of Control* 77, 789-799 (2004)

Mu, X., "Dynamic Modeling and Motion Regulation of a Five-Link Biped Robot Walking in the Sagittal Plane", University of Manitoba Ph.D. Thesis, (2005)

Muller, P.C., "Calculation of Lyapunov Exponents for Dynamic Systems with Discontinuities", *Chaos, Solitans and Fractals* 5, 1671-1681 (1995)

Nicolis, C. and Nicolis, G., "Reconstruction of the Dynamics of the Climatic System from Time-Series Data", *Proc. Natl. Acad. Sci.* USA (83), 536-540 (1986)

Nusse, H.E. and Yorke, J.A., Dynamics: Numerical Explorations, *Springger-Berlag,* New York (1998)

Oseledec, V.I., "A Multiplicative Ergodic Theorem: Lyapunov Characteristic Numbers for Dynamical Systems", *Trans. Moscow Math. Soc.* 19, 197 (1968)

Olsson, H., Åström, K.J., Canudas de Wit, C., M. Gäfvert and P. Lischinsky, "Friction models and friction compensation", (1997)

Packard, N., Crutchfield, J., Farmer, J. and Shaw, R., "Geometry from a time series", *Phys. Rev. Lett.*, vol. 45, no. 9, pp. 712-716, (1980)

Parker, T. S. and Chua L. O., "Chaos: a tutorial for engineers", *proc. IEEE*, vol. 75, no. 8, pp. 982-1008, (1987)

Parker T. S., Chua L. O., "Practical numerical algorithms for chaotic systems", *Springer Verlag* (1989)

Porter, B., and Tatnall, M.L., "Performance characteristics of an adaptive hydraulic servo-mechanism", *Int. J. Control*, (1970), 11

Paden, B.E., and Sastry, S.S., "A Calculus for Computing Filippov's Differential Inclusion with Application to the Variable Structure Control of Robot Manipulators", *IEEE Transactions on Circuits and Systems* 34, 73-82 (1987)

Parlitz, U., "Identification of True and Spurious Lyapunov Exponents from Time Series", *International Journal of Bifurcation and Chaos* 2,155 (1992)

Pavlov, A.V., Yansons N.B., and Anishchenko, V.S., "Application of Statistical Methods to Solve Global Reconstruction Problems", *Technical physics Letters* 23, 297 (1997)

Pavlov, A.N., Yanson, N.B., Kapitaniak, T., and Anishchenko, V.S., "Reconstruction of Dynamic systems using Short Signals", *Technical Physics Letters* 25(6), 424-426 (1999)

Pettis, K. W., Bailey, T.A., Jain, A.K. and Dubes, R.C., "An intrinsic dimensionality estimator from near-neighbor information", *IEEE Trans.* Pattern Analysis and Machine Intelligence PAMI-1, (1979)

Ponzo, P.J., "On the stability of Certain Non-linear Differential Equations", IEEE Trans. Automatic Control 10, 470 (1965)

Rad, F. and Ahmed, H.M., "Calculation of Lyapunov exponents though nonlinear apaptive filters", *IEEE*, (1991)

Raibert, M. H., Brown, H.B., "Experiments in Balance with a 2D One- Legged Hopping Machine", *ASME Journal of Dynamic Systems, Measurement, and Control* 106, 75-81 (1984)

Rauf, F, and Ahmed, H.M., "Calculation of Lyapunov Exponents through Nonlinear Adaptive Filters", *Proceedings IEEE International Symposium on Circuits and Systems*, Singapore (1991)

Sakai, M., Homma, N., Yano, M. and Abe, K., "Lyapunov Spectrum Analysis of Reconstructed Attractors from Observed Time Series", *SICE Annual Conference in Fukui*, (2003)

Sano, M. and Sawada, Y., "Measurement of the Lyapunov Spectrum From Chaotic Time Series", *Physics Review Letter* 55, 1082 (1985)

Sekhavat, P., Sepehri, N. and Wu, Q., "Contact task stability analysis via Lyapunov exponents", *IEEE International Symposium on Intelligent Control (ISIC'02)*, pp. 148-152(2002)

Sekhavat, P., "Design and Stability Analysis of a Switching Contact Task Control for Hydraulic Actuators", University of Manitoba Ph.D. Thesis, (2004)

Sekhavat, P., Sepehri, N. and Wu, Q., "Calculation of Lyapunov Exponents Using Nonstandard Finite Difference Discretization Scheme: A Case Study", *Journal of Difference Equations and Applications* 10 (4), 369-378 (2004)

Sekhavat, P., Wu, Q. and Sepehri, N., "Impact Control in Hydraulic Actuators", *ASME Journal of Dynamic Systems, Measurement, and Control* 127(2), 197-205 (2005)

Small, M., Applied nonlinear time series analysis: applications in physics, physiology and finance, World Scientific, (2005)

Swinney, H. L. and Gollub, J. P., "Characterizaiton of hydrodynamic strange attractors", *Physica 18D*, 448-454, (1986)

Shimada, I. and Nagashima, T., "A numerical approach to ergodic problem of dissipative dynamical system", *Prog. Theor. Phys.*, 61, pp 1605-1616(1979)

Shimada, I. and Nagashima, T., "Chaos phenomena in 2-link manipulator with dead time and

its control", *SICE*, (2002)

Takens, F., "Dynamical Systems and Turbulence", Lecture Notes ion Mathematics 898, edited by Rand, D.A., and Young L.-S. *Springer-Verlag*, Berlin (1981)

Takens, F. "On the numerical determination of the dimension of an attractor", *Dynamical Systems and Bifurcations*, Springer-Verlag, Lecture Notes in Mathematics, vol. 1125, pp. 99, (1985)

Tanaka, Y. and Horio, Y., "An Estimation Algorithm of the Lyapunov exponents From Data With Noise AND/OR Quantization", *IEEE International Symposium on Circuits and Systems*, (1997)

Vakakis A. F., Burdick J. W., "Chaotic motions in the dynamics of a hopping Robot", *Proceedings of IEEE international Conference on Robotics and Automation*, pp. 1464-2469 (1990)

Verduzco, F. and Alvarez, J., "Bifurcation analysis of a 2-DOF robot manipulator driven by constant torques", *International Journal of Bifurcation and Chaos 9*, 617–627, (1999)

Verduzco, F. and Alvarez, J., "Homoclinic Chaos in 2-DOF Robot Manipulators Driven by PD Controllers", *Nonlinear Dynamics* 21: 157–171, (2000)

Williams, G.P., Chaos Theory Tamed, Joseph, *Joseph Henry Press*, Washington, D.C. (1997)

Wolf, A. and Swift, J., "Progress in computing Lyapunov exponents from experimental data, in: Statistical Physics and Chaos in Fusion Plasmas", W. Horton and L. Reichl, eds. (Wiley, New York, 1984), p. 111.

Wolf, A., Swift, J.B. Swinney, H.L. and Vastano, J.A., "Determining Lyapunov Exponents from a Time Series", *Physics* 16D, 285-317 (1985)

Wu, Q., Sepehri, N., Thornton-Trump, A.B. and Onyshko, S., "An Extended Integral Method to Derive Lyapunov Functions for Nonlinear Systems", *International Journal of Control* 62, 717-736 (1995)

Wu, Q., "Lyapunov Stability Analysis of a Class of Base-Excited Inverted Pendulums with Application to Bipedal Locomotion Systems", University of Manitoba Ph.D. Thesis, (1996)

Wu, Q., Thornton-Trump, A.B. and Sepehri, N., "Lyapunov Stability Control of Inverted Pendulums with General Base Point Motion", *Int. J. Non-Linear Mechanics* 33, (1998a)

Wu, Q., Onyshko, S., Sepehri, N, and Thornton-Trump, A.B., "On Construction of Smooth Lyapunov Function for non-smooth systems", *International Journal of Control* 69, 443-457 (1998b)

Wu, Q., Sepehri, N., Thornton-Trump, A.B. and Alexander, M., "Stability and Control of Human Trunk Movement during Walking", Computer Methods in Biomechanics and Biomechanical Engineering 1, 247-259 (1998c)

Wu, Q. and Sepehri, N., "On Lyapunov's Stability Analysis of Non-Smooth Systems with Applications to Control Engineering", *International Journal of Nonlinear Mechanics* 36, 1153-1161 (2001)

Wu, Q., and Sqain, R., "A Mathematical Model of Stability Control of Human Thorax and Pelvis Movement during Walking", Computer Methods in Biomechanics and Biomechanical Engineering 5, 67-74 (2002)

Wu, Q., Sepehri, N., Sekhavat, P. and Peles, S., "On Design of Continuous Lyapunov's Feedback Control", *Journal of Franklin Institute* 342 (6), 720-723 (2005)

Young, L.S., "Dimension, entropy, and Lyapunov exponents, Ergodic Theory and Dynamical Systems 2", (1982)

Zeni, A.R., and Gallas, J.A.C., "Lyapunov Exponents for a Duffing Oscillator", *Physic* D89, 71-82 (1996)

Zeng, X., Pielke, R.a., and Eykholt, R., "Extracting Lyapunov Exponents from Short Time Series of Low Precision", *Modern Physics Letters* B 6 (2), 55-75 (1992)

Zheng, Y.F., and Shen, J., "Gait Synthesis for the SD-2 Biped Robot to Climb Sloping Surface", *IEEE Transactions on Robotics and Automation* 6, 86-96 (1990)